Aspects of Dynamic Anterior Surface Aberrations

By

Varadharajan Jayakumar

A thesis

presented to the University of Waterloo

in fulfillment of the

thesis requirement for the degree of

Master of Science

in

Vision Science

Waterloo, Ontario, Canada, 2013

Author's declaration

I hereby declare that I am the sole author of this thesis. This is a true copy of the thesis, including any required final revisions, as accepted by my examiners.

I understand that my thesis may be made electronically available to the public.

Abstract

Introduction: The measurement of tear film stability/regularity is very critical in the diagnosis of dry eye. The tear breakup time, which is used as a diagnostic tool in diagnosing dry eye, is very subjective in nature and variations among individual clinicians exists. The exact mechanism of the tear breakup is also unclear due to the involvement of so many other factors other than the tear film itself. As the prevalence of dry eye is increasing, the need for an objective technique which can be used universally to differentiate between dry eye and normal values increases. Studies have shown that aberrations can be used as an objective technique in diagnosing dry eye, as there is a direct involvement of the tear film in the optics of the eye. However, very few studies have studied the dynamic nature of the anterior surface using aberrations and suggested using dynamic surface aberrations as an objective measure of surface quality. Hence, a series of studies were conducted to understand the aberrations produced by the anterior surface of the eye (tear film and corneal surface) and to measure objectively the anterior surface quality using surface aberrometry.

The objectives of each study chapter are as follows:

Chapter 3 i): To obtain the noise associated with the instrument using a non-dynamic measuring surface, and ii) to design appropriate acquisition settings for the measurements with ocular surface.

Chapter 4: To determine i) the spectral characteristics of the Placido disc light sources of two corneal analysers, ii) the thermal characteristic for a variety of inanimate objects, human ocular surface and the adnexa in the presence of Placido disc light source at normal working

distance, and iii) to compare the ocular surface aberrations obtained using both the corneal analysers

Chapter 5: To determine i) the optimal method for acquisition with respect to normal physiological processes, by examining the blink regimen and head position that elicits the most consistent response over the largest region on repeated measurement; and ii) the largest region selected for analysis by investigating the effect on the individual and summary aberration metrics of the inclusion of non-measurement areas (i.e. where the Placido disc cannot be projected onto the cornea or contact lens). The proportion of non-measurement area that elicits a significantly different result will be determined.

Chapter 6: To evaluate i) a new method of analyzing dynamic ocular surface aberrations using segmented liner regression, and ii) the inter-ocular characteristics of the dynamic ocular surface aberrations using the segmented linear regression.

Methods:

Chapter 3: The characteristics of the surface aberrometer and the noise associated with the measurements of surface aberrations were evaluated using a non-dynamic surface (model eye). Measurements were obtained in different frame rates and focus positions to evaluate the optimal acquisition technique. At each focus position, a set of three repeated measurements were obtained to analyse the repeatability of the measurements obtained using a surface aberrometer.

Chapter 4: The spectral characteristics of the Placido disc light source were obtained by using a PR650 SpectraScan photometer and the thermal characteristics of the objects were obtained

using THI-500 non-contact infrared thermometer. The surface aberration measurements were compared between the corneal analysers. The spectral measures were obtained from the light sources, whereas the thermal measures were obtained from three different surfaces and surface of the eye and adnexa of ten participants. The dynamic anterior surface aberrations were obtained after obtaining the thermal measurements from the surface of the eye.

Chapter 5: Twelve participants were enrolled by screening twenty participants. Participants were screened with their habitual lenses for contact lens wettability and non-invasive tear breakup time (NITBUT) without contact lenses. The participants were enrolled according to the inclusion and exclusion criteria and categorized into normal and dry eye group for study visits. The measurements of NITBUT and surface aberrations were obtained with and without contact lenses, and study lens wettability were also obtained in two visits on consecutive days. The surface aberration measurements were obtained in natural and forced blinking condition and in two different head positions. All the measurements were randomized between eye and between instruments.

Chapter 6:

Seventeen non- symptomatic and non- contact lens participants were recruited in this study. NITBUT and dynamic anterior surface aberration measurements were obtained. The order of the measurements was randomized between the eyes. Two open intervals of at least 10 sec and a maximum of 15 sec were used in the analysis of segmented fit. The dynamic vertical prism coefficients and higher order aberrations were used for the analysis.

Results:

Chapter 3:

i. Data acquisition at an inter-frame interval of 0.25s gave the least number of dropped frames across focus positions, therefore this is the preferred frame rate for data acquisition.

ii. Data obtained in the initial ~15s reflects the focusing procedure and needs to be manually removed prior to analysis of tear dynamics.

iii. Even in the optimal focus position there were significant (small) differences in the distributions between repeated measures. For this reason repeated samples have to be obtained where possible.

iv. The green and red focus positions showed the most consistency within repeated measurements. The variability of the measurements was also more similar between the red and green focus positions than the blue focus positions, both at the extreme positions of defocus and with incremental defocus away from the optimal focus position. When obtaining the dynamic sampling of human ocular surface measurements, the optimal position of focus should be obtained at the blink such that as the tear film dissipates between blinks the measurements are obtained in the (relatively) red focus position.

Chapter 4:

i. CA200 is the preferred device because of the consistent luminance.

ii. Although aberrations were not significantly different between devices, the HOA RMS were higher with the CA200 and, combined with different luminance and possible tear response, indicates the devices are not interchangeable.

In both instruments, there was no indication that there was a thermal response induced by the power of the light source. Therefore, this aspect of the source does not likely contribute to any difference in the aberrations measured by the two devices

Chapter 5:

i. Obtain data in the straight-ahead position, as there is no significant increase in target size with head turn.

ii. With the CA100F, the forced blink paradigm is preferred as this enables blink dynamics to be examined. With the CA200F, either forced or natural blink paradigms are interpretable for tear dynamics.

iii. Differentiation between dry eye and normal groups was best determined with the slope of the RMS aberrations within a blink.

iv. Differentiation between performance with and without a contact lens in the dry eye and normal groups was best determined by analysing the width of the confidence interval of the moving average.

Chapter 6:

i. The location breakpoints one and two are significantly different between eye, open eye interval and order of the measurements for both vertical prism and HOA RMS values.

ii. The highest positive slope for the HOA RMS was, on average, higher in the second eye measured ($p= 0.0407$) and tended to occur later after the blink ($p= 0.0676$).

iii. The location of breakpoint 2 is not significantly different from the NITBUT values ($p>0.05$), even though the correlation was found to be low and not significant.

iv. The average HOA RMS for segmented fit parameter intervals of vertical prism was found to be higher in the second open eye interval compared to first open eye interval.

Conclusion:

From the results of each chapter, it was observed that choosing the blink paradigm is very important to obtain and analyse the dynamic anterior surface aberrations. Choosing a forced blink paradigm (chapter 5) was showed to be useful when the information regarding blink location were not available. The repeatability of the measurements using a non-dynamic surface (chapter 3) shows that the measurements of surface aberrations are repeatable and it is important to choose a criterion closer to the natural tear film dynamics to obtain more repeatable measurements of anterior surface aberrations (chapter 4, 5 and 6). It also shows that the three phased segmented linear regression techniques can be used to analyse the anterior surface aberrations. The segmented linear regression technique was able to differentiate different stages of the tear film and the location of the second breakpoint calculated using segmented regression was closer to the clinical values of tear breakup time, indicating a possible use of segmented linear regression as an objective measure of surface quality.

Acknowledgement

I wish to express my sincere gratitude to my supervisors, Dr. Natalie Hutchings and Dr. Lyndon Jones for their support, guidance, encouragement and valuable suggestions that helped me in all aspects to complete this thesis work successfully.

I would like to thank my committee members, Dr. Trefford Simpson and Dr. Sruthi Srinivasan for their assistance and valuable comments.

I would like to thank Abbas Ommani for providing precious suggestions and help whenever needed.

I would like to acknowledge all the members of Center for Contact Lens Research for their help and support throughout my stay.

The computing support provided by Jim Davidson and Chris Mathers is greatly appreciated.

My special thanks to all the participants involved in the study.

I would like to thank the graduate officers, graduate coordinators, staff and faculty of School of Optometry & Vision Science, and all the graduate students for making my stay nice and enjoyable.

Many thanks to Topcon Canada Inc. for providing the corneal analyser instruments and support whenever needed. This study was partly funded by Canadian Optometric Education Trust Funds (COETF).

I would also like to thanks all my friends, in particular Ashwini Margabandu and Veena Thangavelu for their help, motivation and advice whenever desired.

I would like to express my deep sense of gratitude to my parents, brother, sister-in-law and all my family members for their love and support.

Dedication

To my parents, brother, sister-in-law

and

to my friends

Table of contents

List of tables

List of figures

List of abbreviations

CCD	Charge-Coupled Device
NITBUT	Non- Invasive Tear Break Up Time
RMS	Root Mean Square
HOA	Higher Order Aberrations
CI	Confidence Interval
ANOVA	Analysis Of Variance
µm	Microns (or) micrometres
nm	Nanometres
OD	Ocular Dexter (or) right eye
OS	Ocular Sinister (or) left eye
cd	Candela
ANCOVA	Analysis Of Covariance
BOZR	Back Optic Zone Radius
df	Degree of Freedom
RM	Running Mean

SD	Standard Deviation
m	Metres
Max	Maximum
Min	Minimum
°C	Degree Celsius

Chapter 1 : Review of Tear Film Stability and Ocular Surface Aberrations

1.1 Tear film:

The tear film is a three-layered clear fluid covering the anterior surface of the cornea and the conjunctiva.[1] It forms a uniform fluid surface over the anterior surface of the eye and inside the eyelid to reduce the drag and avoid friction between the eyelid and cornea.[2] This lubricating action of the tear film not only helps in maintaining the integrity of the cornea but also acts as a protective surface for the cornea against microbes and other environmental factors.[3] It is also important in providing nourishment to the anterior epithelial layer of the cornea.[2,4]

Recent research shows the tear film to be a metastable structure formed by an aqueous gel.[5–7] That is, the aqueous layer of the tear film is found to have a gradient level of mucin from bottom to top forming an aqueous gel anterior to the epithelial surface of the cornea, with the highest concentration of mucin at the bottom over the surface of the corneal epithelium.[6] The aqueous gel is protected at the anterior surface from evaporation with a layer of lipid forming the outermost layer of the tear film.[8] The lipid layer can prevent up to 95% of the loss of the aqueous layer due to evaporation. Each layer of the tear film is produced by different glands in the eyelid and conjunctiva, which is released and spread over the anterior surface during the process of blinking. The meibomian glands within the eyelids produces the lipids, whereas the lacrimal glands produce the aqueous layer of the tear film and the mucin layer is mainly produced by the goblet cells of the conjunctiva.[8]

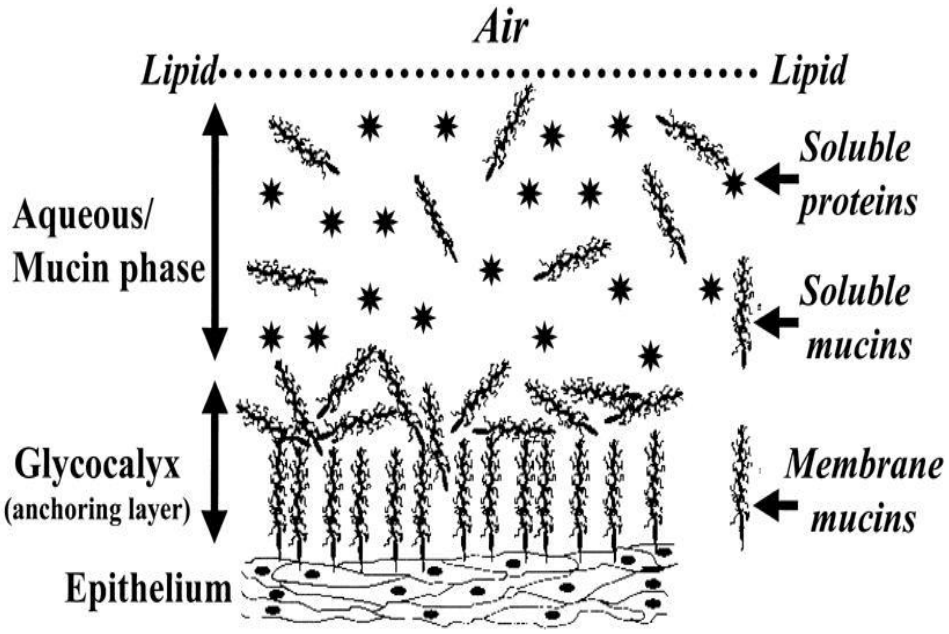

Figure 1-1: Updated structure of the tear film with outermost lipid layer and an aqueous layer with gradient levels of soluble mucus adhering to the corneal epithelium Reprinted from Cornea. The Diagnosis and Management of Dry Eye. A Twenty-five-Year Review. Cornea 2000,19(5):644-649, with permission from Wolters Kluwer Health (Appendix 1).

With every blink, the tear film spreads smoothly over the cornea and conjunctiva by the action of the eyelids. It is important to have a proper blinking action, because study by Carney L et al.[9] have shown that improper or incomplete blinking causes poor tear film quality and lead to dry eye disease if untreated. Following a blink, the tear film undergoes three phases during the inter-blink period.[10] The first phase happens immediately post-blink and is called the tear film buildup or formation phase.[10] In this phase, the tears start spreading throughout the surface of the eye due to the spreading action of the eyelid. After the first phase, when the eyes are fully open, the second phase is when the tear film settles over the cornea and conjunctiva to form a smooth and clear surface. If the eyes remain open for long enough following the second phase, the tear film starts breaking up to form an irregular surface over the cornea and conjunctiva. This is known as the tear film breakup phase[10]. This third phase produces a sensation of dryness and/or irritation, causing the eyes to blink and reform an

intact tear film. The time taken from the eye opening to the breakup of the tear film is the time evaluated when determining tear breakup time measurements.

King-Smith et al [11]suggested that there are three possible reasons for tear film thinning or breakup. These are i) the "outward flow" of the tear film due to evaporation of the tear film, ii) absorption of the tears into the cornea, and iii) "tangential flow" of the tears causing local tear film thickening. It was shown by Nichols et al[12] that the osmosis mechanism of the cornea only helps in outward flow of the tears out of the cornea, which increases the tear evaporation rather than absorption into the cornea. This finding was supported by an increase in the osmolarity of the tears due to evaporation.[13] The third possibility of tangential flow was also later rejected by King-Smith et al.[14] and Begley et al.[15] in their studies of fluorescein self-quenching and fluorescent dimming, which showed a trend of evaporation as the reason for thinning, rather than tangential flow of tears. Thus, it would appear that the major reason for tear film thinning and subsequent rupture is tear film evaporation.

The stability of the tear film is very important in maintaining a clear corneal surface and to produce good retinal image quality.[4,9,16] Chronic dry eye disease may lead to corneal inflammation.[17] If the inflammation remains untreated, it is possible that the increased tear film evaporation may eventually result in scarring of the cornea, which can produce permanent damage to the quality of vision.[6] Studies have also shown a deteriorative effect in the quality of vision and visual comfort during the tear film breakup. According to DEWS classification, "Dry eye is a multi factorial disease of the tears and ocular surface that results in symptoms of discomfort, visual disturbance, and tears film instability with potential damage to the ocular surface. It is accompanied by increased osmolarity of the tear film and

inflammation of the ocular surface".[18] Dry eye disease is the most common cause for ocular discomfort and the main reason for discontinuation of contact lenses.[5,19] It has been estimated that at least 4.4% to more than 50% of the population (of varying age groups) are affected by dry eye disease in the world and it is considered a growing economic burden.[5] The use of different criteria and different diagnostic procedures to diagnose dry eye in various epidemiological studies make the estimation of dry eye a difficult task.

1.2 Diagnostic techniques:

There are several non-invasive and invasive diagnostic techniques which have been adopted to analyse the quality of the tear film. The fluorescein based tear breakup time,[20] Schirmer's test and phenol red thread test are frequently used clinical techniques to evaluate the quality and quantity of the tear film but all these tests have a common problem of being invasive in nature and thereby altering the usual conditions of the tear film. The fluorescein breakup time remains the most widely used clinical diagnostic test for dry eye. It was found that the instillation of the fluorescein dye causes changes to the physical properties of the tear film,[20] and these changes produce variation in the measurements between patients and between eyes of the same patient. Quantification of the fluorescein breakup test is also subjective.[20]

Measurement of tear film osmolarity was considered a "gold standard" for the diagnosis of dry eye due to its high predictive accuracy of 89%, which is higher than many other tests.[6,21] Even though osmometers are commercially available, the need for collection of a large quantity of tears (5-10µl), which is especially difficult in dry eye patients, limits the widespread use of this testing method.[22,23]

To avoid the alteration of the tear film produced by invasive procedures, non-invasive subjective and objective methods are being developed. Placido discs were initially developed to measure the regularity of the cornea (in cases such as keratoconus) by observing the changes in the regularity of the concentric black and white circles. Later, using the same Placido disc principle, video keratoscopes were designed to measure tear film breakup time as well as corneal curvature.[24,25] The reflected light from the Placido disc is captured by the CCD sensor in the instrument and the examiner waits for a break in the image of the Placido ring to develop. The time taken for the Placido ring to break from the time when the eyes are opened is calculated as the non-invasive tear break up time (NITBUT). While this test is used widely in both clinical and research environments, the time for the breakup to occur remains subjective in nature.

Objective tests such as meniscometry,[26] interferometry[27–30] and wavefront sensing[31] have been developed to bring more accuracy to the tear film measurements obtained and to avoid the limitations of fluorescein instillation and the subjectivity of the Placido disc-based tear breakup time measurement. However, even these objective techniques have their limitations due to the structural anatomy of the eye and it's positioning. In meniscometry, the profile of the tear prism height over the lower eyelid margin and the inability to find the exact demarcation point of the apex of the tear prism cause variation in the measurement.[10] Eye movements negatively impact the measurements of the tear film in interferometry, whereas the area of the cornea measured is dependent on the participant's pupil size for wavefront sensing.[10]

1.3 Aberrations:

Aberrations are the deviation in the path of the light from its original path, when it is refracted or reflected from the surface of an object.[32] These aberrations are used to explain the quality of an optical system or individual element of any optical system. The lower the aberrations, the more perfect the optics of the system measured.[33] The quality of the optics of the eyes or its components can be analysed similar to any optical system, by examining the aberrations through the ocular system. There are two categories of aberrations which are of major interest.[34] Chromatic aberration is produced by dispersion of polychromatic light and monochromatic aberrations describe the departure from perfect imagery of a single wavelength of light. Monochromatic aberrations are measured using aberrometers and the overall magnitude of aberrations in an optical system is usually described by the root mean square values (RMS), with higher RMS values describing larger aberrations produced by the optical system. These aberrations can further be classified into different components based on their characteristics.[32]

The Zernike polynomials may be used as a mathematical decomposition of the components of monochromatic aberrations and are continuous, orthogonal and designed for circular pupils. For these reasons, it is often preferred over other polynomial decompositions.[33] If the Zernike polynomials are normalized, each individual coefficient of the polynomial represents the contribution to the RMS wavefront aberrations obtained. An infinite set of complete polynomials can be obtained with each polynomial independent of each other and each measures a distinct quality of the surface. Since these polynomials are directly attributable to

the surface quality, a direct measure of the change in the tear film surface can be analysed using aberrations.[32]

1.4 Dynamic measurements of aberrations:

Early research using dynamic aberrations found the aberrations of the eye to be dynamic and suggested that the reason for the dynamic change may be due to changes in the micro fluctuations in the accommodation of the eye.[34,35] Later, it was realized that the change in aberrations were related to the change in the tear film, and that during the tear breakup the aberrations were high compared to at other time.[31,36,37] This was supported by studies which measured change in contrast sensitivity and visual acuity with time.[38,39] It was also found that there is an unknown compensatory mechanism going on inside the eye to compensate for the changes in aberrations produced by the dynamic tear film.[40] Due to advances in refractive surgery and the importance of dry eye disease evaluation, greater interest was expressed in analyzing dynamic anterior surface aberrations. More recently, studies have used topography of the corneal surface to determine the stability of the tear film. These studies were done based on the change in the curvature or topography of the cornea[24,41,42] or by using the surface regularity and asymmetry indices[43] to observe a variation in the tear film over time.[44]

Montes-Mico et al[37] were able to measure the dynamic aberrations of the anterior surface aberrations from the time of blink to the start of next blink and showed a common pattern of change in corneal aberrations among the participants. They observed higher aberrations immediately after the blink, followed by a decrease in the aberrations with time. After a few seconds, the aberrations reached a low point and then started to increase again.[37,41] This

pattern appears to follow fairly well with the stages of tear film formation and rupture explained by Caniero et al.[10]

From the basics provided by Montes-Mico et al.,[41] this thesis analyse the temporal change in the tear film aberrations and refine the methodology of an objective method to explain the change in tear film quality/stability over time.

Chapter 2 : Methods

2.1 Topcon corneal analysers:

Topcon manufactures both corneal analyser devices used in this thesis. The devices used are the CA100 and CA200 corneal analysers (Figure 2-1). The CA200 is a modified and advanced version of the CA100 corneal analyser . In this section of the thesis, the device setup and general operating procedure of both the corneal analysers will be explained. The methods pertaining to each experiment are discussed in their respective chapters.

2.2 Similarities between CA100 and CA200 corneal analysers:

Both corneal analyser devices used in this thesis feature 24 equally spaced black and white concentric rings in the Placido disc. During the measurements, the white rings in the stimulus are internally illuminated by a 640nm light source for imaging purposes. The light from the stimulus is projected onto the surface of the cornea and the reflected light is captured using the inbuilt CCD camera located at the centre of the stimulus. The captured images or videos (depending on the type of the test) of the reflected light are analysed through a series of algorithms to calculate the elevation of anterior surface of the tear film/cornea. The data describing elevation of the surface obtained from each image frame are used to calculate the anterior corneal surface curvature and the anterior surface aberrations. The algorithm to acquire and analyse the dynamic anterior surface aberrations was developed by Hesp Technology S.r.l., Italy and is incorporated in both corneal analysers. Each corneal analyser device has its own version of software inbuilt.

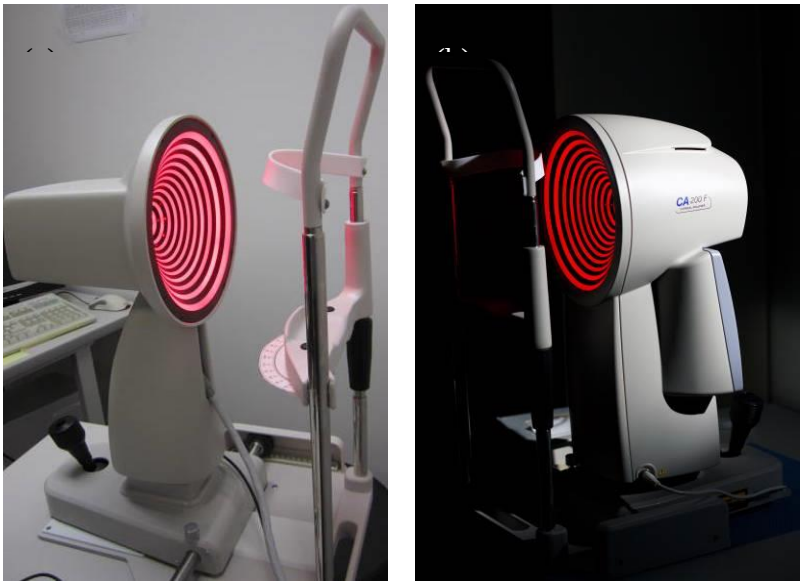

Figure 2-1: (a) Topcon CA100 corneal analyser device; (b) CA200 corneal analyser device.

2.3 Topcon CA100 corneal analyser:

2.3.1 Device setup:

The CA100 corneal analyser device was connected to the control unit and then to the computer which has the proprietary software installed. The attached computer was used, via a control unit to operate the device. All the data from the CA100 are analysed and stored in the computer connected to the instrument.

2.3.2 Operating instructions:

The frame rate, focus and video capture are controlled manually by the examiner. Before obtaining any measurement, the patient's data is entered into the database for a first time measurement or (if recalled) selected follow up measurements are taken. To measure dynamic corneal aberrations, the "BUT" algorithm is selected (Figure 2-2). A popup measurement

window is seen, along with the activation of the Placido disc stimulus of the CA100 . The measurement window consists of a live view window, focus assist, sampling time input area and the progress bar (Figure 2-3). The sampling time is set to the desired level before start of the video acquisition and can be set in 0.05s steps from 0.1 second to 32 seconds according to the study protocol. The video can be captured at a maximum frequency of 10fps using the CA100.

After setting the desired frame rate, the Placido disc reflected from the surface of the object are focused by the use of live view windows. At a tentative clearest mire position, the video capture is initiated by pressing the button in the joystick of the device. Immediately after the initiation the focus assist appears on the side of the live view window and is used to obtain optimal focus. For the right eye measurement, the focus assist appears in the left side of the live view window for the observer and vice versa for the left eye (Figure 2-3). The focus assist shows a blue down arrow, a red up arrow or a green colored double arrow according to the focus of the mires. The green arrow in the side of the measurement window was considered to represent optimal focus. The blue and red arrow indicates slightly defocused mires. The arrows disappear when the mires were completely out of focus or distorted. The progress bar at the bottom of the screen shows the length of the video captured. Usually, the videos can be obtained for a maximum period of 50sec using the CA100.

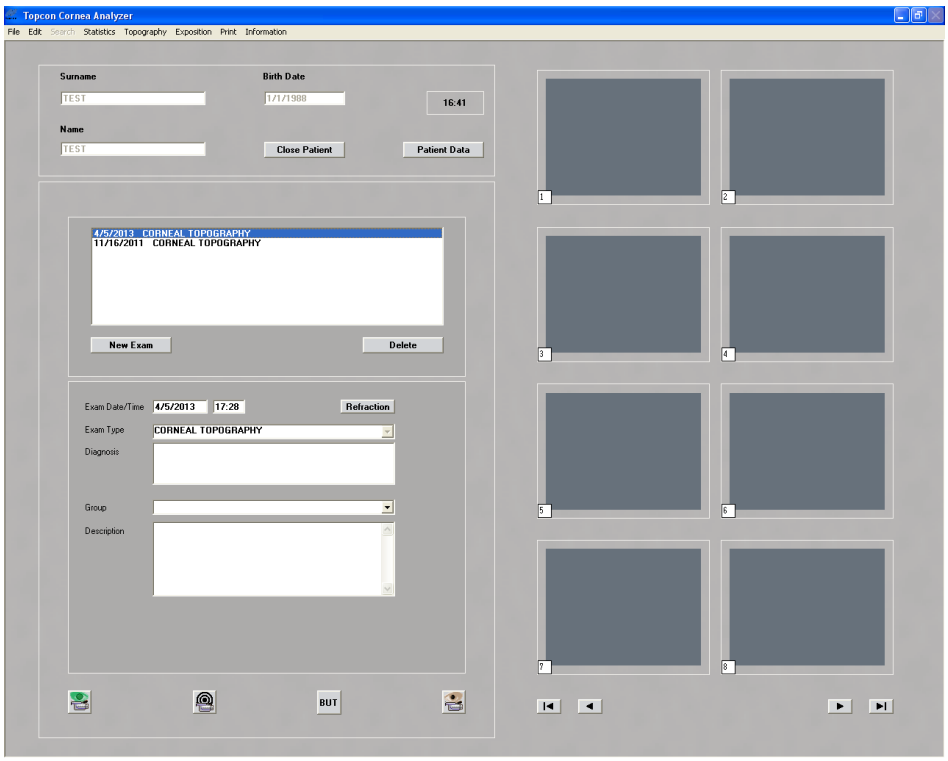

Figure 2-2: Patient data and test selection window of CA100 corneal analyzer device.

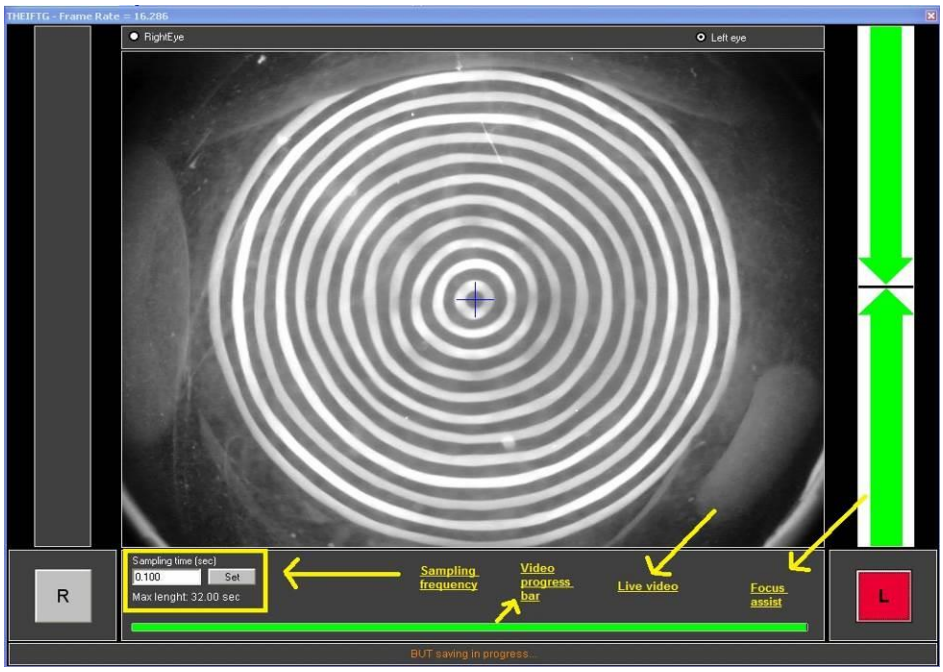

Figure 2-3: Live view window of CA100 corneal analyzer during the dynamic aberration measurement.

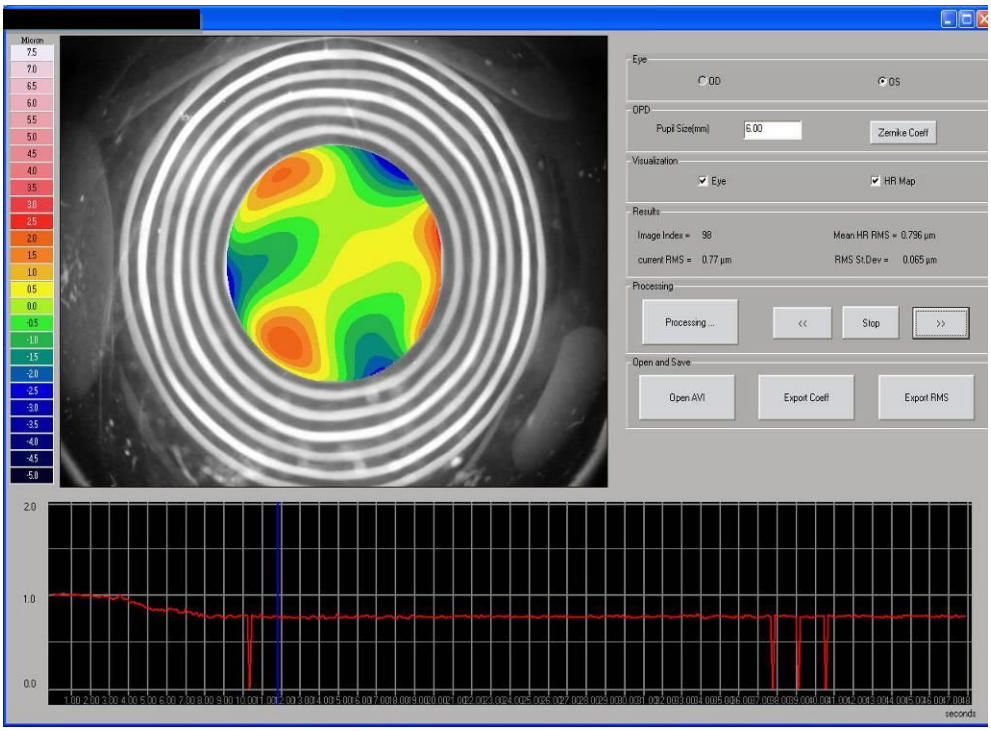

Figure 2-4: Video processing window of Topcon corneal analyzer software.

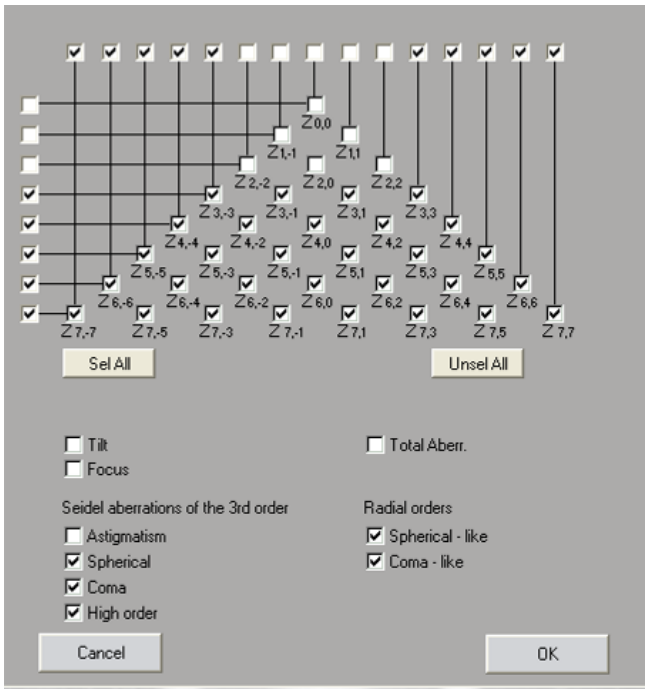

Figure 2-5: Zernike polynomial selection window for analysis of dynamic surface aberrations

After each measurement, a popup window is automatically generated to process the captured video (Figure 2-4). In this window, the desired pupil diameter and Zernike coefficients (Figure 2-5) for analysis can be selected according to the study protocol. The window below the image shows the graph of total RMS variation over time for each analysed time frame during image processing. A 6mm pupil diameter was used for all the studies in this thesis. After processing the video for dynamic aberration measures, the RMS, individual Zernike coefficients data upto the 7^{th} order and the video with or without aberration overlay can be exported.

2.3.3 Topcon CA200 corneal analyser:

2.3.3.1 Device setup:

Unlike the CA100 corneal analyser device, the CA200 connects to the computer through a wireless adaptor and all data transfers are performed wirelessly. The CA200 is provided with user interface software to add patient details and obtain the measurements. These features increase the portability of the instrument. After obtaining the measurements, the data obtained is either stored internally or transferred to a backup computer. The analysis of dynamic aberrations can be performed only in the desktop software, so all data pertaining to this thesis were transferred to the computer immediately after the video acquisition.

2.3.3.2 Operating instructions:

As with the CA100, patient data is either created new or imported from the database before starting the data acquisition (Figure 2-6). After creating the patient data, a new popup acquisition window opens with a live view window, progress bar below and measurement

selection bar in the side. To measure dynamic surface aberrations the 'BUT' algorithms should be selected. The mires reflected from the surface measured are focused to obtain sharp and clear mires with the help of the joystick. The video acquisition is initiated by pressing the button on top of joystick and, with the help of focus assist, the mires are focused to get an optimal focus (Figure 2-7).

The focus assist in the CA200 are blue and red arrows, located at four corners of the live view window. The optimal focus is the position where no arrows are present. The blue arrow indicates defocus away from the surface and red arrow indicates over focusing of the mires. Out of focus or decentered mires are indicated by the appearance of yellow center ring.

Each measurement can be obtained for a maximum period of 2 min and all the measurements are obtained at 25 fps time interval. Once the video acquisition is complete, the data from the device is transferred wirelessly to the remote computer for processing. The proprietary software installed in the computer imports the data directly from the device.

Using the software, the RMS and Zernike coefficients upto 7^{th} order are calculated for a given pupil diameter. The pupil diameter can be changed according to the protocol of the study. In this thesis, all the analysis for the CA200 was obtained for a 6mm pupil diameter. During the analysis, the window shows an aberration overlay of the surface analysed for each frame analysed and a trend graph of RMS values for each analysed frame in the window below the images (Figure 2-8). The trend graph also gives the location of the blinks using a yellow highlight bar.

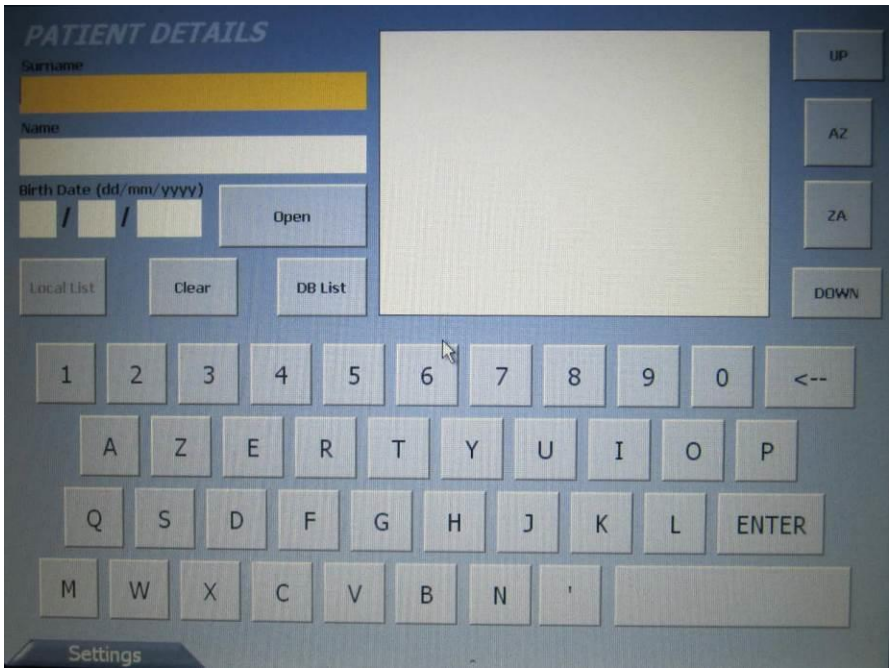

Figure 2-6: Patient selection window of CA200 corneal analyzer device.

Figure 2-7: Measurement window with live capture window.

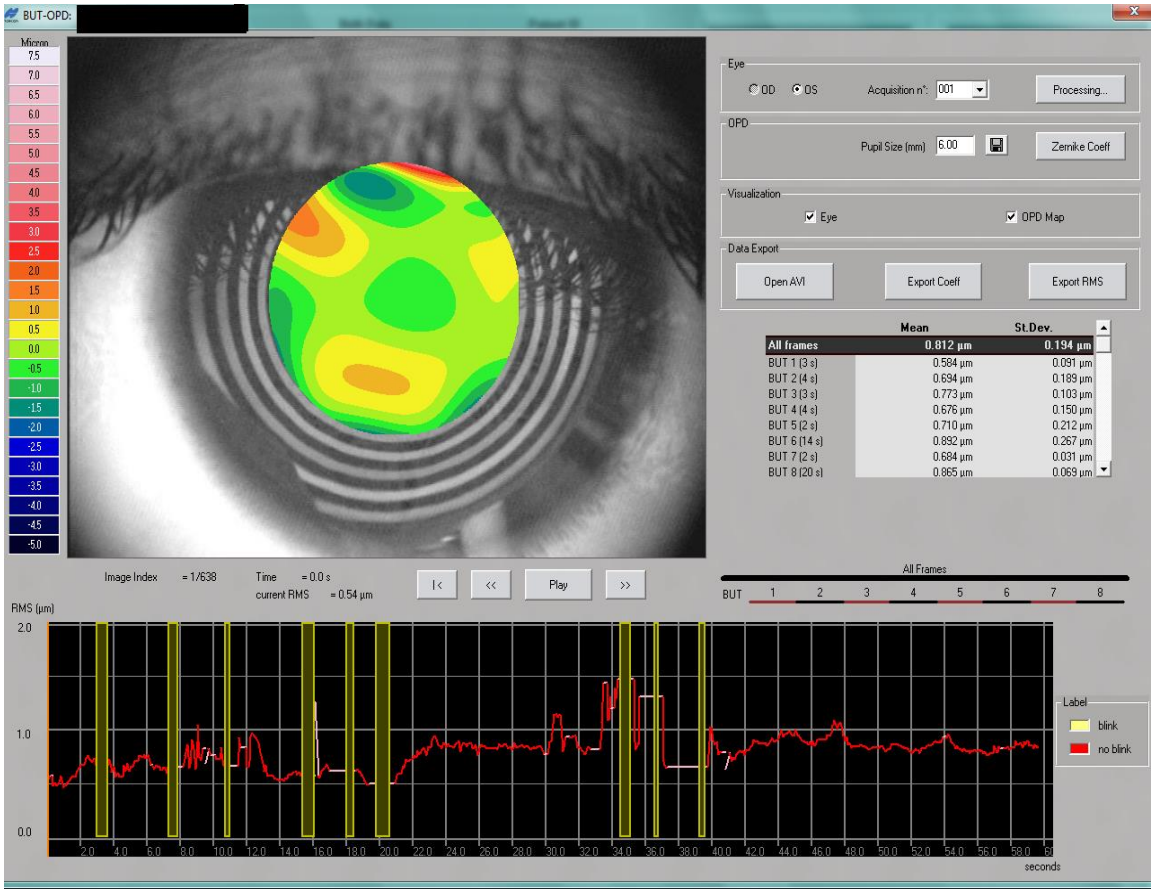

Figure 2-8: Dynamic aberration processing window of CA200 corneal analyzer device. Yellow highlight in the trend graph below indicates the location of the blink.

	CA100	CA200
Optimum frame rate	4 fps	25 fps
Source power	35 µm	6.8 µm
Focus assist	Red, green and blue arrows. Green is considered as optimal focus. Needs thresholding to find optimal focus	Only blue and red arrows. Yellow circle for out of focus and away from center of Placido disc
Blink detection	Detects and delete blinks from the output data	Location and duration of the blinks are shown in output data

Table 2-1: Differences between Topcon CA100 and CA200 corneal analysers.

Figure 2-9: Placido disc light source of (a) CA100 and (b) CA200 corneal analyzer devices.

2.4 Differences between the corneal analysers:

The major difference between the CA100 and CA200 corneal analyser devices are the frame rate, brightness of the light source and the blink data. The CA200 captures video at a higher frame of 25fps compared to 10 fps by the CA100. The larger number of data points obtained with the CA200 allows more precise the analysis of the dynamic aberrations. The detection of the location of the blinks by CA200 also helps in easy identification of "between blinks" data points. The CA100 also identifies the blink, but the location of the blink and data associated with it are permanently removed from the data obtained and no indications are given in the output from where the data has been removed. The source power of the Placido disc also varies between the instruments. The power output of the CA200 is much lower at 6.8 µW, when compared to the CA100 of 35µW. This difference in output power of the light source produces a noticeable difference in the brightness of the light of the Placido disc source (Figure 2-9). The table below highlights the overall difference between the two corneal analysers used in this thesis from the description given above. (Table 2-1)

Chapter 3 : Evaluating the Topcon CA100 Surface Aberrometer Measurement Using A Model Eye

3.1 Background:

The Topcon CA100 corneal analyser is a Placido-based corneal topographer featuring a built-in module to measure dynamic anterior surface aberrations. Measuring the dynamic surface aberrations might involve various external and internal factors other than just variation due to the surface of the eye. There are studies which analysed factors concerning tear film stability, but no studies were found that looked into the influence of external factors like instrument temperature and luminance of the light source on the dynamic anterior surface aberrations measurements. The noise or the variation due to instrument factors also plays a major role in these external factors. The effect of the noise or the defocus on the dynamic surface aberration has not been studied before. To identify the noise associated with the instrument, a non-dynamic reflective surface which can be used to measure surface aberrations was needed. It is equally important to get the appropriate acquisition setting to measure the dynamic aberrations of the eye. In this study, using a model eye, the aim was to gain insight into both these factors.

3.2 Objective:

The main objectives of the study were to determine the noise associated with the instrument using a non-dynamic measuring surface and to design appropriate acquisition settings for the

measurements of the ocular surface. In the acquisition settings, the aim was also to measure the effect of defocus on the measurements of surface aberrations.

3.3 Methods:

3.3.1 Instrument characteristics:

The CA100 setup and operating procedures were explained in general methods chapter (See chapter 2.3). The flowchart (Figure 3-2) explains the methods used to test the hypothesis. To test the validity of the measurements, a non-varying or a non-dynamic surface of a model eye was used. Initially, the optimal frame rate to be used for the measurements was analysed, and then effect of displacement in the optimal focus on dynamic aberrations was measure with different protocols as described below.

3.3.2 Frame rate and dropped frames:

The optimal frame rate to acquire video was tested by calculating the number of dropped frames in the processed data. Dropped frame are the frames which had zero RMS and Zernike coefficient values as a result of processing error due to frame rate (inter-frame interval) selected (Figure 2-4). Five samples of surface aberrations were obtained in three sampling times at each focus position (Figure 3-1). The three sampling times used to acquire data were 0.20, 0.25 and 0.30 seconds. The number of dropped frames in each sample was obtained and averaged across each time point and focus position.

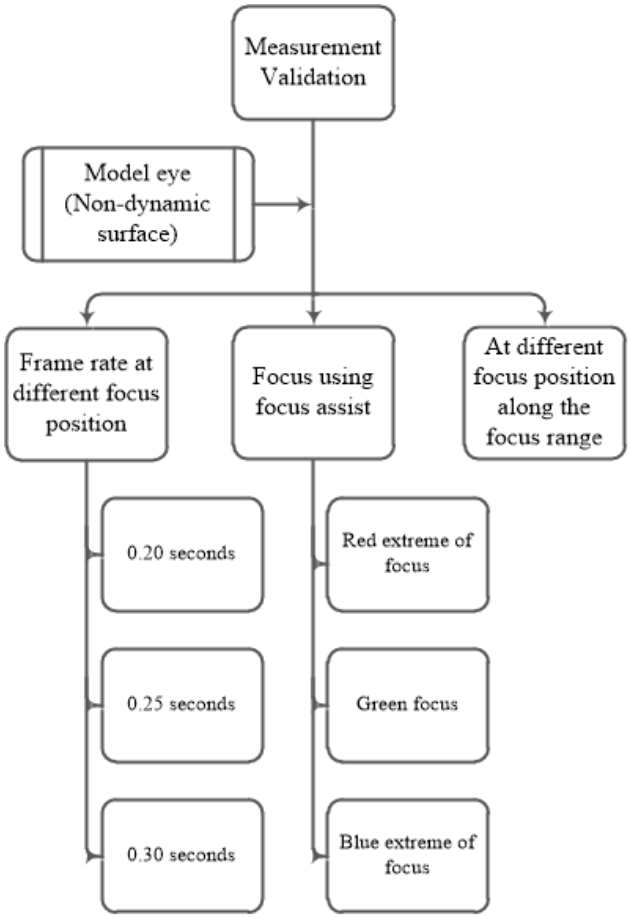

Figure 3-2: A flow chart showing the measurement categories

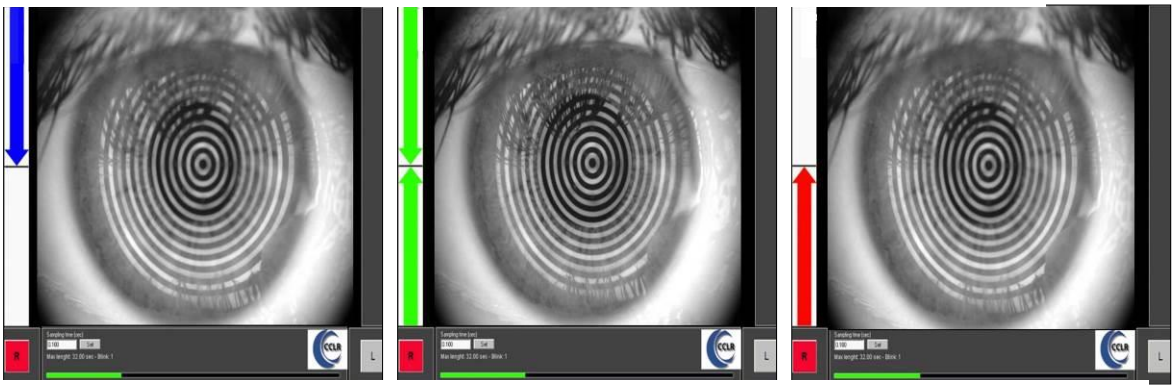

Figure 3-1: Live view acquisition window showing blue, green and red focus arrows.

3.3.3 Focus positions:

To evaluate the variability of the data, three separate samples were obtained in each of the green, red and blue focus positions. The protocol used to obtain each data acquisition was to begin a measurement to find the focus position and then lock the base of the instrument in position. The measurement acquistion was then stopped and restarted. In the case of the red and blue measurements, they were obtained at the outermost limit of defocus (Figure 3-1). This was achieved by moving the base away from the green defocus in the direction of the red or blue arrows until they disappeared, then moving back to the position where the red or blue arrows just appeared again. This protocol was followed so that a consistent position in the red or blue defocus region could be obtained. The abberrations were obtained in 0.25 sec sampling time intervals.

Figure 3-3: Setup for measuring distribution of RMS values in different degrees of defocus. Measurements were obtained when the pointer attached to the base were at 1 and 2 cm interval in both sides of green focus position using the scale attached next to the base.

To examine the effect on the distribution of the measurements of the degree of defocus from the optimal (green) position to the outer limits of defocus a small centrimetre scale was attached to the base of the device. Data acquisitions were obtained at 1and 2cms away, in both the red and blue defocus directions, from the optimal focus position (Figure 3-3). The measurements were obtained in 0.25 sec sampling time intervals.

3.3.4 Data analysis:

In this chapter, the summary data, kernel density plot for different focus positions (Appendix 3, R.code 2) and tests for quantile distribution (Appendix 3, R.code 3) were performed in R statistical programming software. The analysis of variance (ANOVA) and post-hoc tests to analysis the difference between the samples were performed using SPSS version 16.[45] The code for the R [46] are listed in the Appendix 3 under each analysis heading.

3.4 Results:

3.4.1 Obtaining the green focus:

To make the green focus arrows visible in the measurement screen, the threshold of clear focus must be crossed at least twice to make it visible. This was consistently observed during all the measurements which were obtained at green focus position. When the values of root mean square (RMS) of higher order aberrations were plotted against time (Figure 3-4), there were two peaks and troughs within the initial 15 secs of measurement, indicating the crossing of the threshold twice, followed by a steady state for all the subsequent measurements obtained using green focus position. So, the first 15 sec of the data were removed for further analysis.

3.4.2 Dropped frames:

The numbers of dropped frames were calculated for each frame rate at each focus position. Table 3-1 gives the average number of dropped frames for each category. On average, a 50 sec measurement acquisition period with 0.20 sec sampling rate gave 219 time points; a 0.25 sec sampling rate gave 164 time points and a 0.30 sec sampling rate gave 146 time points. When the dropped frames were analysed for each category, the 0.25 sec time interval was observed to be optimal due to a lower number of dropped frames and gave an average of 20 time points more than other frame rates. Maximizing the number of frames is beneficial due to the dynamic nature of the ocular surface. The higher the number of data points obtained, the more detailed the analysis of the dynamic aberrations was possible.

	Dropped frames					
	Green focus		Red focus		Blue focus	
Rate	Total #	Mean	Total #	Mean	Total #	Mean
0.20 s	19	3.8	15	3	5	1.25
0.25 s	9	1.8	8	1.6	6	1.25
0.30 s	6	1.2	14	2.8	6	1.2

Table 3-1: Average number of dropped frames in each focus position and for each sampling rate.

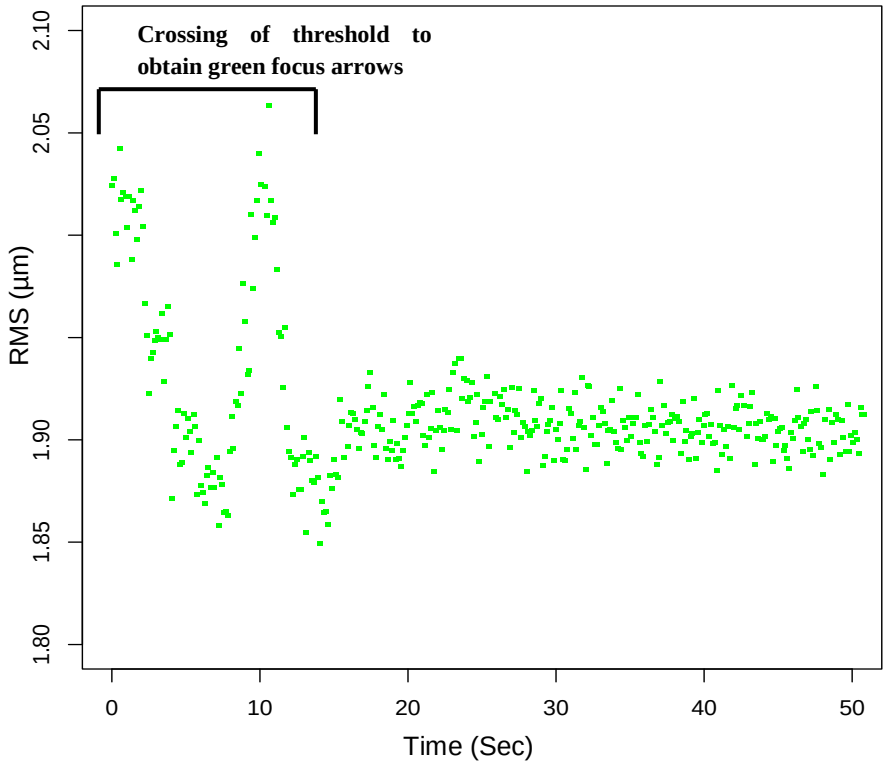

Figure 3-4: Raw RMS measurements plotted versus time for the optimal position of focus

3.4.3 Comparison of distribution with repeated measures within a focus position:

The quantile test for homogeneity of variations[47,48] was used to compare the distribution of three samples of the repeated measures within a focus position. This tests the variation of the outer 5%, 10% and 15% of the tails of the distribution between samples. For the analysis, the samples were centered on the median values of each acquisition, as shown in Figure 3-5. The kernel density plot shows the distribution of the samples along the RMS values in the x-axis and its density in the y-axis. The first 15sec of the values were removed on all the samples analysed. Univariate RM-ANOVA was used to examine the differences in the mean of the distribution of RMS measurements between the samples.

3.4.3.1 Green focus position:

There was a small but statistically significant difference in the centers (RM-ANOVA, $F_{(2,338)}$=6.217; p=0.002) and this difference arose between sample 1 and sample 2 (mean difference =0.009; Tukey p= 0.005), and sample 1 and sample 3 (mean difference =0.009; Tukey p<0.05). Sample 2 and sample 3 were not different (mean difference =0.0006; Tukey p>0.05).

Among all three samples, sample 2 and 3 showed no statistically significant difference (all p>0.05) for the 5%, 10% and 15% tails of the distributions. Sample 1 was different from sample 2 for the outer 10% (p=0.004) and 15% (p=0.022) of the distribution, and was different from sample 3 for the outer 5% (p=0.0002), 10% (p=0.015) and 15% (p=0.012) of the distribution.

3.4.3.2 Red focus position:

The mean of the RMS distributions was not significantly different between all samples (RM-ANOVA, $F_{(2,348)}$ =0.272; p=0.762). The mean difference in RMS between samples ranged between 0.003 and 0.008.

There were no significant differences in the homogeneity of variation for all three samples for the outer 5% of the distributions (p>0.05). The outer 10% and 15% were significantly different between samples 2 & 3 (p=0.039 (10%), p=0.047 (15%)). All other comparisons for the outer 10% and 15% were not significantly different (p>0.05).

3.4.3.3 Blue focus position:

The mean of the RMS distributions was significantly different between samples (RM-ANOVA, $F_{(2,327)} = 28.325$; $p=0.000$). Post-hoc testing revealed that this difference arose between samples 1 & 3 (mean difference=0.01; Tukey $p<0.05$) and samples 2 & 3 (mean difference=0.02; Tukey $p<0.05$). There was no significant difference in the centre of the RMS measurement distributions for samples 1 & 2.

There were significant differences in the homogeneity of variances for all three samples for the outer 15% of the distributions ($p<0.05$). The outer 5% and 10% were significantly different between all samples except samples 1 & 2.

3.4.4 Comparison of distributions with repeated measures between focus positions

Homogeneity of variation was also examined between focus positions for each of the repeated samples. A Bonferroni correction was made to account for multiple comparisons and a p-value of 0.002 was taken as significant. Figure 3-6 shows the box plot distributions of the RMS measurements for each sample at each focus position.

Green samples 2 & 3 were significantly different at the outer 5%, 10% and 15% of the distribution from all samples obtained for the extreme position of red defocus (all comparisons, $p<0.02$). Green sample 1, which showed longer tails of the distribution from Green2 and Green3, was not significantly different from all samples of red defocus.

The outer 5%, 10% and 15% of the distributions were significantly different between all samples obtained at the optimal (green) focus position and all samples of the extreme blue defocus (all comparisons, $p<0.002$).

3.4.5 Comparison of distributions for intermediate positions of defocus:

Data acquisitions were made at intermediate positions between the optimal and maximum defocus positions, in each of the red and blue defocus positions. Figure 3-7 shows the box plots of the RMS measurement distributions for each of these data acquisitions. As expected, the value of the mean RMS value is different between focus positions. It can be seen that the distributions are similar between the green and red focus positions, and that the distribution for the blue focus positions was larger.

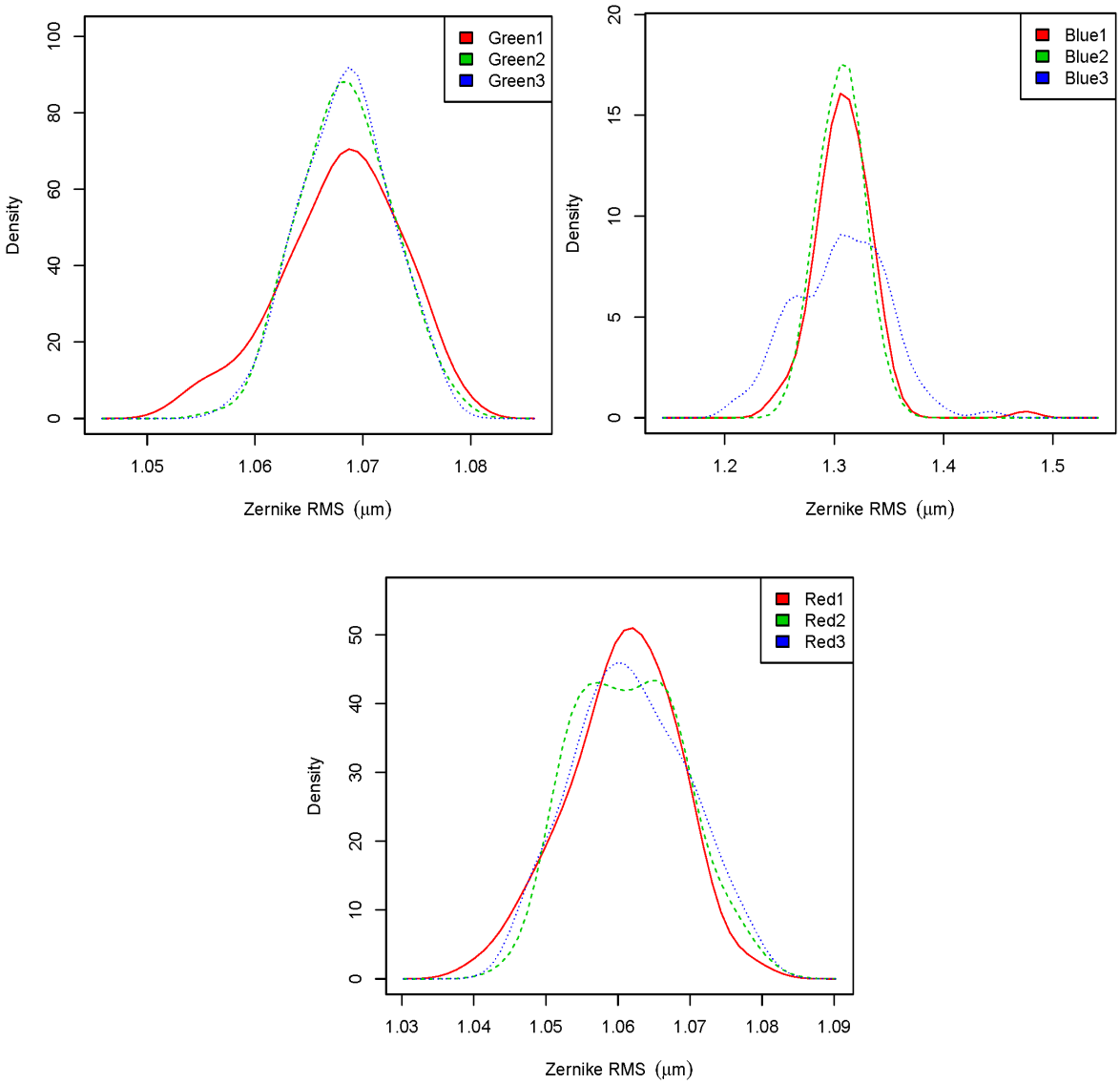

Figure 3-5: The kernel density plot for comparing the repeated measures samples at 3 focus position; Green(optimal), extreme blue and extreme red focus positions..

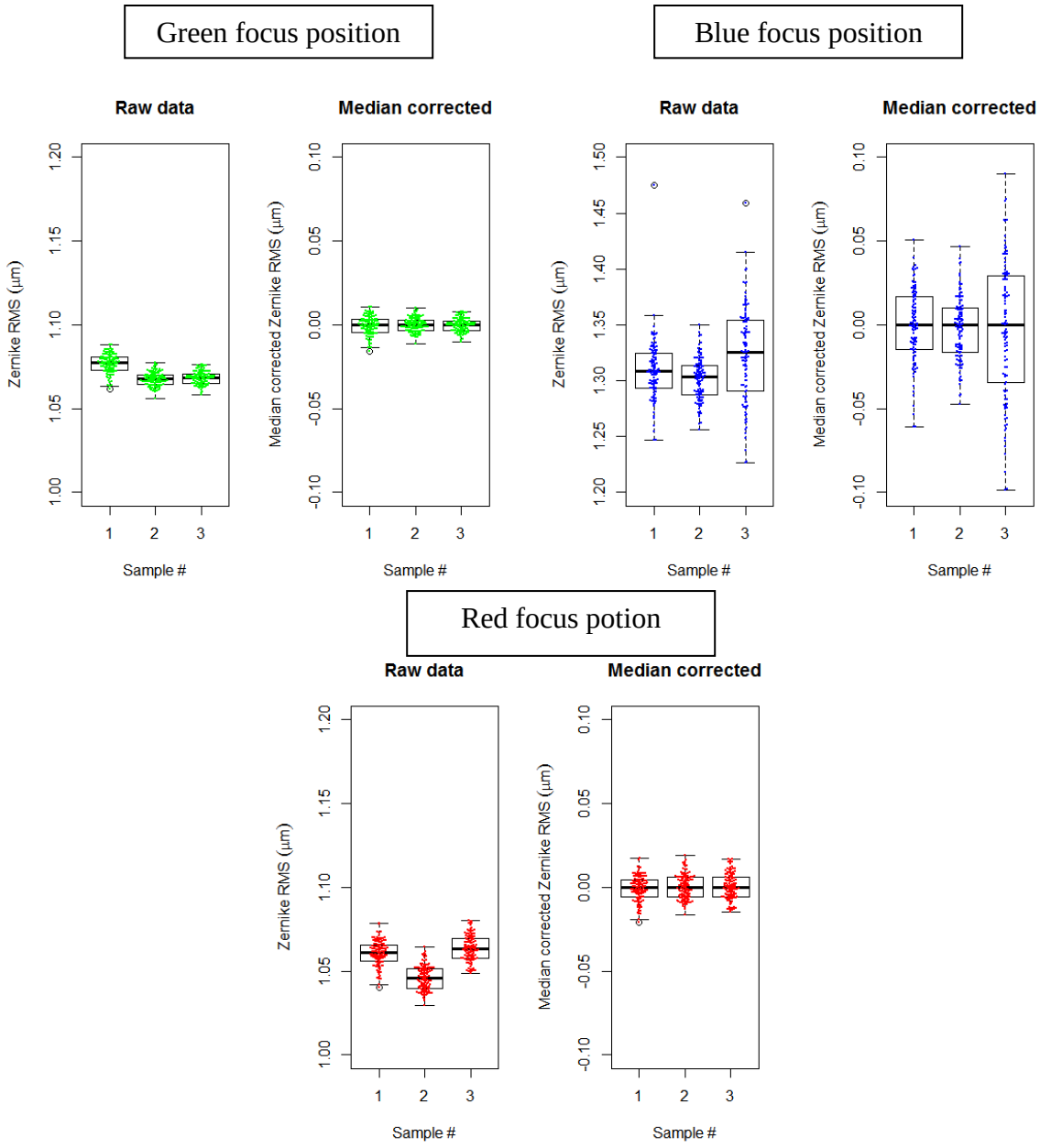

Figure 3-6: Comparison of distribution of the RMS values and median corrected RMS values for green, blue end and red end focus positions. The center bold line represents the median of the distribution, outer boxes are the 25th and 75th quantiles and the whiskers are ± 2 standard deviation.

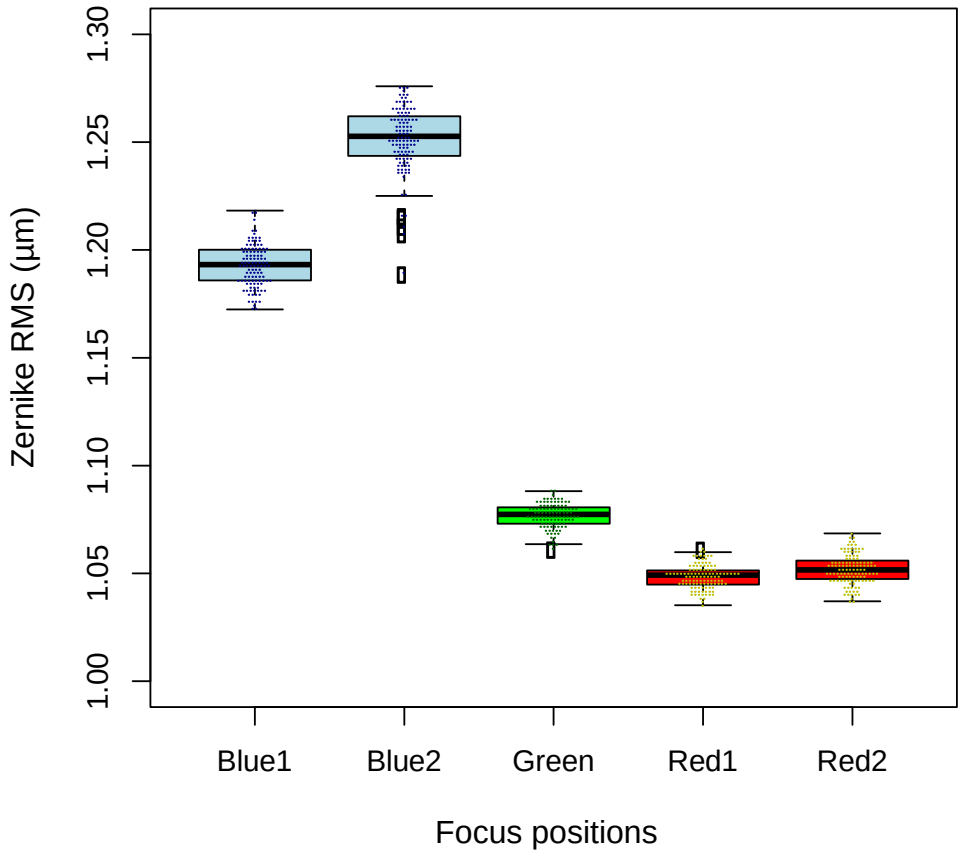

Figure 3-7:Distribution of RMS measurements at 1cm and 2cm from the optimal focus position in the blue defocus direction (Blue1 & Blue2, respectively) and in the red defocus direction (Red1 & Red2, respectively) See Figure 3-3 for description on focus positions.

3.5 Discussion:

The blue focus position shows greater measurement variability than either the green or red focus positions for a static surface target. In addition, the blue focus position showed significant differences in the centre of the RMS distributions across samples and, although there were significant differences found between the centres of the RMS distributions of the green sample, the magnitude of the difference between the blue samples was much larger. Thus, this study concludes that the green focus position and red focus positions show more consistent sample distributions on repeated measurement than the blue focus position.

For all samples, the red samples positions did not show homogeneity of variation in the outer 5%, 10% and 15% of the distribution, whereas green and blue samples showed a significant difference in the tails of the distribution. The comparisons between focus positions, the green, red and blue focus positions showed narrower but consistent variability between the red and green focus positions. The samples that had not been consistent within the green focus position, showed similar variability as red focus position samples. The comparison between blue and other focus positions showed a higher variability in the distribution of the tails of the measurements. This study concludes that the variability is more similar between the red and green samples than between the green and blue samples or red and blue samples.

As for the extreme, defocus positions, the distribution of the RMS measurements are similar between the green and red focus positions and vary by a greater amount in the blue focus position and that this variability increases as defocus away from the optimal focus position increases.

The change in the focus position during dynamic anterior surface aberration measurements can be expected due to dynamic tear film surface. As there are dynamic changes in the thickness of the tear film in an open eye interval, it is difficult to maintain optimal focus during the measurement. The movement of the joystick during the acquisition to maintain optimal focus might introduce a motion artefact in the obtained measurements (as observed in Figure 3-4). Therefore, it is important to maintain a steady instrument focus during the measurement.

The changes in the tear film, especially during the tear thinning phase, shifts the focus position towards the red focus position. It was observed in this study that the measurements obtained in the red focus position are less variable and similar to the green (or optimal focus) position compared to the variability of measurements in the blue focus position. These results suggest that it is optimal to keep the focus position either in the red or – ideally - green focus positions during the measurements without moving the joystick.

3.6 Conclusion:

Moving forward to the human subjects measurements the following measurement protocols were implemented, based on the findings of the measurement of a static target.

i. Data acquisition at an inter-frame interval of 0.25s is the preferred frame rate for data acquisition, to give the least number of dropped frames across focus positions.

ii. Data obtained in the initial ~15s reflects the focusing procedure and needs to be manually removed prior to analysis of tear dynamics.

iii. Even in the optimal focus position there were significant (small) differences in the distributions between repeated measures. For this reason, repeated samples should be obtained where possible.

iv. The green and red focus positions showed the most consistency within repeated measurements. The variability of the measurements was also more similar between the red and green focus positions than the blue focus positions, both at the extreme positions of defocus and with incremental defocus away from the optimal focus position. When obtaining the dynamic sampling of human ocular surface measurements, the optimal position of focus should be obtained at the blink such that as the tear film dissipates between blinks the measurements are being obtained in the (relatively) red focus position.

Chapter 4 : Spectral and Thermal Characteristics of an Illuminated Placido Disc during Dynamic Measurement of Anterior Surface Aberrations

4.1 Background:

Ocular surface temperature has been investigated as a factor contributing to our understanding of tear film stability and dry eye. Studies have examined the relationship between ocular surface temperature and tear film evaporation[49] and blood flow[49,50]. It was also shown in studies that the tear film stability depends on various environmental factors, including humidity, room temperature and pollution.[3,51]

Paschides et al.[3] observed that a change in room temperature or humidity level can cause changes to the lipid layer of the tears and induce a higher evaporation rate. It was also observed in most of the studies that participants with dry eye had a steeper decrease in the ocular surface temperature with time.[52] Along with ocular surface temperature, ocular aberrations[53,54] and surface aberrations[42] were also found to change with changes in tear stability over time. However, the exact mechanism explaining the influence of external factors (like temperature variations and humidity) on the stability of the tear film was not well established.

Placido discs are used in collecting temporal variation of corneal surface aberrations of the eye. Due to the close working distance of these topographers, a local variation was expected

in the humidity and the temperature between participants and the eye, causing variations in ocular surface aberrations and tear film stability. No previous studies have analysed the instrument target as a factor related to the variation of ocular surface aberrations and tear film stability. In this study, the ocular surface temperature in the presence of two illuminated Placido discs in front of the eyes at normal working distance was measured.

4.2 Study Objectives:

The objectives of this study were:

1. To determine the spectral characteristics of the Placido disc light sources of two corneal analysers.

2. To determine the thermal characteristic for a variety of inanimate objects, human ocular surface and the adnexa in the presence of Placido disc light source at normal working distance.

3. To compare the ocular surface aberrations obtained using both the corneal analysers.

4.3 Methods:

The two corneal analysers used in this study were the Topcon CA100 and CA200. Both use the Placido disc principle for the measurement of anterior surface aberrations, but the power output of the stimulus is markedly different from each other. This difference in power introduces a difference in object brightness and a potential change in the spectral distribution and thermal radiation of the source. The properties of the stimulus are examined and the

methods to obtain the spectral and thermal characteristics of the stimulus are explained in this section.

4.3.1 Stimulus characteristics:

The CA100 and CA200 setups are explained in the general methods chapter (Chapter 2). The main difference between the corneal analysers while acquiring corneal surface aberration measurements is the power output of the Placido discs. The output of the CA100 is 35µW compared with 6.8µW of CA200. This difference in the power output produces a noticeable difference in the brightness of the stimulus (Table 2-1).

4.3.2 Measurement of spectral and thermal characteristics:

Spectral and thermal measures were obtained in this study using the PR650 SpectraScan photometer (Figure 4-1) and a Tasco THI-500 non-contact infrared thermometer (Figure 4-6). Spectral measures were obtained from the surface of the illuminated Placido disc of the corneal analysers and the thermal measures were obtained from air (room temperature), a piece of tissue paper and a model eye, as well as from the anterior surface of the eye and adnexa of ten human participants. In all cases the measurement procedures for the thermal characteristics was the same.

4.3.2.1 Spectral Characteristics of the Placido discs:

4.3.2.1.1 Properties of the photometer:

The properties of the photometer includes a detection range of 380-780nm, with an accuracy of ±2 nm. The wavelength resolution of the photometer is <3.5nm/pixel. The accuracy of the luminance data obtained using the photometer is ± 2% of the calculated luminance, at 2856K

@ 23ºC. When the photometer was set to focus at infinity, it provided a measuring angle of 1 degree, with a viewing angle of 7 degrees. The measurement area in the photometer is seen as a dark black opaque circle in the center of the viewing area. The auto-sync function of the photometer helps in adjusting the exposure time of the sensor according to the refresh rate of the target. This helps in obtaining an accurate measure of the spectral characteristic and provides a refresh rate of the target measured. All the spectral measures were obtained with the photometer mounted on a camera tripod for stability.[55]

Figure 4-1: PR-650 SpectraScan photometer used to measure spectral characteristics of the Placido disc

4.3.2.1.2 Spectral measures:

This phase of the study did not involve any human participants. As provided in the manual for each instrument, the Placido disc of the CA100 and CA200 were illuminated by different powered light sources for measuring dynamic anterior surface aberrations. The spectral distribution of each target was obtained using the photometer.

The measurement obtained included (Figure 4-3):

1) Spectral characteristics of each individual ring in the Placido disc (each ring from left end of the Placido disc to right end, along the central horizontal axis);
2) Spectral distribution of each quadrant (entire target divided into 4 quadrants) of the Placido disc (upper, lower, right and left side);
3) Spectral distribution of the whole Placido disc;
4) Spectral distribution of the entire ring of the Placido disc (i.e., measures of the outer ring, including the rings within it).

For each type of measurement indicated above, the distance between the stimulus and the photometer was increased or decreased to accommodate the area measured into the measurement area of the photometer (Figure 4-2). For example, to measure individual rings, the distance between the photometer and stimulus was 50cms, whereas to measure the whole Placido disc the separation was around 7m.

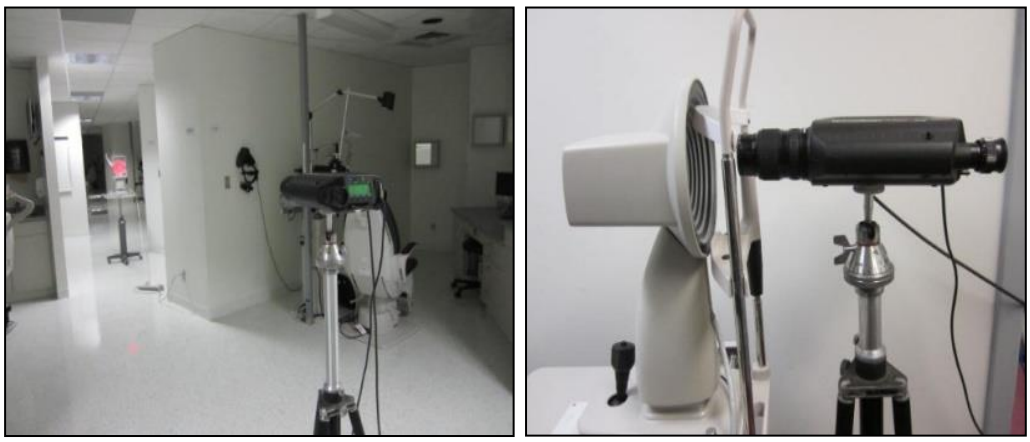

Figure 4-2: Photometer setup during spectral measurements

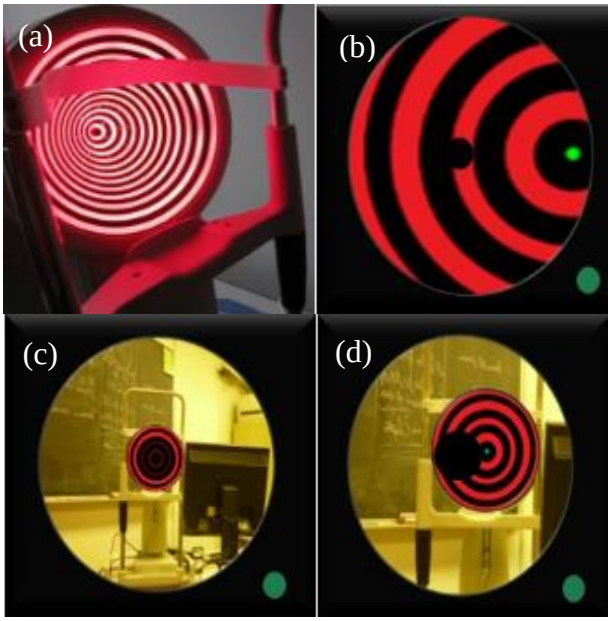

Figure 4-3: Illustration explaining the setup of Placido disc during each type of spectral

(a) Normal appearance of the illuminated Placido disc of a corneal analyzer;

(b) Spectral measures of an individual Placido disc obtained by the photometer. The central black circle indicates the measuring area of the photometer;

(c) View using eyepiece of the photometer while measuring spectral characteristic of the Placido disc;

(d) Eyepiece view of photometer showing the setup for a quadrant measure.

4.3.2.2 Thermal Characteristics of the Placido disc:

4.3.2.2.1 Properties of thermometer:

The Tasco THI-500 infrared non-contact thermometer was used to obtain corneal, conjunctival and eyelid temperatures during the measurements of surface aberrations. It was evaluated by other investigators for its reliability and repeatability while measuring corneal and conjunctival temperatures.[50,56] The thermometer can evaluate temperatures between 0°C and 300°C, with a resolution of 0.1°C within a measured wavelength of 8-16µm. It features a red visible point source to obtain the temperature measurements exactly from the area of interest.

4.3.2.2.2 Measures from three different surfaces:

Initially, the thermal measures were obtained from air, tissue paper and a model eye before measuring the surface of the eye. These measures were obtained from three different surfaces to determine if there was a dependency of the change in temperature on the nature of the surface tested. The model eye (Figure 4-6) is a uniform clear surface of fixed curvature made from a plastic material. The model eye was positioned in front of the stimulus and the thermometer was introduced from the side for measuring the temperature from the surface of the model eye. Similarly, a piece of tissue paper was attached to the head rest and the chin rest of the instrument in front of the stimulus and thermal measures were obtained. For each surface, two temporal measures of surface temperatures were obtained using each corneal analyser. Each measure was obtained for a three minute time interval.

4.3.2.2.3 Measures from the surface of the eye:

Ten participants were involved in this study. The thermal measures were obtained using the same infrared thermometer, but the measurements were obtained from the center of the eyelid, temporal bulbar conjunctiva and temporal cornea when illuminated by the stimulus Placido disc.

The order of the measurements (CA100 then CA200 or vice versa) was randomized between participants to minimize any bias in the temperature measurements due to differences in the stimuli. Both corneal analysers were used in a random order to compare the effect of the thermal radiations on the anterior surface of the eye. The measures were obtained only in the right eye of each participant.

The participants were seated in front of the instrument with their chin placed in the chin rest. The infrared thermometer was introduced from the side and was set to measure when the guiding light from the thermometer formed a point target over the region of interest (Figure 4-6). Measurements were obtained for a total of 3 minutes. All the measures from the thermometer were recorded using a digital camera. The measures were extracted manually from the recorded videos. In the open eye condition (conjunctival & corneal measures), participants were asked to blink normally. At the end of the thermal measures, a measure of dynamic ocular surface aberrations was measured for a period of approximately 50 seconds.

4.3.3 Study measures:

In this study, the photometric data and surface temperature measurements were obtained. The photometric data obtained are the spectral luminance, radiance along the light spectrum and

the peak wavelength. The measure of spectral luminance provides the amount of light emitted by the Placido disc towards the eye, and the peak wavelength of the light determines the color of the light emitted by the light source. The luminance of the light measured is given in candelas/square meter ($cd.m^{-2}$) and wavelength in nanometers (nm). The radiance is the measure of amount of light emerging from a source per unit area per unit solid angle. The radiance is given in Watts per steradian per square meter ($W.sr^{-1}.m^{-2}$). The surface temperatures were measured in degree Celsius (^oC).

Figure 4-6: Tasco Thi-500 non- contact infrared thermometer used to measure surface temperatures

Figure 4-6: Model eye

Figure 4-6: Setup for thermal measurements.

4.4 Results:

4.4.1 Spectral measures:

The luminance of the whole Placido disc of both corneal analysers was found to be significantly different (t-test, df= 10, $p<0.001$), with an average luminance of 31.95 ±0.1cd.m^{-2} and 5.79 ±0.01cd.m^{-2} for the CA100 and CA200 respectively (Figure 4-7). The integration time (using the auto-sync function in the photometer), which is related to the refresh rate of the light source, differed between the corneal analysers. The average integration time for the Placido disc was 427ms and 2563ms in the CA100 and CA200 corneal analysers respectively. The larger integration time for measuring the Placido disc indicates that the light source of the Placido disc was smoother and more regular in the CA200 than the CA100 light source. The peak wavelength of both the Placido discs was in the red spectrum of the visible light spectrum at 645nm throughout the measurement period.

Along with the peak wavelength, the radiance of the light source across the wavelengths of the visible light spectrum was also obtained. The log radiance of each trial was plotted across the wavelength of the visible spectrum and a cumulative mean was obtained (Figure 4-8). The ggplot2 package in R statistics was used to plot the radiance across different time points. The solid line in the plot represents the global mean of the data set across different wavelengths of the visible spectrum. The grey shaded region around the solid line represents the confidence interval of the data set.

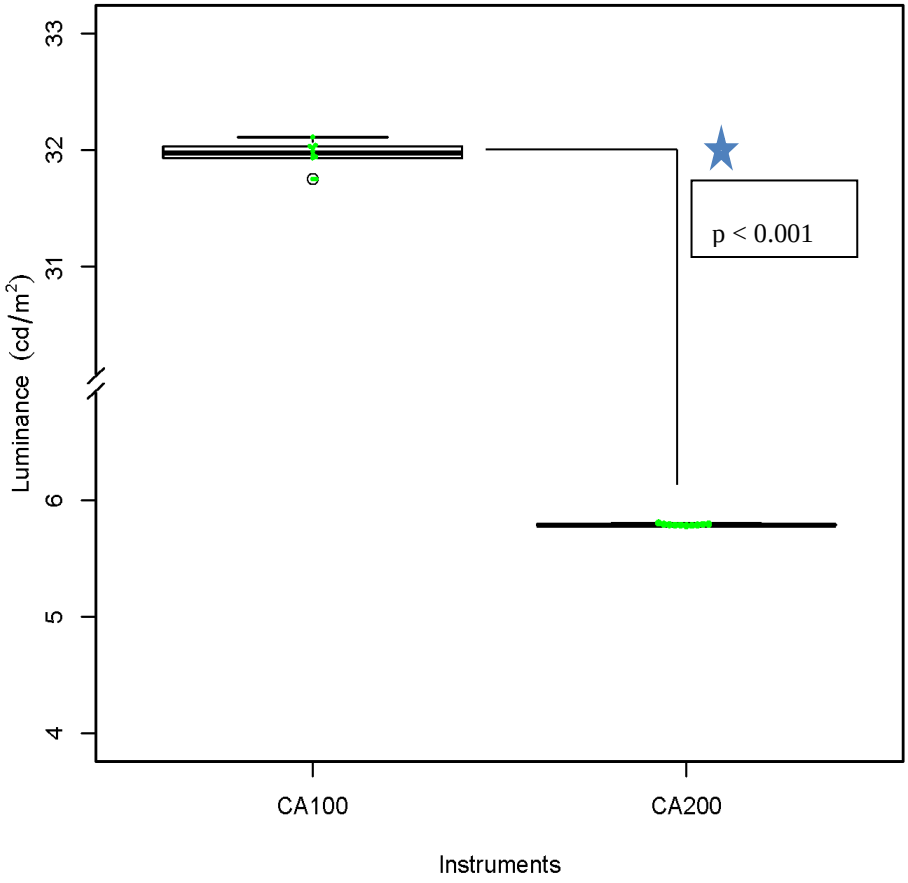

Figure 4-7: Comparison between the luminance of CA100 and CA200 Placido discs.

Distribution of the data points are shown as green points in the centre of box plot using beeswarm package in R. In addition, due to larger difference in the values, the Y-axis has a customized axis break (using Plotrix package of R) to show both box plot in a single plot. (Appendix 3, R.code 4)

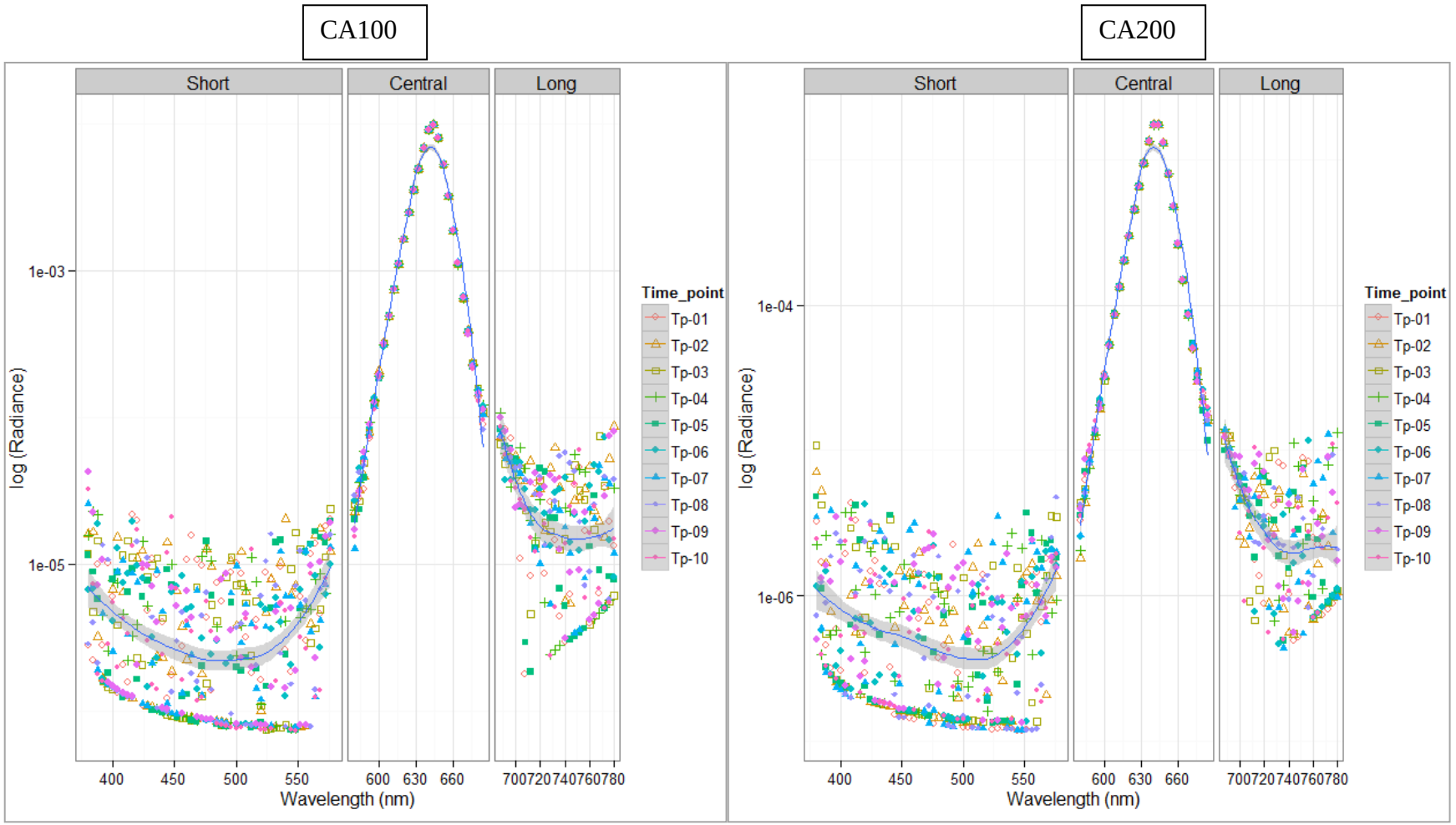

Figure 4-8: Geom plot (using ggplot2 package in R) with radiance in y-axis and wavelength in x-axis for measures from CA100 and CA200 Full Placido disc measures. (Appendix 3, R.code 5)

4.4.1.1 Individual rings:

Similar to the full Placido disc measure, the spectral characteristics of the individual rings in the Placido discs were measured. This was done to measure the individual contribution of each ring to the overall spectral characteristics of the Placido disc. The photometer was located 50cm from the disc during the measurements. The black concentric rings showed no spectral data on all the trials obtained. The spectral measures of the individual rings were analysed.

As mentioned in the methods (chapter 4.3.2.1.2), the spectral measures were obtained on each illuminated ring of the Placido disc from left to right along the central horizontal axis of the disc. The overall average luminance of the right and left side of the CA100 were 92.7cd.m^{-2} and 67.24 cd.m^{-2} respectively. Similarly, in the CA200 the averages were 20.46cd.m^{-2} and 15.79cd.m^{-2} in the right and left side of the Placido disc (Figure 4-9). The difference between the average luminance of right and left side of each instrument was significantly different (t-test, df=11, p=0.038) with difference of 25.27cd.m^{-2} and 4.67cd.m^{-2} in CA100 and CA200 respectively. The peak wavelength was obtained and it was averaged across all the rings. The average luminance values for each individual rings are listed in table below. The average peak wavelength was 644nm and 642.13 ±1.98nm in the CA100 and CA200 corneal analysers respectively (Figure 4-11).

	Luminance of CA100 ($cd.m^{-2}$)		Luminance of CA200 ($cd.m^{-2}$)	
Individual rings (from center)	Towards left side	Towards right side	Towards left side	Towards right side
1st ring	60.8 ± 0.16	111.45 ± 0.5	12.17 ± 0.022	28.6 ± 0.24
2nd ring	66.67 ± 0.21	33.71 ± 0.23	16.94 ± 0.041	44.1 ± 0.13
3rd ring	42.63 ± 0.11	94.24 ± 0.78	11.32 ± 0.027	24.4 ± 0.083
4th ring	38.49 ± 0.1	69.9 ± 0.6	9.74 ± 0.027	18.21 ± 0.065
5th ring	50.89 ± 0.13	75.88 ± 0.44	12.92 ± 0.036	21.63 ± 0.092
6th ring	60.06 ± 0.22	87.73 ± 0.64	15.49 ± 0.06	23.48 ± 0.053
7th ring	59.22 ± 0.14	84.99 ± 0.52	14.17 ± 0.035	18.33 ± 0.055
8th ring	64.90 ± 0.53	84.42 ± 0.52	12.96 ± 0.03	16.85 ± 0.055
9th ring	88.12 ± 0.25	115.4 ± 1.21	17.85 ± 0.04	19.85 ± 0.06
10th ring	78.38 ± 0.26	89.5 ± 1.21	16.8 ± 0.09	13.30 ± 0.04
11th ring	98.53 ± 0.72	155.34 ± 1.17	28.36 ± 0.07	8.68 ± 0.015
12th ring	97.01 ± 0.3	106.5 ± 0.62	20.72 ± 0.031	8.03 ± 0.02

Table 4-1: Average luminance values for each individual ring and side in CA100 and CA200 corneal analysers

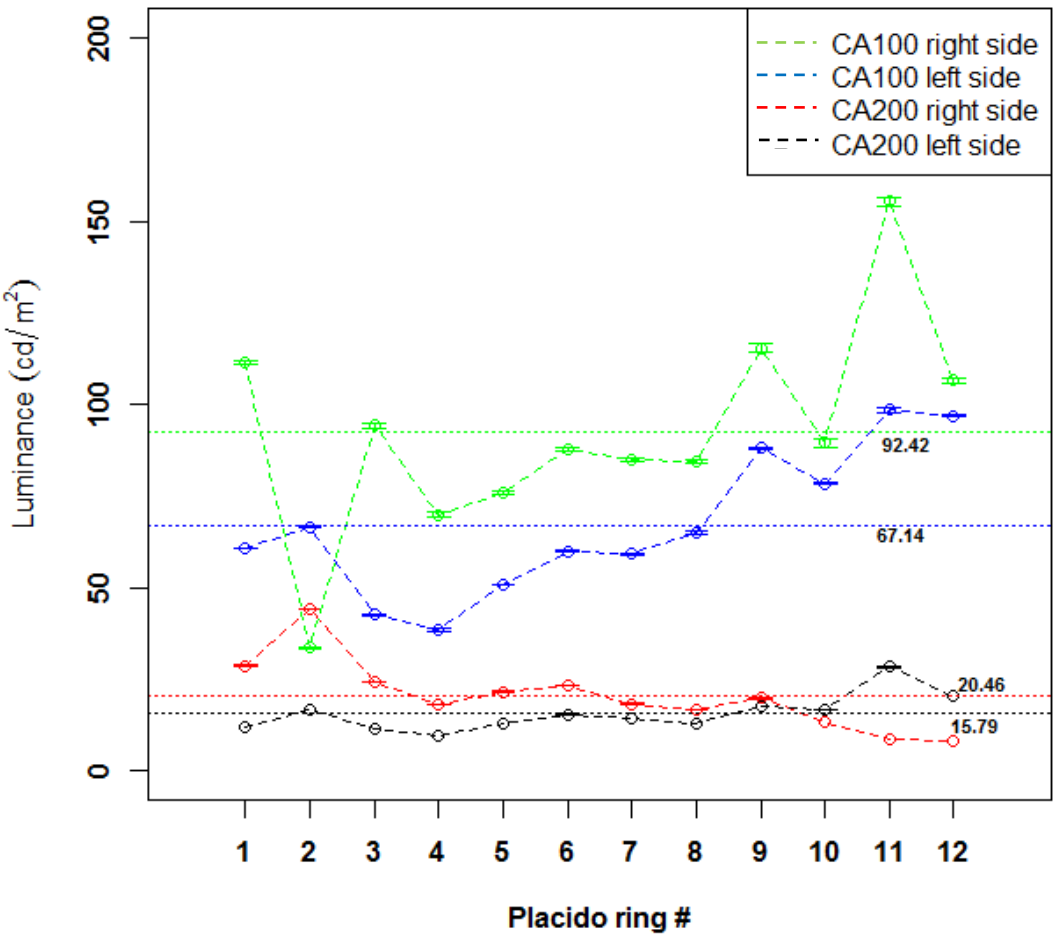

Figure 4-9: Scatter plot with error bars (using plotrix package in R) for luminance of each ring of Placido disc across the ends of horizontal axis in CA100 and CA200 corneal analyzers. (Appendix 3, R.code 6)

4.4.1.2 Quadrant measures:

The quadrant measures were obtained to confirm the discrepancy in the luminance difference obtained in spectral measures of individual rings between sides. The Placido disc was divided into four quadrants and spectral measures were obtained for both corneal analysers. The measurements involve the cumulative luminance of both black and illuminated rings. As observed in the individual rings, the difference in the luminance of the right and left sides of the CA100 is higher compared to the luminance of the CA200. The luminance obtained in the CA200 was more repeatable, with a standard deviation of 0.88cd.m^{-2} compared to the standard deviation of 2.53cd.m^{-2} in the CA100 across all quadrants (Table 4-2). The average luminance of all quadrants was 44.17cd.m^{-2} and 9.99cd.m^{-2} in the CA100 and CA200 respectively. The box plot in Figure 4-10 also shows the distribution of the luminance between quadrants.

4.4.1.3 Disc measures:

The disc measure was obtained by changing the distance between the photometer and the Placido disc. The centre of the measuring area of the photometer was overlapped with the center of the Placido disc and measurements were obtained with each illuminated ring in the Placido disc as the edge of the measuring area. The cumulative luminance of the Placido disc was found to change with the inclusion of each illuminated and black concentric ring from the first ring. The change in the luminance was negative in the CA200 with the inclusion of each ring, whereas in the CA100 there was a decrease in luminance up to the 5th illuminated ring, after which there was an increase in luminance and then a sharp decrease in the luminance of the whole Placido disc (to the 12th ring; Figure 4-12).

The wavelength for each concentric ring of the Placido disc was the same and consistent across rings between the CA100 and the CA200, as shown in Figure 4-11. The peak wavelength of both the corneal analysers was 644nm across all the illuminated rings.

	Luminance in CA100 ($cd.m^{-2}$)	Luminance in CA200 ($cd.m^{-2}$)
Whole Placido disc	31.94 ± 0.1	5.79 ± 0.01
Quadrants		
Right	48.15 ± 0.083	8.56 ± 0.025
Left	41.24 ± 0.086	10.91 ± 0.03
Inferior	43.65 ± 0.11	10.45 ± 0.03
Superior	43.67 ± 0.11	10.05 ± 0.017

Table 4-2:List of average luminance values of the Placido disc in different quadrants and the whole Placido disc for the CA100 and CA200 corneal analyzers during measurement of dynamic anterior surface aberrations.

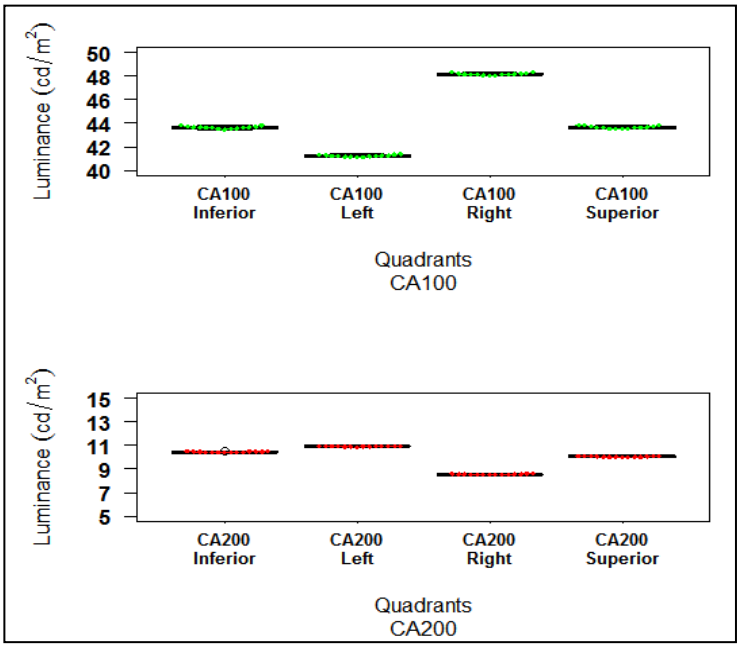

Figure 4-10: Comparison of luminance measures from each quadrant of CA100 and CA200 Placido discs. (Appendix 3, R.code 4)

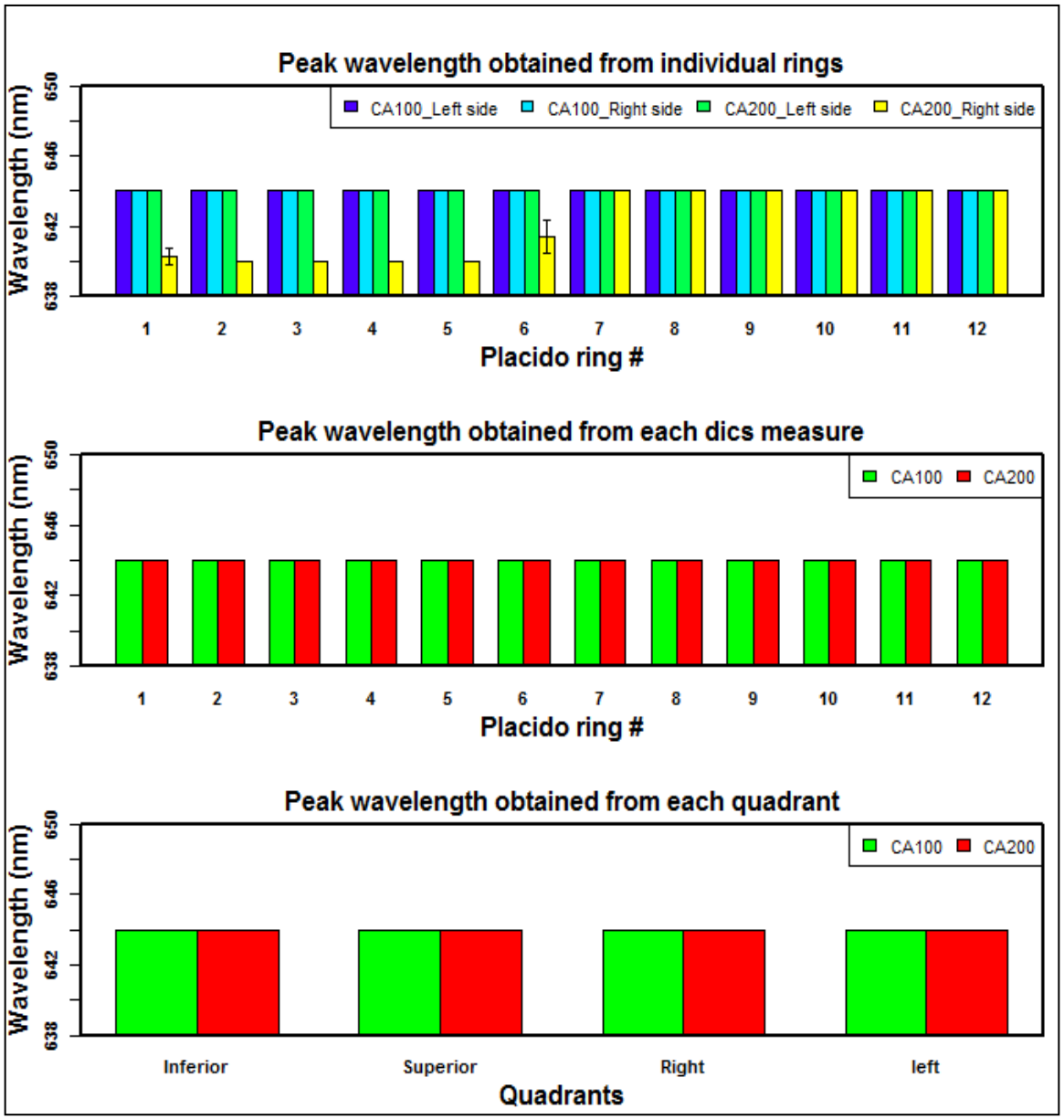

Figure 4-11: Peak wavelength of the light source across each type of measurement. (Appendix 3, R.code 8)

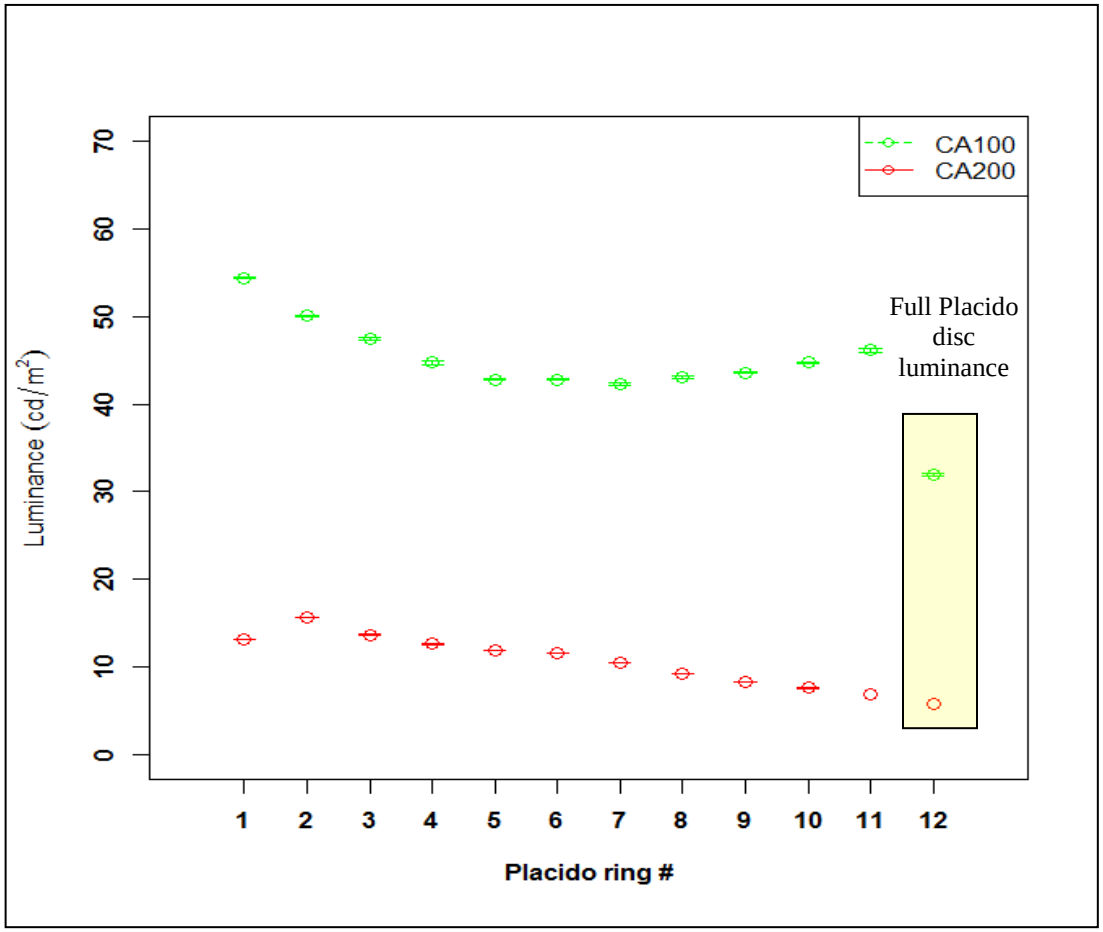

Figure 4-12: Luminance of the light sources across each disc measure of Placido disc. (Appendix 3, R.code 6)

4.4.2 Thermal measures:

The thermal measures were obtained on the surface of the eye or the surface of the inanimate objects, unlike the spectral measures, which were measured on the surface of the Placido disc. This was undertaken to check the influence of thermal radiation on the surface of the eye during the measurement. As mentioned in the methods section, the inanimate objects were measured before measuring the surface of the eye. The results of both the ocular surface and inanimate objects are listed below.

4.4.2.1 Inanimate objects measures:

The inanimate objects used were air, a piece of tissue paper and a model eye placed at the approximate position of the corneal plane in the headrest. The results of temperature variation across a 3-minute period showed varying levels of change in temperature among the different object types. The surface temperature also depended on the type of object measured. A linear regression analysis was used to evaluate the amount of change in temperature over time with each object. A summary of slope and its significance from zero was listed in Table 4-3 below. There was a positive increase in temperature with all the objects using both corneal analysers. However, the rate of change in the temperature was very slow, which is shown by low positive slope values. With the model eye, there was an increase of 0.2ºC at the maximum with both instruments. Similarly, with tissue paper and air, there was no steep rise in the surface temperature in the presence of the illuminated target (Figure 4-13). These results indicate that the surface temperature measured depends on the type of object measured.

	CA100		CA200	
	Slope (ºC/s)	p-value	Slope (ºC/s)	p-value
Air	0.00046	0.082	**0.00048**	**0.00178**
Tissue paper	**0.00091**	**0.0019**	**0.00064**	**0.0152**
Model eye	0.00033	0.068	**0.00063**	**0.0001**

Table 4-3: List of slopes and its significance for different object types.

	CA100 (º C)	CA200 (º C)
Eyelids	34.13 ± 0.31	34.26 ± 0.38
Conjunctiva	33.60 ± 0.65	33.76 ± 0.57
Cornea	33.87 ± 0.38	33.72 ± 0.40

Table 4-4: Average surface temperatures obtained during aberration measures using the corneal analysers.

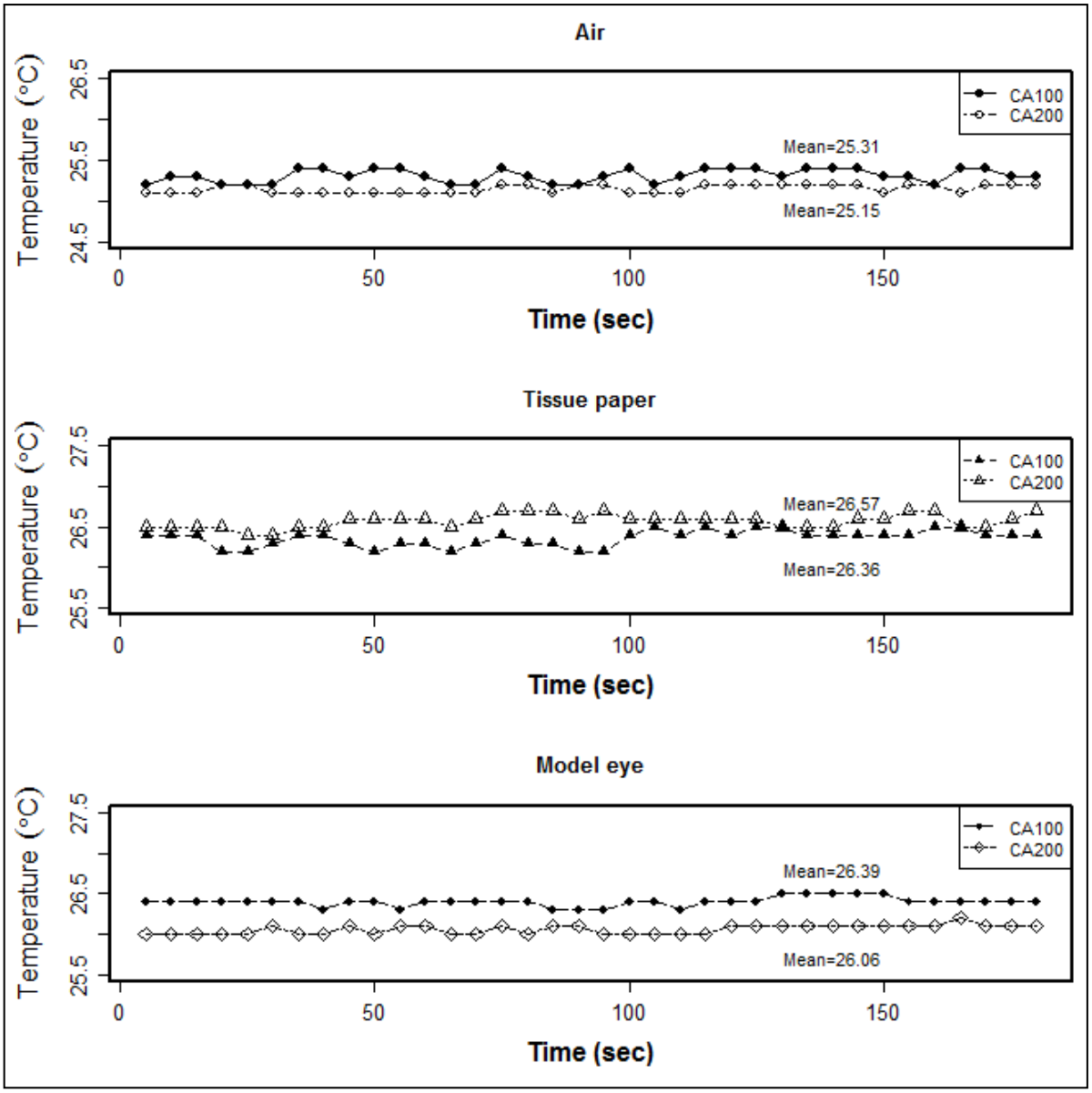

Figure 4-13: Multi plot showing change in temperature of inanimate objects over time. (Appendix 3, R.code 9)

4.4.2.2 Ocular surface temperatures:

The ocular surface measures were obtained from the cornea, conjunctiva and eyelids of human participants. The mean age of the group of participants involved in the study was 27.8 ±4.9 years of age. Out of 10 participants, 4 were males and 5 were females. Aberration measures were also obtained on the same participants following surface temperature measures. The thermal measures obtained from all 10 participants were averaged for each location. The corneal surface temperature was 33.87 ±0.38ºC and 33.72 ±0.40ºC in the presence of CA100 and CA200 corneal analysers respectively (Table 4-4).

To analyse the temperature variation over time between instruments, the analysis of covariance (ANCOVA) was used to find the changes in the trend of ocular surface thermal measures from all participants. The slopes were fit for each participant and then the slopes compared between instruments (Table 4-5).

4.4.2.2.1 Eyelid:

The average slope over the 180s time period for the CA100F was +0.00065ºC/s and for the CA200F was +0.00048ºC/s. Across subjects, the data was not significantly different between the CA100F and CA200F (paired t-test; df=9; p=0.487). Most of the participants (CA100-8, CA200-7) showed an increase in ocular temperature with time (Figure 4-14).

4.4.2.2.2 Conjunctiva:

The average slope over the 180s time period for the CA100F was -0.00104ºC/s and for the CA200F was +0.01079ºC/s. Across subjects, the data was not significantly different between the CA100F and CA200F (paired t-test; df=9; p=0.336). Only a few participants (CA100-1,

CA200-3) showed a significant increase in ocular temperature with time. Most of the participants (CA100-6, CA200-5) showed no significant change in temperature with time (Figure 4-15).

4.4.2.2.3 Cornea:

The average slope over the 180s time period for the CA100F was +0.00268ºC/s and for the CA200F was +0.00234ºC/s. Across subjects, the data was not significantly different between the CA100F and CA200F (paired t-test; df=9; p=0.758). Only a few participants (CA100-4, CA200-2) showed an increase in ocular temperature with time. Most of the participants with CA200 (n=6) showed no significant change in temperature with time (Figure 4-16).

4.4.3 Surface aberrations:

The higher order RMS was obtained for all the participants. Out of 10 participants, the data were extracted for 7 participants. We were not able to process the video obtained from the remaining three participants due to an unknown error during image processing. The average HOA root mean square (RMS) values obtained from each participant was 0.599 ± 0.2345µm (n=7) and 1.0477 ± 0.692µm (n=7) in the CA100 and the CA200 corneal analysers respectively (Figure 4-17). The HOA RMS obtained were not statistically significant different between instruments. Individual coefficient data were also obtained for all participants. The average spherical aberrations were -0.144 ± 0.1488µm and -0.2848 ± 0.0704µm for the CA100 and the CA200 corneal analyser devices. A list average of individual coefficients is shown in Table 4-6.

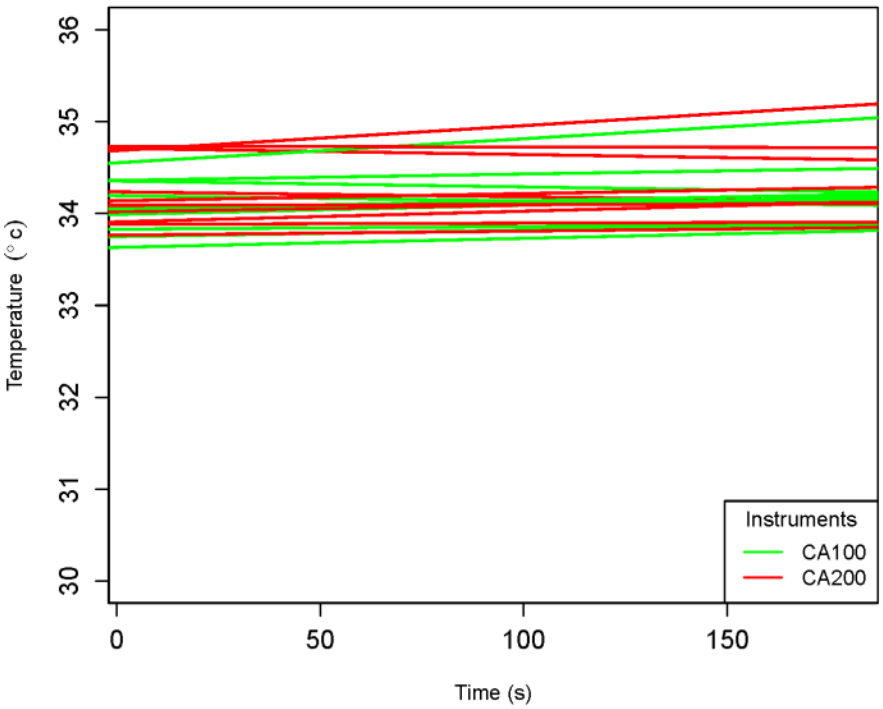

Figure 4-14: Multilevel plots showing slopes of change in temperature of the eyelid over time for each corneal analyzer by participant.(Appendix 3, R.code 10)

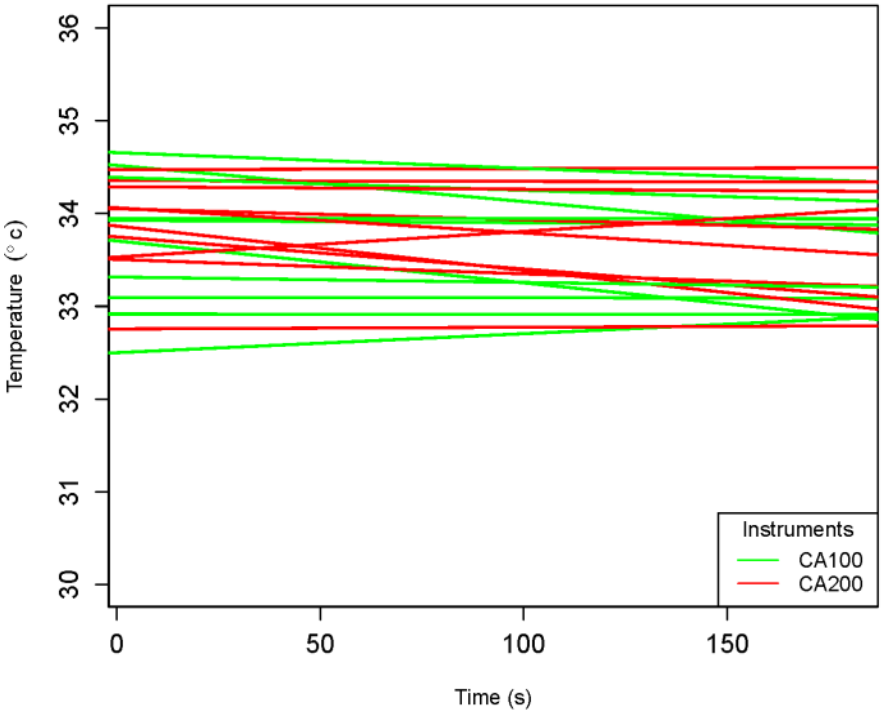

Figure 4-15: Multilevel plot showing slopes of change in temperature of the conjunctiva over time for each corneal analyzer by participant. (Appendix 3, R.code 10)

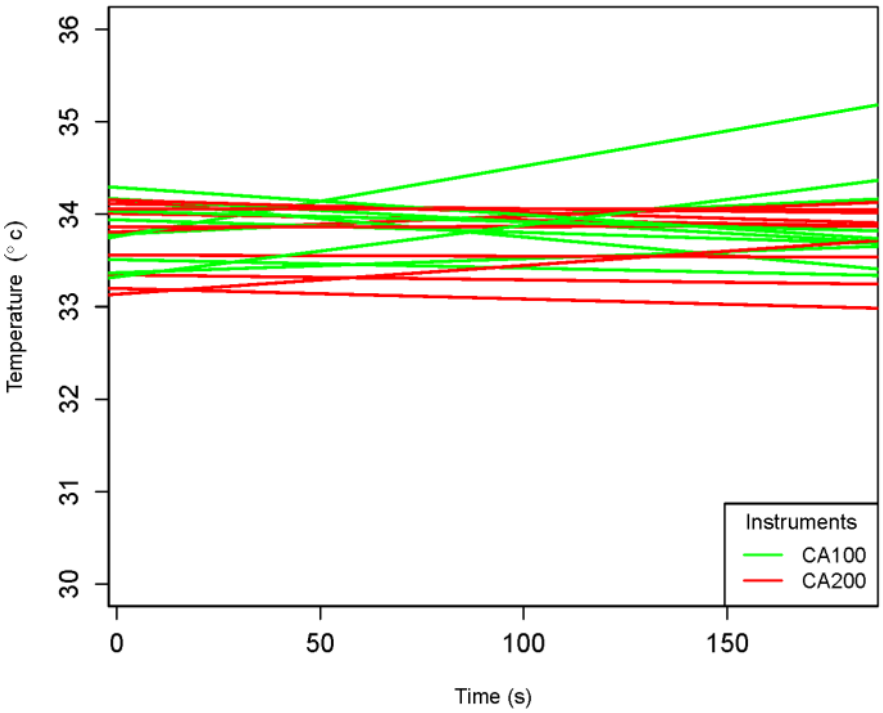

Figure 4-16: Multilevel plots showing slopes of change in temperature of the corneal surface over time for each corneal analyzer by participant. (Appendix 3, R.code 10)

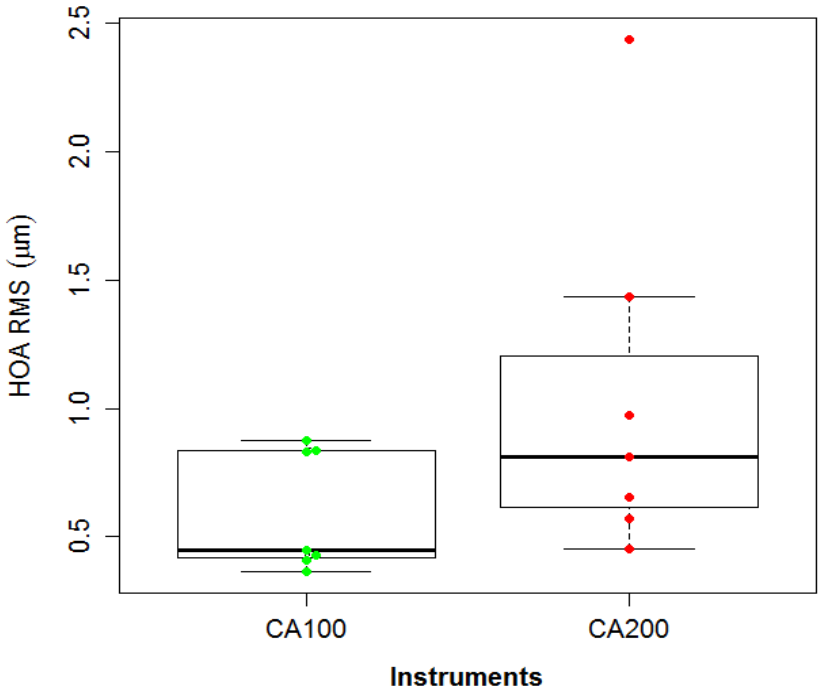

Figure 4-17: Comparison of HOA RMS obtained from participants using CA100 and CA200 corneal analyzers (Appendix 3, R.code 4)

Sub.id	Eye lids			Conjunctiva			Cornea		
	CA100	CA200	Comparison between instruments	CA100	CA200	Comparison between instruments	CA100	CA200	Comparison between instruments
	Slope (ºC/s)	Slope (ºC/s)	p < 0.05	Slope (ºC/s)	Slope (ºC/s)	p < 0.05	Slope (ºC/s)	Slope (ºC/s)	p < 0.05
1	0.0003	**-0.0005**	*	-0.0004	**-0.0048**	*	**0.0249**	**0.0246**	
2	**0.0010**	**-0.0007**	*	0.0021	**-0.0035**	*	**0.0076**	-0.0007	*
3	**0.0026**	**0.0027**		**-0.0039**	0.0001	*	**-0.0040**	**-0.0005**	*
4	**0.0007**	0.0001	*	-0.00003	0.0002		**-0.0014**	-0.0005	
5	**-0.0007**	-0.0001	*	**-0.0017**	-0.0009		**-0.0025**	**-0.0013**	
6	0.0007	0.0007		-0.0003	**-0.0012**		**0.0015**	-0.0012	*
7	**-0.0006**	**0.0005**	*	**-0.0045**	**-0.0016**	*	-0.0009	0.0001	
8	**0.0010**	**0.0012**		-0.00001	**-0.0027**	*	-0.0011	-0.0001	
9	**0.0009**	**0.0008**		-0.0006	**0.0028**	*	**0.0056**	**0.0031**	*
10	**0.0005**	0.0001	*	**-0.0014**	-0.0003		**-0.0030**	-0.0001	*

Table 4-5: List of slope values for thermal measures of each participants and their significance when compared between instruments. The bold values represent the slopes, which are significantly different from zero and '' represents a significant difference between the slope for each instrument (ANCOVA).*

Coefficients	CA100 (µm)	CA200 (µm)
Vertical coma Z_3^{-1}	0.0186 ± 0.1201	0.1353 ± 0.2142
Horizontal coma Z_3^{1}	0.0547 ± 0.2409	0.1133 ±0.4506
Spherical aberrations Z_4^{0}	-0.1445 ± 0.1488	-0.2848 ± 0.0704
Vertical trefoil Z_3^{-3}	-0.0844 ± 0.1147	0.1162 ± 0.1436
Horizontal trefoil Z_3^{3}	-0.1736 ± 0.1147	-0.0877 ± 0.1387

Table 4-6: List of average aberration coefficients obtained in CA100 and CA200 corneal analysers.

4.5 Discussion:

The spectral measures exhibit a definite difference between the luminance of the Placido discs. There was notable difference in the luminance distribution of the light source between quadrants and between sides for the CA100 topographer, whereas the light source was more evenly distributed in the CA200 corneal analyser. The inconsistency in the luminance may be due to the type of light source or the difference in the distribution of the light sources behind the Placido disc. To our knowledge, no studies have analysed the spectral characteristics of the Placido disc light source. The wavelength of the light from both the Placido discs was the same and it did not change over time. This indicates there is no influence of the wavelength of the light source on the corneal aberration measures. Although the peak wavelength was not different between the two devices, the higher luminance of the CA100 might induce a photophobic and/or reflex tear response, which may contribute to a difference in the measured aberrations between instruments.

When it comes to ocular surface temperature, there are many studies, in which ocular surface temperature was reported, using a thermometer or a thermograph.[3,49,50,52,56–61] Most of these studies agree that there is a decrease in the corneal and conjunctival surface temperature with time. They also observed a steeper decrease in the surface temperature with time in dry eye participants compared to normal participants. All these measurements were taken directly on the cornea without the influence of an external source. [49,52,59,61]

In our study, two Placido disc light sources were used at its normal working distance to measure their influence on the ocular surface temperature variation. Corneal temperatures obtained in this study were similar to previous studies and there was no significant difference in the change in surface temperature over time between corneal analysers. A similar trend was observed with the eyelid and conjunctival temperature over time.

The location of the thermometer during the temperature measurement was a limitation in this study. Due to the Placido disc's large diameter and close working distance, the thermometer had to be introduced from the side, between the eye and the Placido disc. A study conducted by Morgan et al.[52] measured ocular surface temperature using an infrared thermograph, which provides ocular surface temperature for the entire ocular surface rather than a reference point. They observed a variation in corneal temperature from the center of the cornea towards the periphery and that it depended on the curvature of the cornea. Thus, because the curvature differences between patients were not controlled or corrected, this may be the reason for differing trends in the temperature between study participants.

The higher order RMS was not significantly different between the corneal analysers, although on average, the higher order RMS was higher for the CA200 compared to the CA100 .

4.6 Conclusion:

This study found that:

i. The CA200 is the preferred device to use for these studies because of the consistent luminance.

ii. Although aberrations were not significantly different between devices, the HOA RMS were higher with the CA200 and, combined with different luminance and possible tear response, indicates that the two devices are not interchangeable.

iii. For both instruments, there was no indication that there is a thermal response induced by the power of the light source. Therefore, this aspect of the source does not likely contribute to any difference in the aberrations measured by the two devices.

Chapter 5 : Assessment of Tear Film Stability / Regularity Using Surface Aberrometry

5.1 Background:

An increase in HOAs has been associated with NITBUT in normal and dry eyes,[41,62–65] and the magnitude of HOA associated with the tear film are higher in individuals with dry eye than in those without.[41,66] An increase in HOA has also been noted with soft contact lens wear,[66,67] with some dependence on soft contact lens design.[68,69] A shorter NITBUT in contact lens wearers has been found to be associated with reduced optical quality, and is thus implicated in blurry visual symptoms with lens wear.[39]

A stable tear film is critical in order to maintain a healthy ocular surface and to provide good optical quality. Both invasive and non-invasive methods exist to evaluate tear film stability; however, they do not provide a good measure of the dynamic nature of the tear film. The use of surface aberrometry may provide an instantaneous, discriminatory measure of tear film stability, as well as a dynamic measure of temporal tear film stability.

Using the results from Chapter 3, the study design for this chapter was altered. The first 15 seconds of the measurements were discarded, measurements were obtained at 0.25 sec sampling time and the focus was maintained at either green focus or red focus positions for maximum accuracy.

This study intended to examine the measurement itself, by obtaining measurements on human participants for different blink regimen, and head position, and the impact on the

measurement of nasal shadow, eyelashes, etc. on the measurement area. It also examined existing output metrics (already published for similar procedures) in addition to other metrics, particularly those that may characterize the dynamic/local nature of the tear film.

5.2 Objectives:

The overall objectives of this study were:

1. To determine the optimal method for acquisition with respect to normal physiological processes, by examining the blink regimen and head position that elicits the most consistent response over the largest region on repeated measurement.

2. To determine the largest region selected for analysis by investigating the effect on the individual and summary aberration metrics of the inclusion of non-measurement areas (i.e. where the Placido disc cannot be projected onto the cornea or contact lens). The proportion of non-measurement area that elicits a significantly different result will be determined.

5.3 Methods:

5.3.1 Study design:

This study was conducted as a non-dispensing assessment in which the methodology for optimizing measurement acquisition was developed. Various methods of data-capture were explored (e.g. blink regimen [natural vs. forced] and head position). Measurements with different head positions was used to analyse the missing area due to shadows from the nose

and/or eyelashes, preventing capture of data across the full cornea or contact lens. The impact of these areas on the outcome measures was determined.

Twenty adapted soft contact lens wearers were screened with the goal of enrolling twelve participants: six who demonstrate poor soft contact lens wettability and poor tear film stability with no lens (Group A) and six who demonstrate good soft contact lens wettability and good tear film stability with no lens (Group B). Participant eligibility was determined at a screening and fitting visit according to the inclusion and exclusion criteria outlined below. Informed consent was obtained from all participants prior to enrolment in the study. There were three scheduled visits by the participants to the CCLR research facility during the study, if they were successfully enrolled into the study, including the initial screening visit and two additional visits on two separate days. Ethics clearance was obtained through the Office of Research Ethics at the University of Waterloo, prior to commencement of the study.

5.3.2 Inclusion and exclusion criteria:

A person was eligible for inclusion in the study if he/she:

1. Was at least 17 years of age and has full legal capacity to volunteer;
2. Had read and signed an information consent letter;
3. Was an adapted soft contact lens wearer;
4. Was willing and able to follow instructions and maintain the appointment schedule;
5. Had had an ocular examination in the last two years;

6. Had clear corneas and no active ocular disease;

7. Had wettability ≥ grade 3 with their habitual lenses and a non-invasive tear break-up time (NITBUT) of < 5 seconds with no lens (group A) or wettability≤ grade 0.5 with habitual lenses and a NITBUT of > 10 seconds with no lens (group B).

A person was excluded from the study if he/she:

1. Had any ocular disease;

2. Had a systemic condition that may affect a study outcome variable;

3. Was using any systemic or topical medications that may affect ocular health;

4. Had known sensitivity to the diagnostic pharmaceuticals to be used in the study;

5. Had undergone corneal refractive surgery;

6. Had any clinically significant lid or conjunctival abnormalities, neovascularisation, corneal scars or corneal opacities.

5.3.3 Study visits:

5.3.3.1 Screening and fitting visit:

On the screening visit, participants were advised to wear their habitual lenses for at least 5 hours before the screening visit and to follow their regular work schedule. The participants were scheduled in the afternoon hours for the screening visit, to allow for five hours' time interval from the time of contact lens insertion. The enrolled participants were screened with

their habitual lenses for lens wettability and tear break up time without contact lenses. The participants were then included or excluded from the study according to the protocol.

From the list of twenty participants screened, twelve participants were recruited for the follow-up visit. These participants had their lens wettability grade and NITBUT values within the limits of inclusion criteria (Table 5-1). Each group (normal and dry eye group) had six participants (5 females and 1 male in each). The normal group's mean age was 26 ± 5.9 years and dry eye group's was 34.7 ± 10.3 years (Table 5-2). Other refractive and habitual contact lens characteristics of the two groups are listed in Table 5-3 and Table 5-4

After the screening visit, the B&L Purevision lenses were fitted on the same day according to the manufacturer's guidelines. If the lenses provided inadequate movement or unacceptable decenteration for a particular participant, that person was not enrolled in the study. The lens parameters of the Purevision lenses are listed in Table 5-5.

	Normal group		Dry eye group	
	OD	OS	OD	OS
Wettability with habitual lenses	0.20± 0.1	0.42± 0.2	3.00± 0.24	2.88± 1.07
NITBUT without habitual lenses (seconds)	8.38± 1.24	10.12± 2.08	4.80± 1.27	5.30± 1.43

Table 5-1: Lens wettability and NITBUT characteristics of each group during screening visit

	Normal group	Dry eye group
Age	26 ± 5.9 (21 to 35 yrs)	34.7 ± 10.3 (24 to 52 yrs)
Gender	1 male, 5 females	1 male, 5 females
Average CL wearing time of habitual lenses	11.5 hrs ± 2.3	10.5 hrs± 3.3
Average no. of days of wear of habitual lenses per week	5.5 days± 1.0	5.0 ± 1.23
Average no. of years of CL wear	5.0 yrs ± 4.3	13.7 yrs± 12.5

Table 5-2: Age and habitual lens characteristics of normal and dry eye group.

		Normal group		Dry eye group	
		OD	OS	OD	OS
K-readings (Dioptres)	Flat K Steep K	43.12± 0.51 44.34± 0.79	42.96± 0.61 44.27± 0.98	44.45± 1.55 45.50± 1.53	44.25± 1.54 45.33± 1.45
Corneal cylinder (Dioptres)		-1.22± 0.43	-1.36± 0.57	-0.96± 0.26	-1.08± 0.27
Refractive error (Dioptres)	Sphere Cylinder	-2.4± 2.22 -0.87± 0.68	-2.67± 2.47 -0.89± 0.93	-3.8± 0.9 -0.5± 0.42	-3.52± 1.28 -0.62 ± 0.46

Table 5-3: Refractive characteristics of normal and dry eye group.

	No. of participants	Normal group	No. of participants	Dry eye group
Lens type	1	Acuvue2	4	Acuvue Oasys
	3	Acuvue Oasys	1	1-Day Acuvue TrueEye
	1	Dailies Torics	1	Air Optix Multifocal
	1	Dailies Aqua Comfort Plus		
Lens care solution	2	OptiFree Replenish	5	ClearCare
	2	ClearCare		
Wearing modality	1	Monthly	2	Monthly
	3	Biweekly	3	Biweekly
	2	Daily	1	Daily

Table 5-4: Habitual lens characteristics of each group during screening visit.

Identifier	PureVision contact lens
Manufacturer	Bausch & Lomb
Material	Balafilcon A
FDA classification	Group III
Health Canada license #	25928 and 22080
Health Canada device identifier	PUREVISION
EWC (%)	36%
Dk/t (-3.00D)	101
BOZR (mm)	8.3, 8.6
Diameter (mm)	14.0
Spherical powers (D)	-0.25D to -6.00D (0.25) -6.50 to -12.00D (0.50) plano to +6.00D (0.25) (8.3 mm) -0.25D to -6.00D (0.25)

Table 5-5: Study lens parameters.

5.3.3.2 Follow up visits:

Following a successful screening and fitting visit, participants returned for the first study visit (Visit 1) after two days of no contact lens wear. Measurements of NITBUT, surface aberrations were obtained before and after insertion of a new pair of study lenses. The measurements of lens wettability were only obtained with the study lenses. Each measurement was randomized between eyes and between measurement types, to avoid order effects influencing the results obtained (Table 5-6 and Table 5-7). The order of measurements in the second visit was repeated in the same order as the first visit. Visits were scheduled in the afternoon and all participants had visits within the same one to two hours (i.e. between 1 and 3 p.m.). These procedures were repeated on a separate day, ± 0.5 hours from the time Visit 1 was conducted (Visit 2). Each study visit included three sets of measurements separated by a 15-minute wait period. Measurements were separated into 3 categories: before study lens insertion, immediately after study lens insertion and 30 minutes after study lens insertion.

Group Normal (N) / Dry eye (DE)	ID. No.	Test 1	Test 2	Test 3
DE	3	Pre lens NITBUT	Aberrometry	Lens wettability
DE	4	Lens wettability	Aberrometry	Pre lens NITBUT
DE	5	Pre lens NITBUT	Lens wettability	Aberrometry
DE	7	Lens wettability	Aberrometry	Pre lens NITBUT
DE	8	Pre lens NITBUT	Lens wettability	Aberrometry
N	10	Aberrometry	Lens wettability	Pre lens NITBUT
N	12	Lens wettability	Aberrometry	Pre lens NITBUT
N	14	Lens wettability	Pre lens NITBUT	Aberrometry
N	15	Aberrometry	Lens wettability	Pre lens NITBUT
N	16	Lens wettability	Aberrometry	Pre lens NITBUT
N	18	Pre lens NITBUT	Lens wettability	Aberrometry
DE	20	Pre lens NITBUT	Lens wettability	Aberrometry

Table 5-6: Randomization table for the order of measurements.

Group (N/DE)	ID. No.	Natural blink	Forced blink	Head position
DE	3	OU	OD	OS
DE	4	OU	OS	OD
DE	5	OU	OD	OS
DE	7	OU	OD	OS
DE	8	OU	OS	OD
N	10	OU	OS	OD
N	12	OU	OS	OD
N	14	OU	OS	OD
N	15	OU	OD	OS
N	16	OU	OS	OD
N	18	OU	OS	OD
DE	20	OU	OS	OD

Table 5-7: Randomization table for aberrometry measurements- forced blink and head position.

5.3.4 Study measures:

5.3.4.1 Contact lens wettability:

Wettability measurements were performed by viewing the specular reflection of the pre-lens tear film under high magnification (32X) and very low illumination (both internal and external light diffusers on the slit lamp). Two examples of the image of the specular reflection used for grading are shown in Figure 5-1.

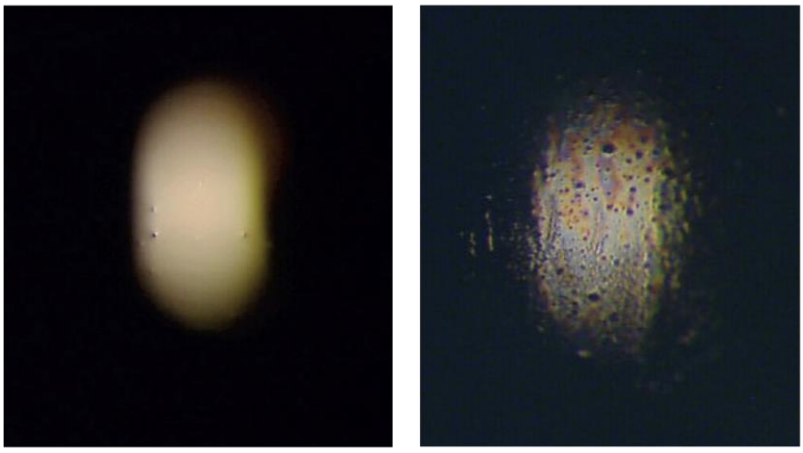

Figure 5-1: Examples of good image quality (grade 0) (left) and poor image quality (grade 4) (right) of the specular reflection off the pre-lens tear film.

Surface drying between blinks and re-wetting with each blink were considered when deciding on the final wettability grade. Nasal and temporal sides of the lens are each graded separately and the final grade was an average between the two. A 0-4 grading scale, with 0.25 grading steps was used. Wettability measurements were repeated on visit 1 and visit 2.

5.3.4.2 Non-invasive tear break up time (NITBUT):

Following wettability measurements at the screening visit, participants removed their habitual lenses and waited for 10 minutes before NITBUT measurements were obtained. NITBUT was assessed by using the Atlas^{TM} corneal topographer. The instrument has a keratoscope unit that

produces concentric rings of light, which are reflected off the cornea and imaged by a CCD camera. Participants looked at a fixation target at the centre of the concentric rings of light and were asked to blink 3 times before each measurement was taken. NITBUT was determined by measuring the time taken for distortions or discontinuities to appear in the reflected image of the concentric ring pattern (Figure 5-2). The time (in seconds) for the first distortion of the rings was measured using a stopwatch, to the nearest 0.1-second. Three measurements were taken for each eye and averaged. On visit 1 and 2, NITBUT measurements were taken before lens insertion, 15 and 30 minutes post-lens insertion.

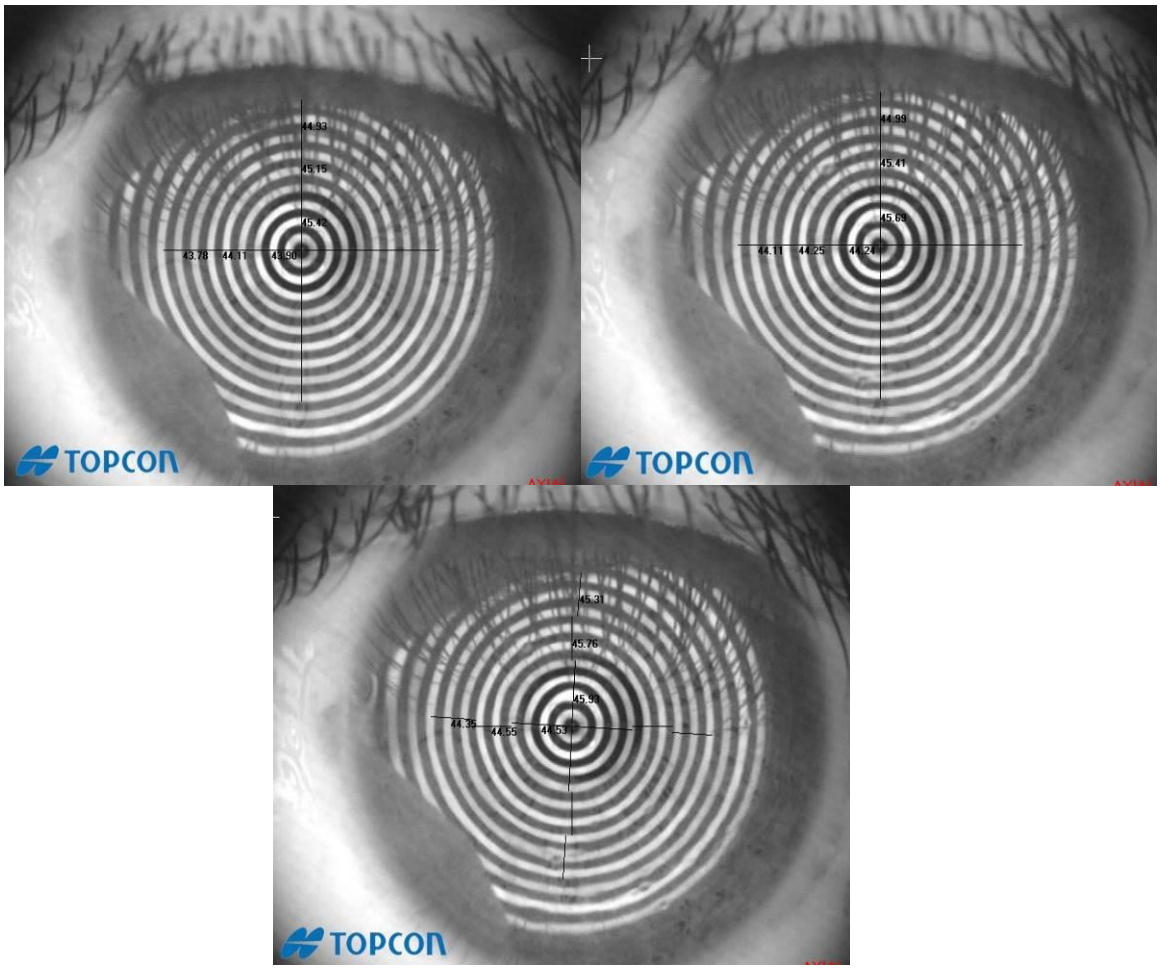

Figure 5-2: A schematic representation of tear breakup during the NITBUT test.

5.3.4.3 Surface aberrometry measurements:

The temporal measurements of ocular surface aberrations were obtained using the Topcon CA100 corneal analyser. The methods to obtain dynamic aberrations using the CA100 corneal analyser was explained in Chapter 2. The methodology for obtaining the surface aberrometry measurements in vivo were determined by the outcomes of Chapter 3 (measurement acquisitions from a model eye).

The acquisition parameters followed while acquiring measurements with human eyes were:

1) Data was acquired with an inter-frame interval of 0.25s;

2) The first 15s of data, obtained while the optimal focus arrows were being obtained, was removed and

3) The green (optimal) focus position was determined immediately post-blink.

At each visit, multiple acquisitions of surface aberrometry measurements were obtained for evaluation of repeatability of the measure and any developed metrics. In addition, measures were obtained in the straight-ahead position, with 10° and with 20° of head turn (Figure 5-4) to allow assessment of the impact of shadows from the lashes and nose on the area of the target projected onto the cornea. To measure aberrations in different head turns, a degree scale (protractor) was attached below the participants chin rest, with 90° located at the center of the chin rest (Figure 5-3). When the participant looked straight ahead, the tip of the nose was aligned with the 90° of the degree scale. With 10° and 20° degree head turn, the tip of the nose was aligned with a head turn to the desired measurement angle. Participants were instructed not to change their head position during the measurement period. Lastly,

measurements were obtained with natural blinking and with forced blinking (blink every ~8 seconds). During the forced blink interval, the examiner activated a metronome calibrated for 1 sec time interval between two sounds and participants were instructed to blink every 8 sec by the examiner.

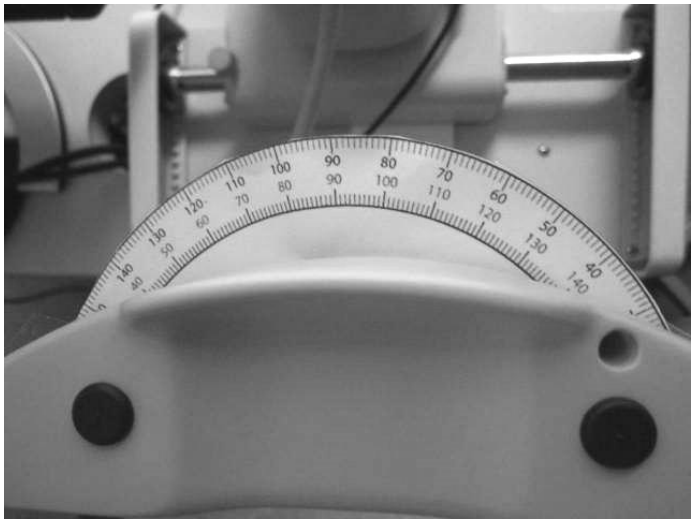

Figure 5-3: The degree scale (protractor) attached to the bottom of the chin rest as a guide for measuring surface aberrations at different head turn angles.

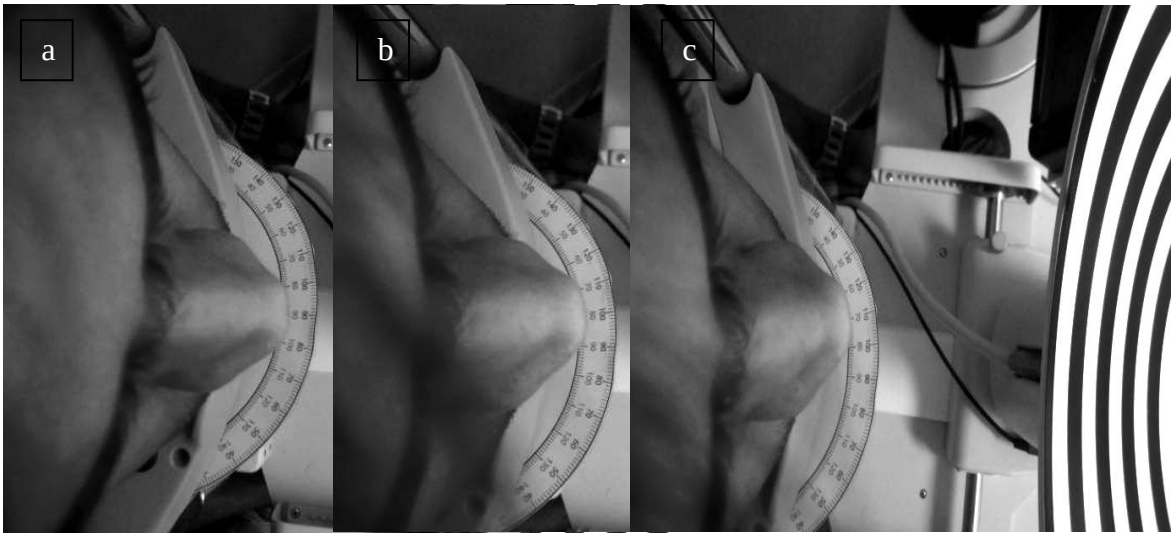

Figure 5-4: Head turn was determined by aligning the nose tip to the center in primary gaze (a,)to 10° (b) and 20° (c) degree off the center.

5.4 Data analysis:

Raw surface aberration data were smoothed using a running mean procedure (k=moving window size=11), with the moving window centred on the central time point of capture. The purpose of this procedure was to minimise the between measurement variability without losing the trend of the data over time. This procedure was undertaken using the caTools[70] package in the R statistical software.[46] The procedure generated a 'running mean' for each point and, in addition a 'running SD' for the window. In this way, confidence intervals could be constructed around the running mean that would describe the variability within a window across time. Therefore, data showing high variability within a window (as might be expected with emergence of areas of surface dryness) would have a wider confidence interval than data exhibiting low variability.

The area covered by the Placido disc each of the in three head turn positions was calculated using ImageJ (v.1.46.a) application software.[71] After obtaining the areas between the eyelids of individual participant, values were compared between the participants and groups using repeated measures ANOVA.

One-way analysis of variance was used to compare between normal and dry eye groups for single estimates of any measure per subject. Repeated measures ANOVA was employed for comparison between normal and dry eye groups with multiple acquisitions of the aberrometry data on the same subject (SPSS v20).[72]

5.5 Results:

5.5.1 Contact lens wettability:

The contact lens wettability obtained in the right eye of each participant was not significantly different between visits (Visit 1, Visit 2; RM-ANOVA $F_{(1,11)}$=0.215; p=0.652) but was significantly higher at the 1hr measure than at the 15mins measure (measure 15min & 1hr); RM-ANOVA $F_{(1,11)}$=8.308; p=0.015) (Figure 5-5). This difference was not different between visits (Visit*Measure; RM-ANOVA $F_{(1,11)}$=3.090; p=0.107).

The lens wettability in the left eye was not significantly different between the 15min and 1hr after contact lens insertion in both groups (Visit; RM-ANOVA $F_{(1,11)}$=0.120; p=0.736; Measure; RM-ANOVA $F_{(1,11)}$=15.619; p=0.002; Visit*Measure; RM-ANOVA $F_{(1,11)}$=0.886; p=0.367) (Table 5-8).

5.5.2 NITBUT:

There was no statistically significant difference between the NITBUT between visits (screening, visit 1 & visit 2; RM-ANOVA $F_{(2,22)}$=1.831; p=0.190), between eyes (OD & OS; RM-ANOVA $F_{(1,11)}$=0.266; p=0.616) or their interaction (eyes*visits; RM-ANOVA $F_{(2,22)}$=3.124; p=0.068).(Table 5-8)

		Normal group- visit 1	Normal group- visit 2	Dry eye group– visit 1	Dry eye group– visit 2
CL Wettability- After 15 min	OD	0.41± 0.21	0.54±0.29	1.63± 1.21	1.92±1.10
	OS	1.00 ±1.24	1.00±0.63	2.50 ±1.38	2.87±0.97
CL Wettability- After 1 hr	OD	1.13± 0.93	1.00±0.39	2.50± 1.04	1.91±0.89
	OS	1.67 ±1.29	1.54±1.08	3.13 ± 0.85	3.08± 0.77
NITBUT- Without CL (sec)	OD	7.41±2.6	8.36±1.99	5.53± 1.05	5.56± 2.17
	OS	7.42±1.81	8.54±2.89	4.72± 1.61	4.79±1.07
NITBUT with CL- After 15 min (sec)	OD	6.9±2.25	6.70±1.58	5.13± 1.71	5.40± 1.90
	OS	5.51±1.03	5.7±2.04	4.48± 1.03	4.23±1.23
NITBUT with CL- After 1 hr (sec)	OD	6.08±0.88	7.11±1.82	4.72± 1.12	5.50±1.3
	OS	5.6±1.6	5.58±1.45	4.00± 1.71	5.19±1.31

Table 5-8: Average and standard deviation of lens wettability and NITBUT measurement of visit 1 and visit 2.

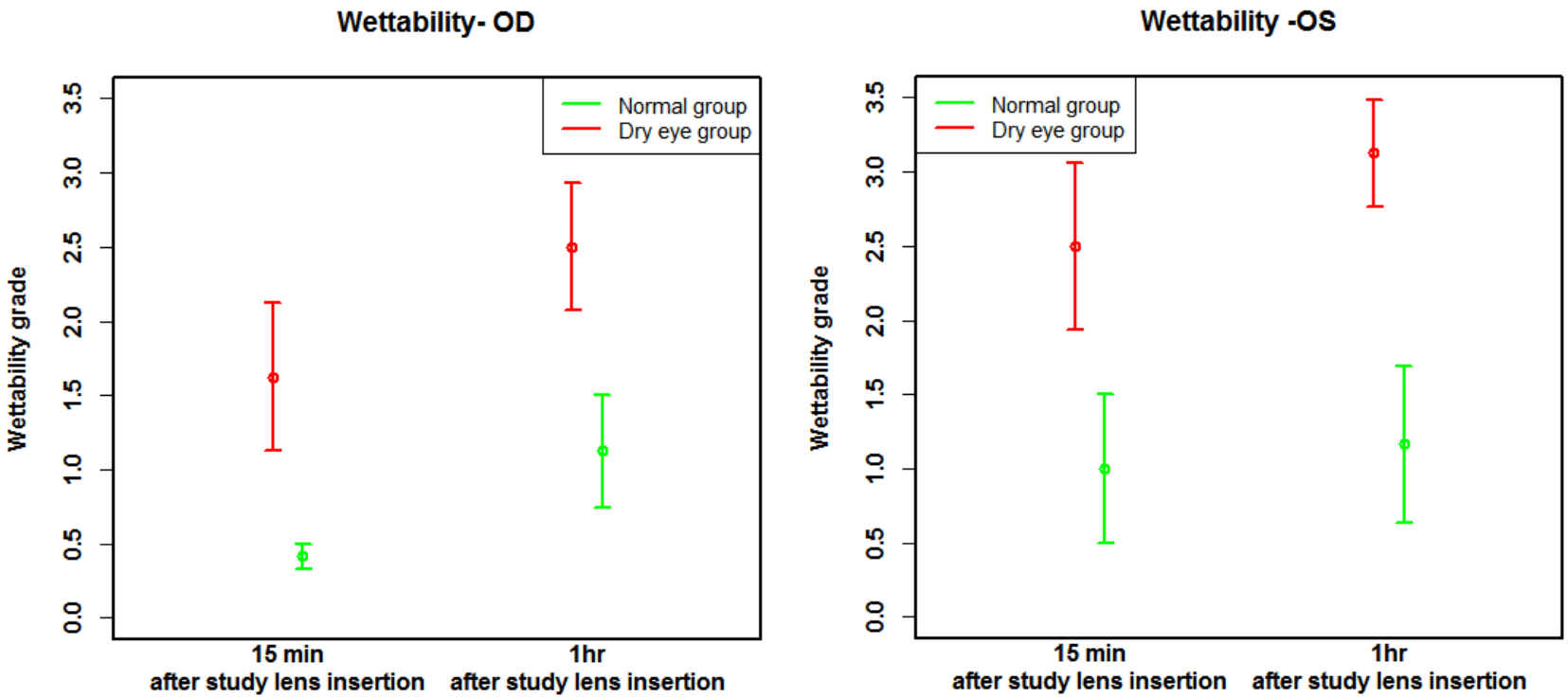

Figure 5-5: Visit 1- lens wettability comparisons between groups and measurements for 15 min and 1 hr post lens insertion. The 1 hr measurement was higher after than the 15 min.

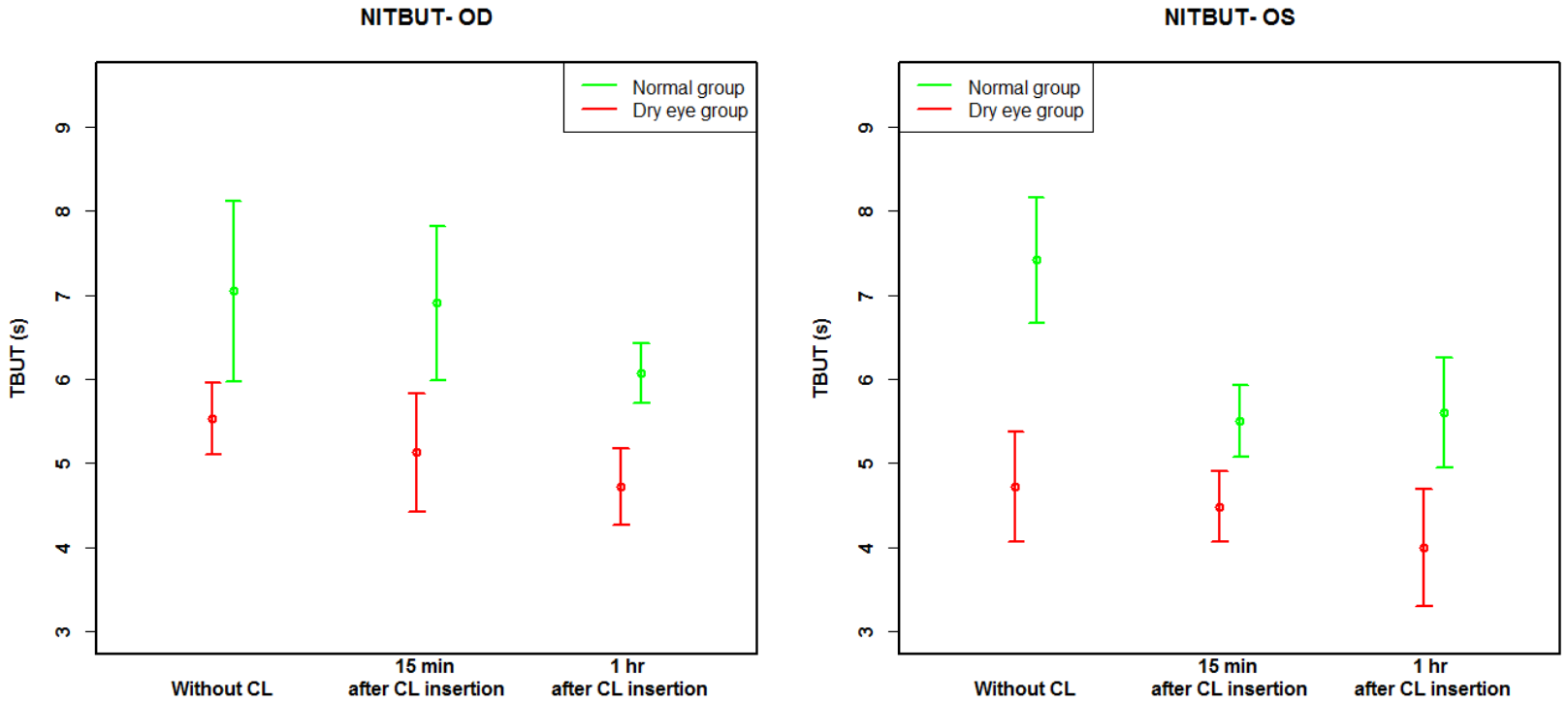

Figure 5-6: Visit 1-NITBUT measurement comparisons between the group and measurements for measurements without contact lens, 15min and 1hr after contact lens insertion.

5.5.3 Clinical measurement optimization:

5.5.3.1 Analysis of target area with head position:

Video of the Placido disc was exported from the TOPCON measurement device without the aberration map superimposed. The video was cropped to a segment that excluded the first 15 seconds (where instrument focusing took place) and included at least 3 blinks. The video segment was then converted to a jpeg-image sequence. A single jpeg was selected from the post-blink phase in which the Placido target rings were clear and was representative of the coverage seen in the image sequence (Figure 5-7(a)).

The selected image was cropped at the limbal region (Figure 5-7 (b)). The image was converted to a binary image using local auto-thresholding (NiBlack with a radius of 8 pixels; ImageJ, v.1.46a NIH Image, Bethesda, MD, USA). This procedure highlighted the white Placido rings in black and all other parts of the image as white (Figure 5-7(c)). Discontinuities in the Placido rings (shadows from eyelashes or nose) where coded as white. The coordinates of the centre of the cornea were located by selecting the inner edge of the central Placido ring (Figure 5-7(d)).

A 500x500 pixel selection box was drawn, centred on the position of the central cornea, and the image was cropped. The percentage area of the 500x500 pixel box that was black was measured and this was analysed across images and in different head positions (Figure 5-7(e)). The number of complete target circles was also determined for each condition.

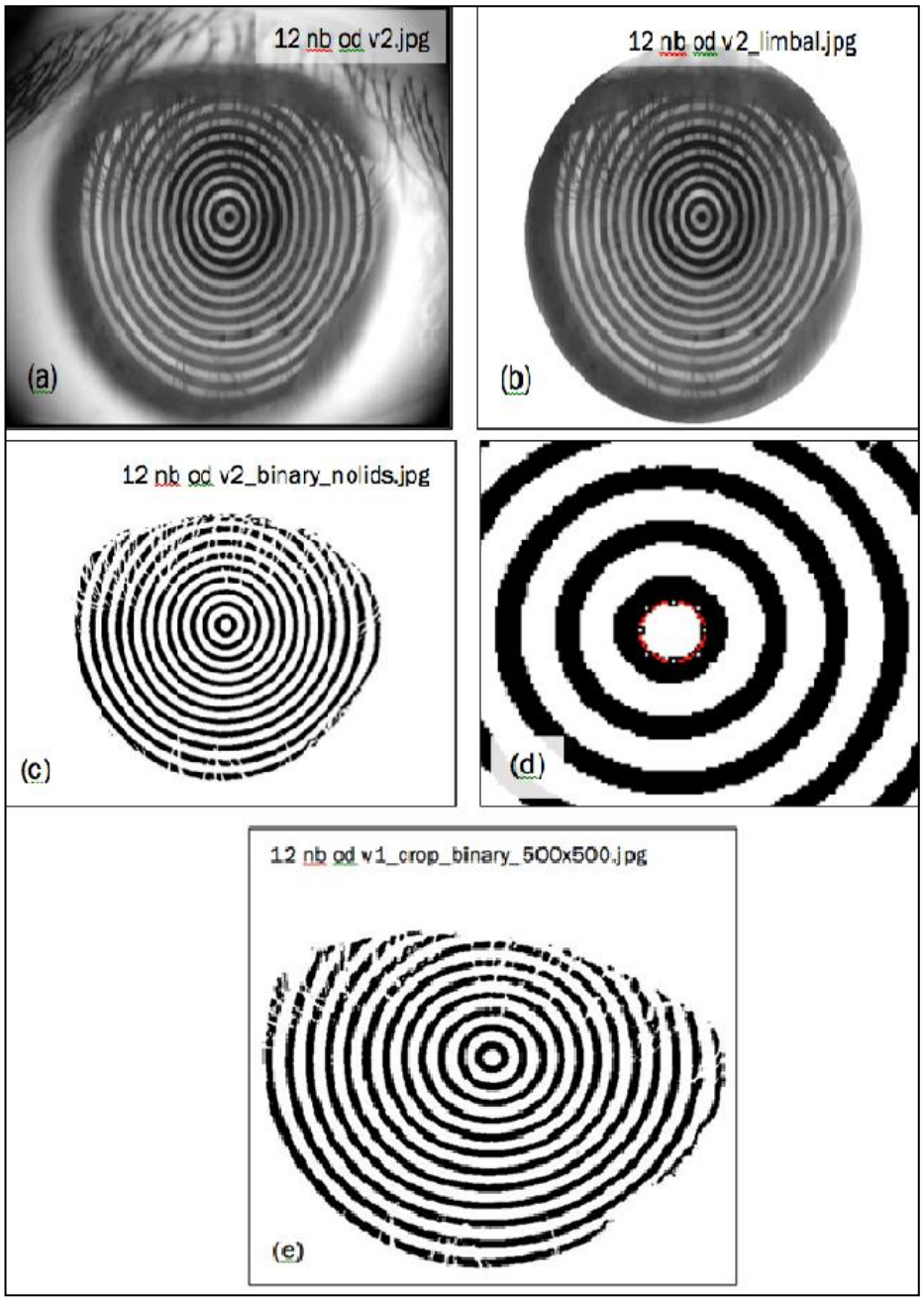

Figure 5-7: Image processing procedures to identify percentage area of 500 x 500-pixel area that is covered by the Placido target. (a) Original jpeg exported from movie; (b) Crop to limbal area; (c) Local auto-threshold (NiBlack, Radius 8pixels); (d) Locating the centre of the cornea; (e) Crop to 500x500 pixel box centred on the corneal centre from which the %area covered by Placido targets is determined

There was no significant difference between the area covered by the target (% of pixels) for a given head position at the first or second measure (RM-ANOVA F=0.054; p=0.816; Figure 5-8). Thus, the values for the area covered by the target were averaged across the repeated measures for each head position and were then re-analysed for the percentage area covered as a function of head position and diagnostic group.

There was no significant difference between the percentage area covered by the Placido targets between head positions (RM-ANOVA F=1.724; p=0.216) for normal/ dry eye groups (RM-ANOVA F=0.235; p=0.639) or for their interaction (RM-ANOVA F=0.203; p=0.756). The same result was found for the number of complete rings in the target. Table 5-9 shows the descriptive data of the percentage of area covered by Placido disc over the corneal surface, as a function of measure number, head position and diagnostic group

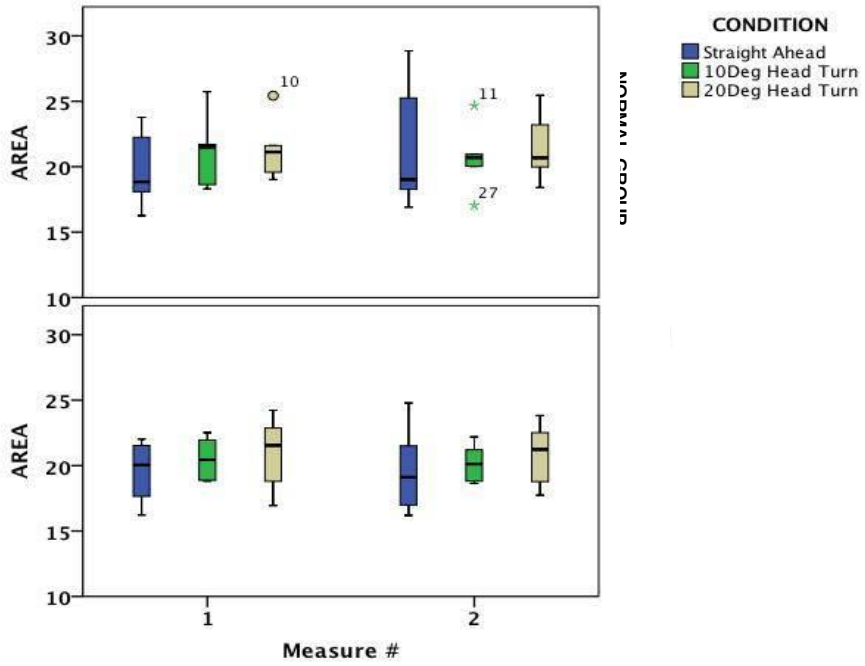

Figure 5-8: Percentage area covered by Placido target as a function of head position and diagnostic group

	Straight Ahead			10° Head Turn			20° Head Turn		
	% Area		# Circles	% Area		# Circles	% Area		# Circles
Measure 1	Mean (±SD)	Median (Range)	Median (Range)	Mean (±SD)	Median (Range)	Median (Range)	Mean (±SD)	Median (Range)	Median (Range)
Normal group	19.8 (3.1)	18.8 (16-24)	4.0 (2-5)	21.2 (3.0)	21.5 (18-26)	4.0 (2-5)	21.4 (2.5)	21.1 (19-25)	3.0 (1-5)
Dry eye group	19.6 (2.4)	20 .0 (16-22)	3.5 (2-6)	20.5 (2.7)	20.7 (19-22)	4.0 (2-6)	21.5 (2.3)	21.5 (17-24)	3.5 (3-6)
Measure 2	Mean (±SD)	Median (Range)	Median (Range)	Mean (±SD)	Median (Range)	Median (Range)	Mean (±SD)	Median (Range)	Median (Range)
Normal group	21.2 (3.0)	20.3 (16-29)	4.0 (2-5)	20.7 (2.7)	20.1 (19-24)	4.0 (2-5)	21.5 (2.3)	20.7 (19-26)	3.0 (2-5)
Dry eye group	19.6 (3.4)	19.1 (16-25)	4.0 (3-6)	20.2 (2.4)	20.7 (19-22)	3.5 (3-5)	20.9 (2.3)	21.2 (18-24)	3.5 (3-5)

Table 5-9: Percentage area of Placido target and number of complete circles as a function of head position and diagnostic group.

5.5.4 Comparison of aberrations between groups – Natural blink

5.5.4.1 RMS Aberrations without contact lens – Natural blinking

The average RMS over the time of acquisition without contact lenses and the average width of the confidence interval are shown for each participant, stratified for diagnostic group in Table 5-10. The change in NITBUT from the screening visit is also shown. The normal group showed a larger change, generally a reduction, in NITBUT from the screening appointment.

The confidence interval over smoothed RMS values was calculated for each time point, as shown in Figure 5-9. On average, the smoothed RMS was relatively constant over the measurement acquisition time. The dry eye group showed slightly more variation in RMS and width of the confidence interval over the time of acquisition, although this was not true for all participants in the dry eye group. (Figure 5-10)

5.5.4.2 RMS Aberrations with contact lenses – Natural blinking

The average RMS over the time of acquisition with the study contact lenses and the average width of the confidence interval are shown for each participant, stratified for diagnostic group in Table 5-11. The change in NITBUT and wettability from the screening visit is also shown.

The dry eye group showed improved wettability after the lenses had been inserted for 15 minutes than the wettability observed with their habitual lenses. In participants #3, #8 & #20 the improvement in wettability seen at 15 minutes did not persist to the same extent after 1 hour of study lens wear. (Table 5-11)

Unlike in the normal group, the dry eye group showed a trend to increasing RMS over the measurement acquisition period with the study lenses. In both visits, the width of the

confidence interval did not differentiate between the two groups without contact lenses, but it showed a difference when the measurements were obtained with study lenses. (Figure 5-10**)**

ID	Average RMS (±SD)	Average RMS CI Width (±SD)	Change in NITBUT from screening
Normal group	(µm)	(µm)	(Sec)
10	0.48±0.01	0.023±0.010	-3.88
12	0.59±0.06	0.062±0.081	-2.87
14	0.44±0.004	0.002±0.002	-1.23
15	0.82±0.45	0.822±1.335	1.88
16	0.44±0.49	0.051±0.029	-1.25
18	0.45±0.01	0.031±0.010	1.47
Dry eye group			
3	0.56±0.04	0.067±0.019	0.26
4	1.21±0.75	0.251±0.719	0.97
5	0.60±0.13	0.058±0.066	-0.63
7	0.44±0.08	0.100±0.208	0.80
8	0.47±0.02	0.030±0.022	-0.84
20	0.50±0.02	0.025±0.010	2.35

Table 5-10: Average RMS and confidence interval (CI) width of the RMS for each study participant without contact lenses at the first visit. Positive change in NITBUT indicates a longer NITBUT at Visit 1(OD)

Groups	SID	Average RMS (µm) (±SD)	Average RMS CI Width (µm) (±SD)	Change in lens wettability after 15 mins	Change in lens wettability after 1 hour	Change in average NITBUT¶ after 15 mins (sec)	Change in average NITBUT¶ after 1 hour (sec)
Normal group	10	0.47±0.013	0.024±0.009	0.25	0.75	-0.02	-3.61
	12	0.84±0.065	0.052±0.020	0.50	2.75	0.66	-2.51
	14	0.44±0.008	0.015±0.005	0.00	0.50	-2.67	-2.37
	15	1.24±0.115	0.224±0.087	0.25	0.50	-4.31	-4.23
	16	0.36±0.080	0.067±0.095	0.25	0.75	-2.31	0.30
	18	0.47±0.034	0.067±0.044	0.00	0.25	-0.23	-1.43
Dry eye group	3	0.47±0.05	0.147±0.075	-2.25	-0.25	1.41	1.25
	4	1.48±0.36	0.574±0.249	-0.50	-0.25	-0.58	0.10
	5	0.56±0.04	0.217±0.279	-2.00	-2.00	-0.43	0.12
	7	0.47±0.16	0.089±0.098	0.25	0.50	1.37	-0.14
	8	0.47±0.16	0.078±0.104	-1.50	0.00	-3.03	-3.01
	20	0.42±0.04	0.071±0.029	-2.50	-1.25	2.78	0.78

Table 5-11: Average RMS and confidence interval (CI) width of the RMS for each study participant with contact lenses at the first visit (OD). Positive change in wettability indicates that the wettability is worse at Visit 1 with the study lenses. Positive change in TBUT indicates a longer NITBUT at Visit 1

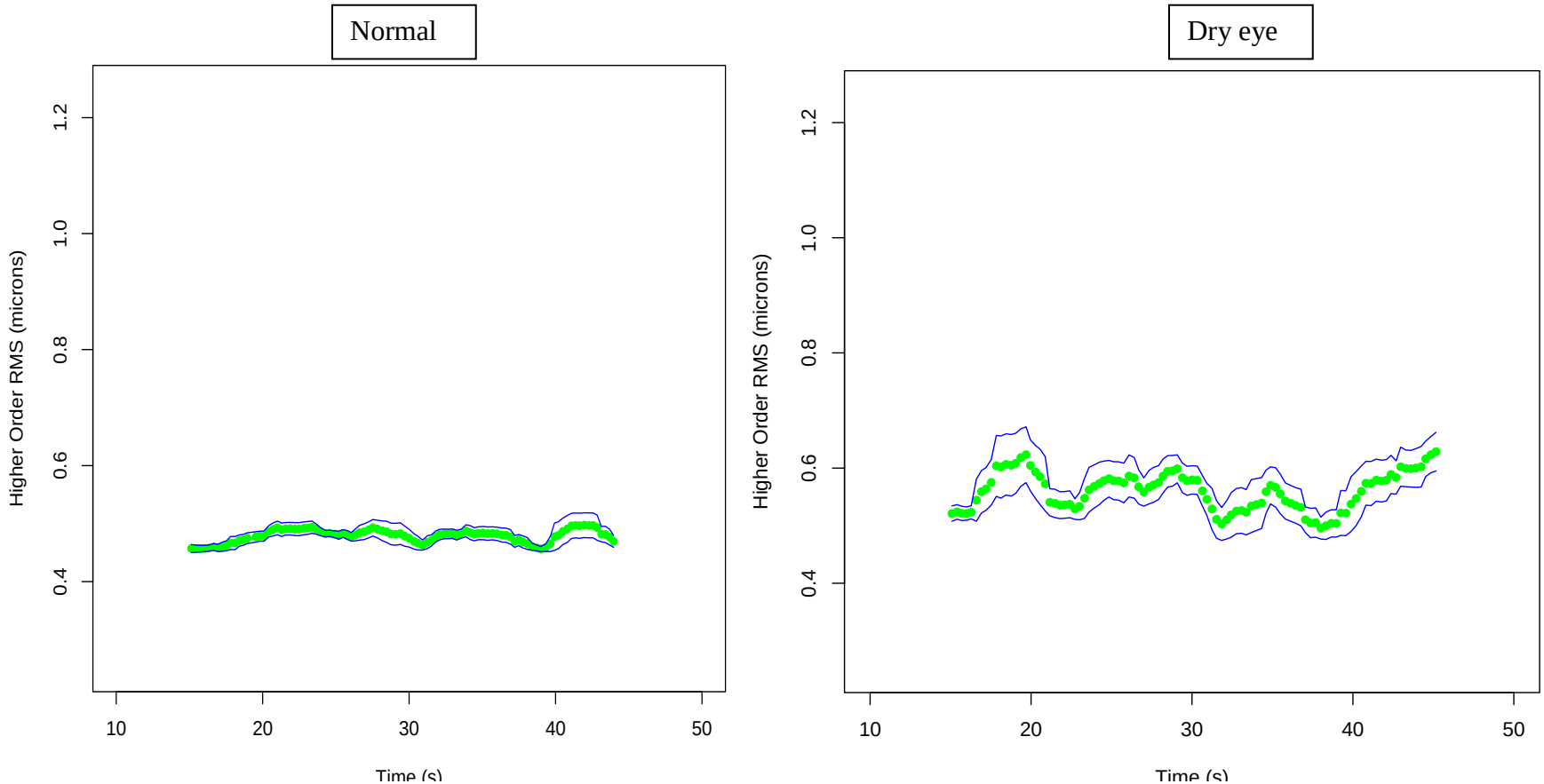

Figure 5-9: Representative scatter plot of smoothed HOA RMS (green dots) with CI (blue lines) of a normal and dry eye participant.

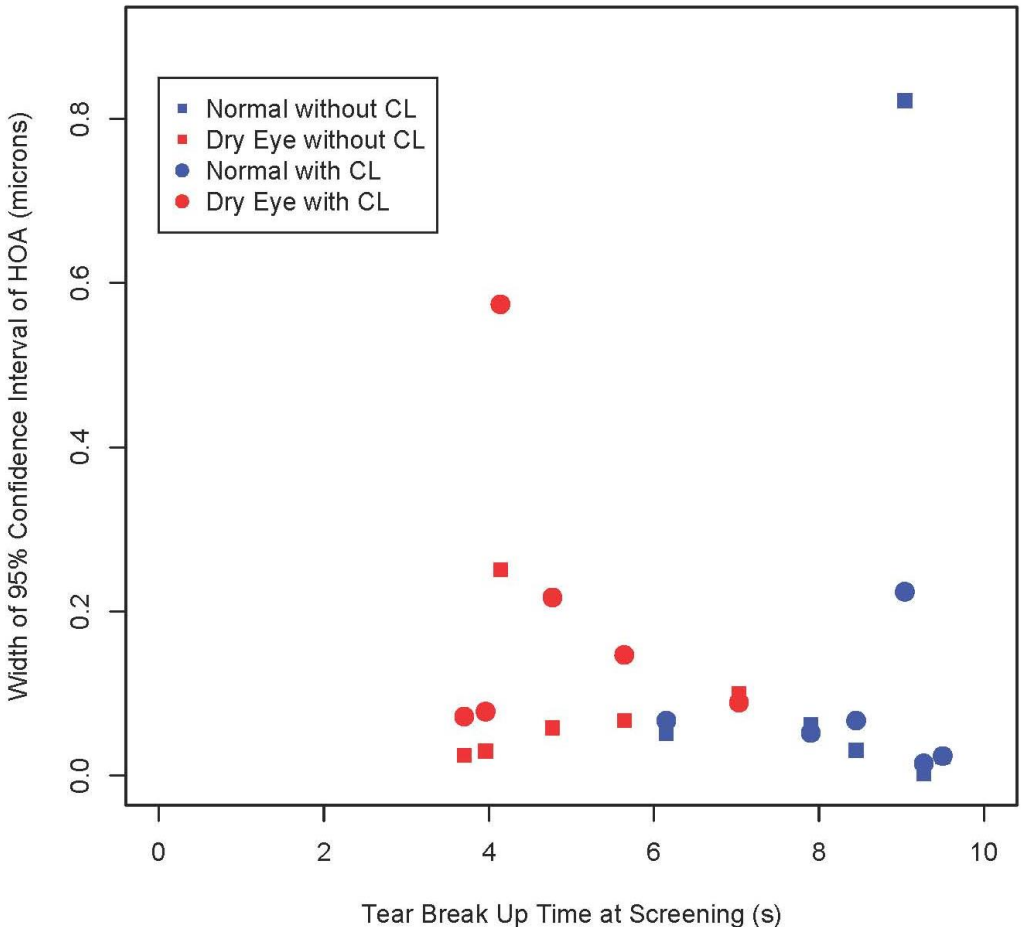

Figure 5-10: Average CI width for normal and dry eye participants with and without contact lenses as a function of tear break-up time in the natural blinking paradigm.

5.5.5 Comparison of aberrations between groups – Forced blink

Data were also obtained without and with contact lenses, where the blinking was regimented. Subjects were instructed to blink every 8s. This procedure was intended to allow investigation of the within-blink dynamics. In the CA-100F, the blink is not identified in the output data of the instrument.

However, due to the forced blink paradigm, the approximate position of the blinks were identified and the data between two forced blinks (an epoch) was used to determine the slope of the data (RMS per unit time). In addition, the minimum and maximum values within each

epoch were determined. Examples of the analysis in a normal and a dry eye participant are shown in Figure 5-11.

5.5.5.1 RMS - Normal participants:

Table 5-12 shows the blink characteristics for the normal participants with and without a contact lens in place. It can be seen that in all conditions, the slope of the RMS in the blink epoch is very shallow (excepting subject #14 without a contact lens). The maximum and minimum values did not illustrate the same trend, but this might be expected, as outliers in the data more heavily influence the trend.

5.5.5.2 RMS - Dry eye participants:

Table 5-13 shows the blink characteristics for the dry eye participants with and without a contact lens in place. It can be seen that in all conditions, the slope of the RMS in the blink period is considerably higher (~4x) than in the dry eye group, in both the without CL (*t*-test, p=0.001) and with CL (*t*-test, p=0.000) conditions. The large positive slope indicates that the RMS aberrations increase from beginning to end of the blink period. Again, the maximum and minimum values did not illustrate the same trend.

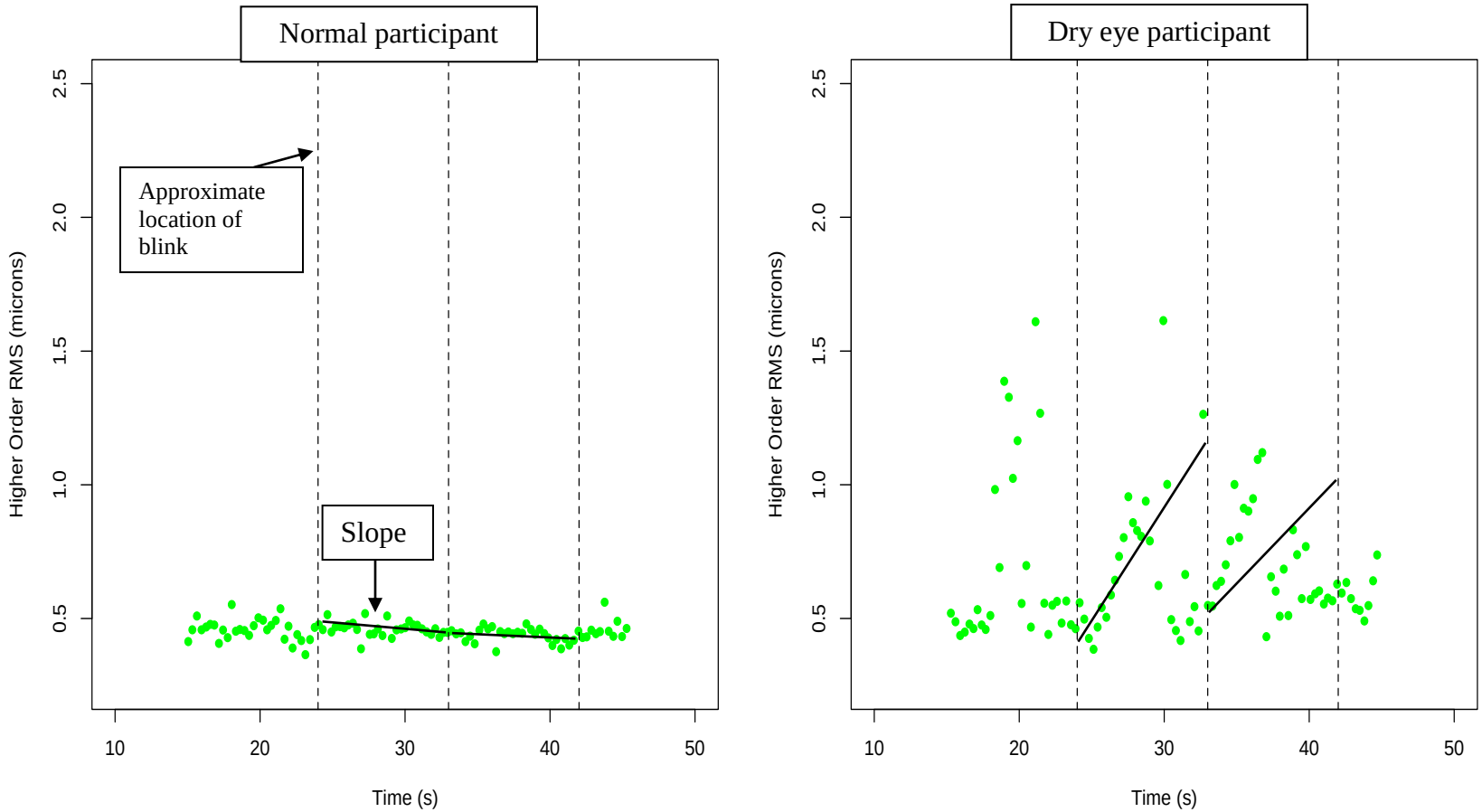

Figure 5-11:Slope of the RMS within a blink illustrated for an normal participant (#18; left) and a dry eye participant (#3; right) without a contact lens in place in the forced blink paradigm. The line was fitted to all the data but for ease of comparison, the scale of y-axis was kept constant.

SID		Time point	#10	#12	#14	#15	#16	#18
WITHOUT CL	Min RMS (µm)	24-32	0.53221	0.53318	0.51257	0.43925	0.34578	0.38699
		32-40	0.56831	0.57435	0.53243	0.38889	0.36871	0.37593
	Max RMS (µm)	24-32	0.66902	0.88661	0.95685	0.67755	0.79521	0.51849
		32-40	0.71507	0.9457	0.89074	0.76097	0.71655	0.48018
	Average Slope		**0.03387**	**-0.5711**	**1.85874**	**-0.1078**	**0.36969**	**-0.6297**
	(Max-Min) RMS (µm)	24-32	**0.13681**	**0.35343**	**0.44428**	**0.2383**	**0.44943**	**0.1315**
		32-40	**0.14676**	**0.37135**	**0.35831**	**0.37208**	**0.34784**	**0.10425**
WITH CL	Min RMS (µm)	24-32	0.48663	0.48462	0.52413	0.38641	0.53568	0.35421
		32-40	0.45179	0.45898	0.54598	0.38125	0.42864	0.36478
	Max RMS (µm)	24-32	0.55041	0.76758	0.64993	1.14037	1.31699	0.7345
		32-40	0.56672	0.74514	0.66923	2.51626	0.69145	0.91773
	Average Slope		**0.06122**	**0.18288**	**-0.0747**	**-0.5734**	**0.31471**	**-0.5645**
	(Max-Min) RMS (µm)	24-32	**0.06378**	**0.28296**	**0.1258**	**0.75396**	**0.78131**	**0.38029**
		32-40	**0.11493**	**0.28616**	**0.12325**	**2.13501**	**0.26281**	**0.55295**

Table 5-12: Blink characteristics for the normal group with and without a contact lens in place in the forced blink paradigm. The data in the table shows the minimum and maximum RMS value within each blink, the average slope of the RMS for the two blinks, and the difference between the maximum and minimum RMS with each blink

SID		Time point	#3	#4	#5	#7	#8	#20
WITHOUT CL	Min RMS (µm)	24-32	0.38467	0.89869	0.49315	0.40044	0.46735	0.4257
		32-40	0.43169	0.68009	0.47205	0.40618	0.45647	0.5057
	Max RMS (µm)	24-32	1.6138	1.54934	0.64628	0.51829	1.02539	1.34333
		32-40	1.26351	1.84161	1.05169	0.52371	0.9194	3.59292
	Average Slope		***2.44990***	***1.26680***	***2.07211***	***2.47948***	***2.16492***	***2.14731***
	(Max-Min) RMS (µm)	24-32	***1.22913***	***0.65065***	***0.15313***	***0.11785***	***0.55804***	***0.91763***
		32-40	***0.83182***	***1.16152***	***0.57964***	***0.11753***	***0.46293***	***3.08722***
WITH CL	Min RMS (µm)	24-32	0.25426	0.38558	0.35333	0.35919	0.47311	0.51786
		32-40	0.32264	0.38949	0.43651	0.33463	0.51356	0.50703
	Max RMS (µm)	24-32	0.70333	0.64433	0.83961	0.72834	0.82613	0.86763
		32-40	0.65233	0.90418	0.85372	0.54033	0.93469	0.82004
	Average Slope		***3.46681***	***2.58041***	***2.53216***	***2.88259***	***2.02702***	***1.95143***
	(Max-Min) RMS (µm)	24-32	***0.44907***	***0.25875***	***0.48628***	***0.36915***	***0.35302***	***0.34977***
		32-40	***0.32969***	***0.51469***	***0.41721***	***0.20570***	***0.42113***	***0.31301***

Table 5-13: Blink characteristics for the dry eye group with and without a contact lens in place in the forced blink paradigm. The data in the table shows the minimum and maximum RMS value within each blink, the average slope of the RMS for the two blinks, and the difference between the maximum and minimum RMS with each blink

5.5.5.3 Width of confidence interval

The average confidence interval width was examined for the forced blinking paradigm. In the natural blinking paradigm, the width of the confidence interval was not different between the two groups (dry eye & normal) without a contact lens in place, but showed a relative shift towards higher RMS in the dry eye group with the contact lens. In the forced blinking paradigm, a similar relationship was seen. In this case, however, the normal group exhibited a higher range of RMS aberrations without the contact lens in place. This may have been because the 8-second interval between blinks was longer than their typical inter-blink interval, leading to greater variability at the end of the blink interval than with the natural blinking paradigm. Nevertheless, with the contact lens in place, the dry eye group tended to show a shift towards higher RMS aberration values, whereas the normal group did not.

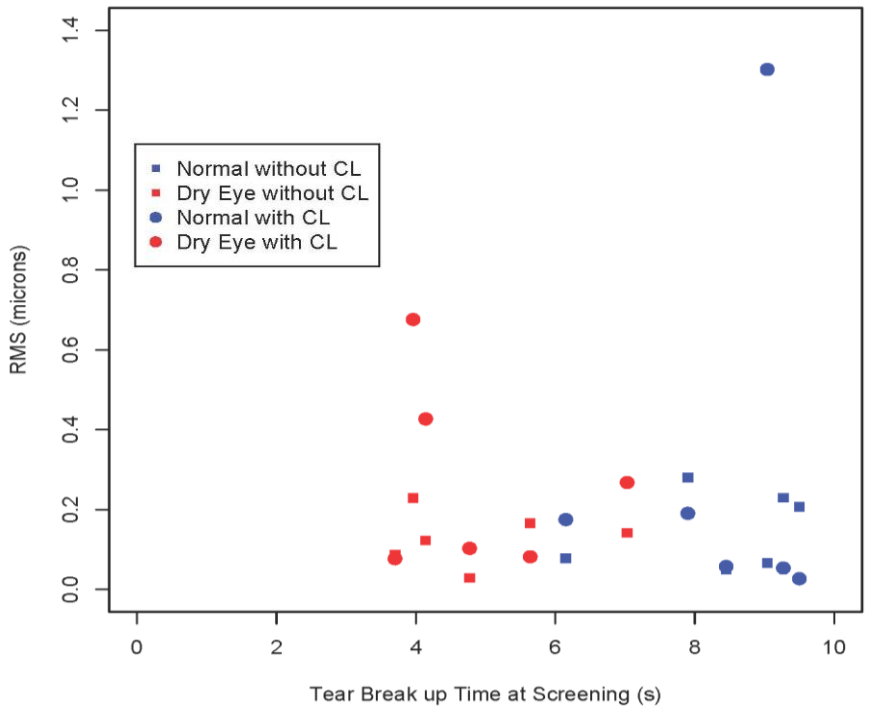

Figure 5-12: Average CI width for normal and dry eye participants with and without contact lenses as a function of tear break-up time in the forced blinking paradigm.

5.6 Discussion

5.6.1 Analysis of target area with head position

There was no significant difference in the size of the target areas or the number of complete rings projected onto the cornea with 10° or 20° of head turn when compared to the straight-ahead position. Thus, this study concludes that the straight-ahead position is optimal for image acquisition with this anterior surface aberrometer.

5.6.2 Comparison of natural & forced blink paradigms

The forced blink paradigm introduced greater variability into the data. However, with the CA100, the forced blink paradigm was the only mechanism by which blink dynamics could be evaluated. The CA100 device deletes identified blink data from the instrument data set and does not export the location of the blink from the device. However, the newer CA200 does keep all of the blink data and allows the blink location to be determined both in forced and natural blinks paradigm. Given that blink dynamics does appear to differentiate between the groups in this pilot study, the newer device would be the preferred device for surface aberration capture.

5.6.3 Comparison of aberrations between groups

In the forced blink paradigm, the slope of the RMS within a blink was different between the normal and dry eye groups, irrespective of whether a contact lens was in place or not. This analysis could not be determined for the natural blink condition, as there were no tools to identify the location of the blink in the data with any accuracy once it had been processed by the CA100 device (the device removes the blink from the raw data). On average, the dry eye

group exhibited a trend of increasing RMS higher order aberrations over each blink period. This trend was consistent despite the clinical evaluation of wettability showing an improvement with the study lenses from the wettability with the subject's habitual lenses at the screening appointment.

5.6.4 Comparison of aberrations with & without contact lenses

The width of the confidence interval around the smoothed raw data was investigated between groups (normal versus dry eye) and for condition (without a contact lens or with a contact lens). While the width of the confidence interval in the natural blink condition was not different between groups without a contact lens, the dry eye group showed a shift towards a greater magnitude of higher order aberrations with the contact lens in place. The same shift was not observed in the normal group. A similar relationship was also observed in the confidence interval width for the forced blink paradigm.

5.7 Conclusion

i. Obtain data in the straight-ahead position, as there is no significant increase in target size with head turn.

ii. With the CA100F, the forced blink paradigm is preferred as this enables blink dynamics to be examined. With the CA200F, either forced or natural blink paradigms are interpretable for tear dynamics.

iii. Differentiation between dry eye and normal groups was best determined with the slope of the RMS aberrations within a blink.

iv. Differentiation between performance with and without a contact lens in the dry eye and normal groups was best determined by analysing the width of the confidence interval of the moving average.

Chapter 6 : Analysis of Dynamic Ocular Surface Aberrations Using Segmented Linear Regression

6.1 Background:

The mechanism of tear thinning is debated frequently, due to its importance in the diagnosis of dry eye and the exact mechanism remains unknown, due to limitations in imaging techniques. Earlier studies have shown the thinning of the tear film is caused by divergent tangential flow of the tears or a combination of tangential flow and evaporation.[73,74] More recent studies using fluorescent quenching have shown that tear thinning is caused only by evaporation rather than by divergent tangential flow or a combined effect.[14,15] They observed a uniform thinning in the tear thickness and variable fluorescent decay between high and low concentration of the fluorescein which is indicative of mechanism to be evaporative.[14]

Even though the fluorescent quenching technique is able to differentiate between the evaporative and tangential flow theories, its repeatability is still under investigation and the test itself is invasive in nature. The instillation of fluorescein changes the physical properties of the tear film, therefore changes the quality of the tear film and the repeatability of the tear breakup time measurements.[13,20,75]

Studies by Montes-Mico et al[42] using dynamic corneal surface aberrations have shown that the tear film breakup can be studied non-invasively. Using the corneal topographer, the corneal elevations were obtained every second of a 10 sec open-eye interval. The elevation data were then used to calculate the higher order RMS and individual prism coefficient values

for each time point. The average for all the participants in their study produced a wave like pattern over time,[37,41,42] the time course of which showed high aberration values immediately after the blink, followed by an approximately linear decrease in aberrations. After the lowest point (trough in a wave) the aberrations again increased in a linear way and the authors considered this inflection point as the breakup point of the tear film.[37,41,42]

Later, Zhu [76] showed that the vertical prism Zernike coefficient of the aberrations can be directly attributed to tear film thickness, since the tears flow vertically after the blink and proposed that analysis of the vertical prism component of aberrations gives more insight about the change in the tear film thickness. Using both the theories suggested by Montes-Mico et al. and Zhu, this study aims to study the change in tear film thickness over time using the prism coefficient and higher order aberrations. This study also aims to provide an objective method to analyse the tear film changes over time of anterior surface aberrations.

6.2 Objectives:

The purpose of this study was

1. To evaluate a new method of analyzing dynamic ocular surface aberrations using segmented liner regression

2. To evaluate the inter-ocular characteristics of the dynamic ocular surface aberrations using the segmented linear fits

6.3 Methods

Seventeen (11 men and 6 women) asymptomatic, non-contact lens users were included in this study, of which one participant discontinued from the study and 4 participants' data were not able to be extracted and/or analysed. The average age group of the participants involved in this study was 27.5 ± 3.3 years of age. Non-invasive tear breakup time (NITBUT) and dynamic corneal surface aberrations were measured during the study visit. The Atlas Corneal Topographer was used to measure NITBUT and the Topcon CA200 Corneal Analyser was used to measure dynamic corneal surface aberrations. NITBUT was measured before the aberration measurements and the order of the eye measured first was randomized across the participants (see Table 6-1). In each eye, three measures of NITBUT were obtained and the average of all three measures was considered for analysis. In this study, NITBUT for each participant ranged between 5.4s and 11.5s, with a mean of 7.3s in the right eye and 7.5s in the left eye, respectively.

The Topcon CA200 corneal analyser uses the Placido disc principle to measure corneal surface aberrations and dynamic measurements were obtained at a frame rate of 24Hz. Similar to NITBUT, the order of the eye measured first was randomized across participants. The time between two consecutive blinks was considered as an open-eye interval and the aberration measures were obtained for two 15-second open-eye intervals. The inbuilt software identified the location of the blinks automatically during the analysis. Participants were asked to hold their eyes open during the open-eye measurement period. A recovery period of 10 minutes was provided between the tests to maintain the tear film in as near normal condition. The aberration measures were calculated for a 6mm pupil diameter.

The instrument provides the corneal aberrations in terms of Zernike polynomials up to the 7^{th} order. Total higher order aberrations (HOA) were calculated as the root-mean-square (RMS) of Zernike coefficients from the 3^{rd} to 7^{th} orders for each frame captured on an open-eye interval were considered for analysis. The prism terms of Z^{-2}_2 and Z^{2}_2 were also separately considered.

The measurements obtained using the Topcon software were exported to a Microsoft Excel datasheet and evaluated using scatter plots. The scatter plot of the extracted raw data showed a variable amount of noise or variation within the extracted data. For better understanding of the data and to reduce noise, the data were subjected to a smoothing procedure (Figure 6-1), as described in Chapter 5.4.

A segmented linear regression was fitted to the smoothed data for each interval of eye-opening using the 'segmented' package in the R statistical program. In all cases, this procedure fitted 3 segments (phase1, phase2, and phase 3) (see Figure 6-2). The phases were denoted by two automatically determined breakpoints. The breakpoints are the location at which there is significant change in the observed trend. For each breakpoint, the slope associated with the trend in the data prior to the breakpoint was calculated. Each phase was assumed to denote a distinct stage in the stability of the tear film.

The segmented fits were reviewed and the blink with the best fit for each of the right and left eye was selected. The initiation of the first positive slope ('positive slope'; i.e. the point at which the ocular surface exhibited increasing aberration magnitudes) and the time point after the blink at which this occurred ('break point') were identified for each vertical prism and HOA RMS measurements.

Subject ID	TBUT 1	TBUT 2	Aberrometry 1	Aberrometry 2
1	OS	OD	OD	OS
2	OD	OS	OD	OS
3	OS	OD	OD	OS
4	OD	OS	OS	OD
5	OD	OS	OD	OS
6	OD	OS	OD	OS
7	OD	OS	OS	OD
8	OS	OD	OS	OD
9	OS	OD	OS	OD
10	OS	OD	OS	OD
11	OS	OD	OD	OS
12	OS	OD	OS	OD
13	OD	OS	OS	OD
14	OS	OD	OD	OS
15	OD	OS	OD	OS
16	OS	OD	OS	OD
17	OS	OD	OS	OD

Table 6-1: Randomization table for NITBUT and aberration measures

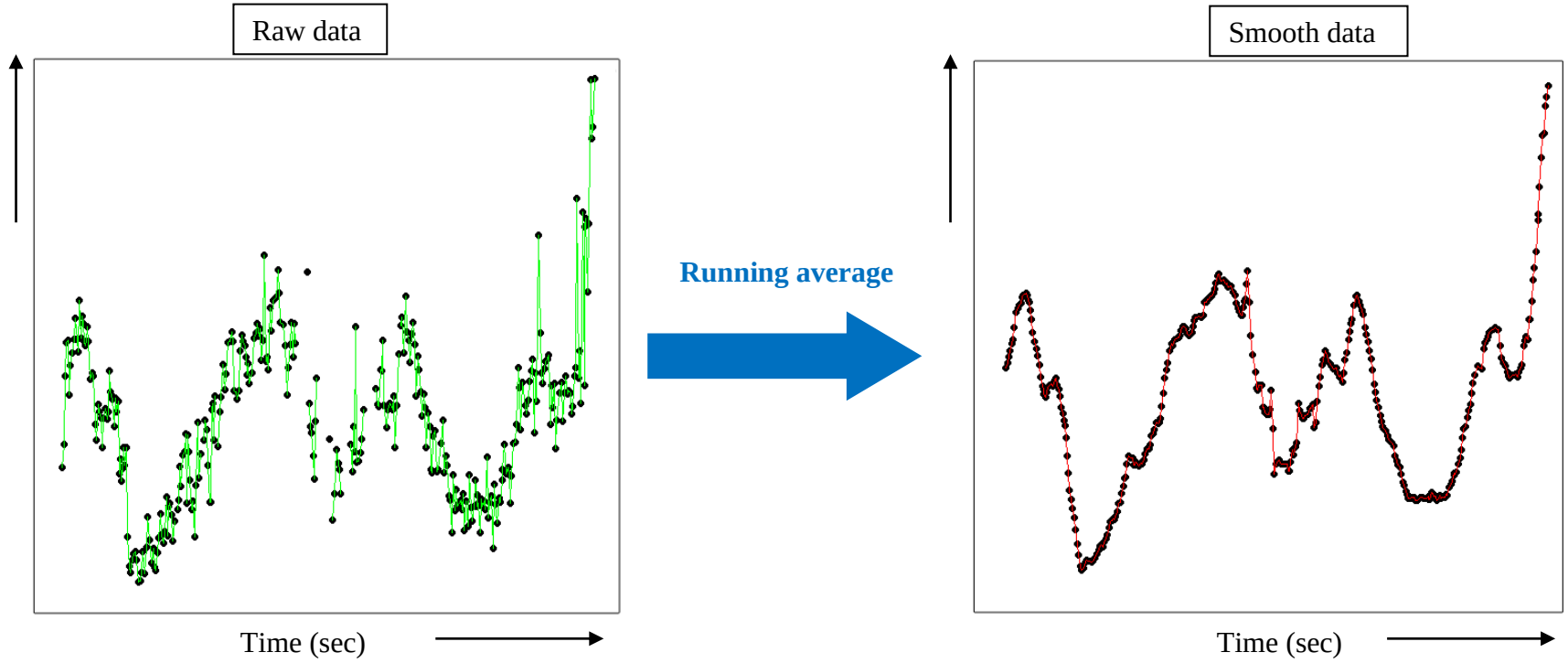

Figure 6-1: Schematic representation of a raw and smoothed data (using running average procedure) across the two open-eye intervals. The procedure is described in Chapter 5.4

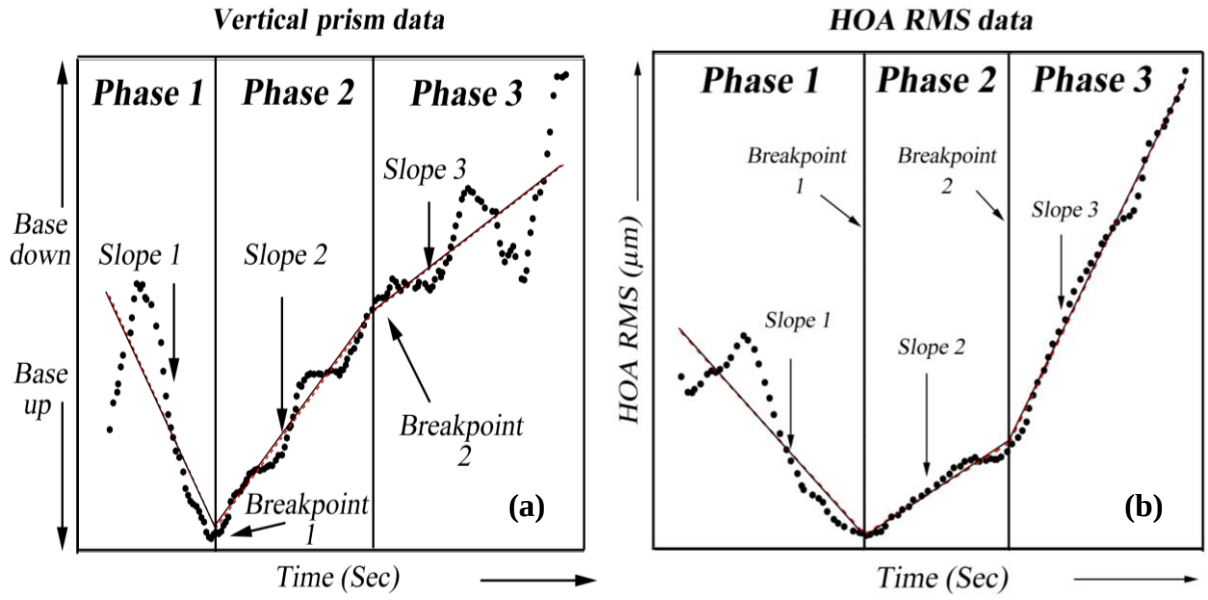

Figure 6-2: Schematic representation of the dynamic (a) vertical prism and (b)HOA RMS data of a segmented linear regression. The X-axis represents the time in second and the Y-axis represents the change in direction of the tear prism base in figure (a) and increase in RMS in figure (b).

6.4 Data analysis:

All the data from the CA200 corneal topographer were exported and stored as comma separated value (.CSV) files for further analysis. The data smoothing process and the segmented linear regression analysis were performed using R statistical program.[46]

The overall analysis of the group was analysed using repeated measures ANOVA with factors of eye (OD/OS), open-eye intervals (1,2) and order (1st eye measured) for each of the segmented fit parameters. The segmented fit parameters used for the RM-ANOVA are the first and second breakpoints and the highest positive slope value after the first phase. The RM-ANOVA analysis was used to analyse the segmented fit parameter of both vertical prism and HOA RMS values. The RM-ANOVA was obtained using the Statistica (v. 11).[77]

Individual participant's data between segmented fit parameters of vertical prism and HOA RMS were analysed using linear regression. The variation in higher order RMS within the first two phases of segmented vertical prism data was analysed using non-parametric Wilcoxon signed rank test.

6.5 Results:

The average RMS, slope and breakpoints for vertical prism and HOA RMS are shown in Table 6-2.

	Vertical Prism (Z_1^{-1})		HOA RMS (3^{rd} to 7^{th} order)	
	OD Mean ± SD	OS Mean ± SD	OD Mean ± SD	OS Mean ± SD
RMS (µm)	-0.0042 ± 0.81	0.2714 ± 0.78	0.7611 ± 0.35	0.8152 ± 0.41
Highest positive slope after first phase	0.25 ± 0.37	0.22 ± 0.22	0.20 ± 0.26	0.23 ± 0.22
First break point (s)	4.4 ± 3.09	3.97 ± 2.97	2.87 ± 2.44	4.09 ± 3.24
Second Break point (s)	8.14 ± 3.07	7.15± 2.87	7.97 ± 2.87	8.36 ± 3.33

Table 6-2: Summary values for vertical prism and HOA aberrations, stratified by phase of the segmented fit.

6.5.1 Group analysis of segmented fit parameters for each factor of dynamic surface aberrations:

6.5.1.1 Vertical prism:

As expected, the location of the breakpoint 1 and breakpoint 2 were significantly different ($p<0.001$) between each other, between eyes, open-eye intervals and order of the measurements. The breakpoints were not significantly different ($p>0.05$) between eyes, open-eye intervals and order of the measurement. The first highest positive slope after the first breakpoint and the breakpoint corresponding to the start of the highest positive slope was obtained for each open-eye interval. RM-ANOVA of all other comparisons involving location of breakpoints and highest positive slope between individual grouping factors showed no significant difference ($p>0.05$).

The NITBUT was significantly different from the time of breakpoint 1 ($p<0.0001$) but not from the time of breakpoint 2 values ($p>0.05$) (Figure 6-3 and Figure 6-4). The correlation between the location of breakpoint 2 and the NITBUT values was not significant in all cases. The correlation between location of breakpoint 2 and NITBUT varied from -0.52/sec for left eye and open-eye interval 1 to a maximum of +0.27/sec for left eye and open-eye interval 2.

6.5.1.2 HOA RMS

Similar to the vertical prism values, the location of the breakpoints 1 and 2 were significantly different ($p<0.0001$) from each other between eyes, open-eye intervals and order of the measurements. The breakpoints were not significantly different ($p>0.05$) between eyes, open-eye intervals and order of the measurement

The first highest positive slope after first breakpoint and the breakpoint corresponding to the start of the highest positive slope was obtained for each open eye interval. RM-ANOVA showed the highest positive slope for the HOA RMS was, on average, higher in the second eye measured ($p= 0.0407$) and tended to occur later after the blink ($p= 0.0676$) (Figure 6-5 and Figure 6-6). All other analysis comparing the breakpoints and the highest positive slopes between individual grouping factors were not significantly different from each other (all $p>0.05$).

There was no significant difference between the time of breakpoint 2 and NITBUT values ($p> 0.05$) obtained initially (Figure 6-7 and Figure 6-8). Even though, ANOVA showed no significant difference between breakpoint 2 and NITBUT values, the correlation was found to be positive but low in the range of 0.02/sec to 0.2/sec. Similar results were obtained for correlation between eyes, between open-eye intervals and between orders of the measurements.

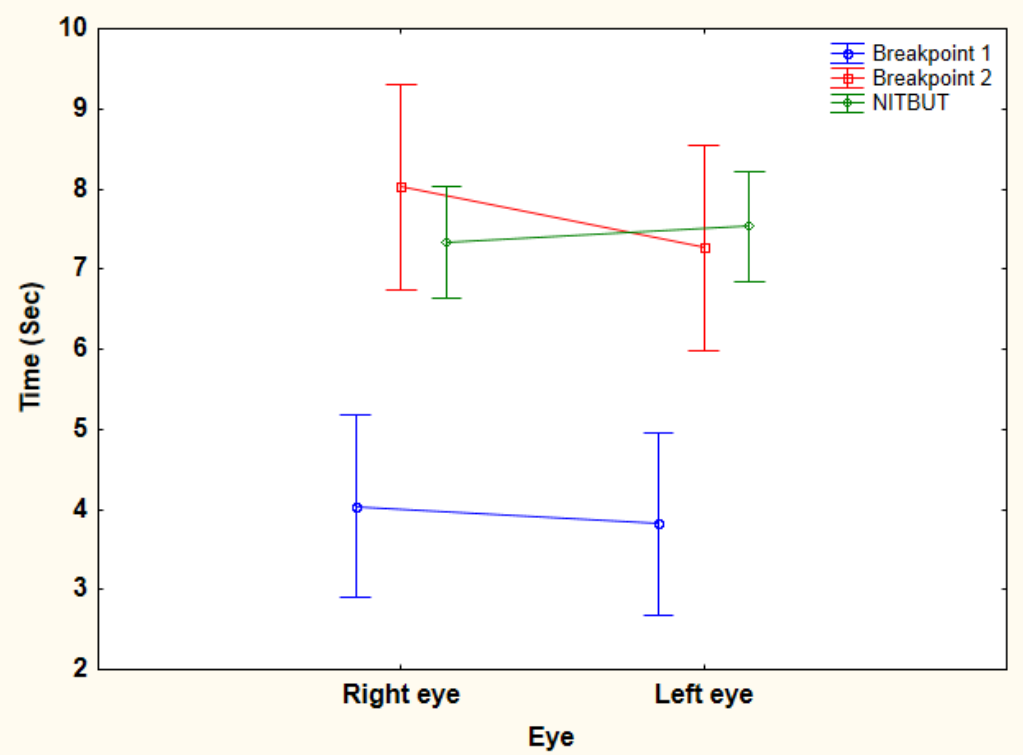

Figure 6-3: Comparison of location of the breakpoints and NITBUT values between eyes for vertical prism measures.

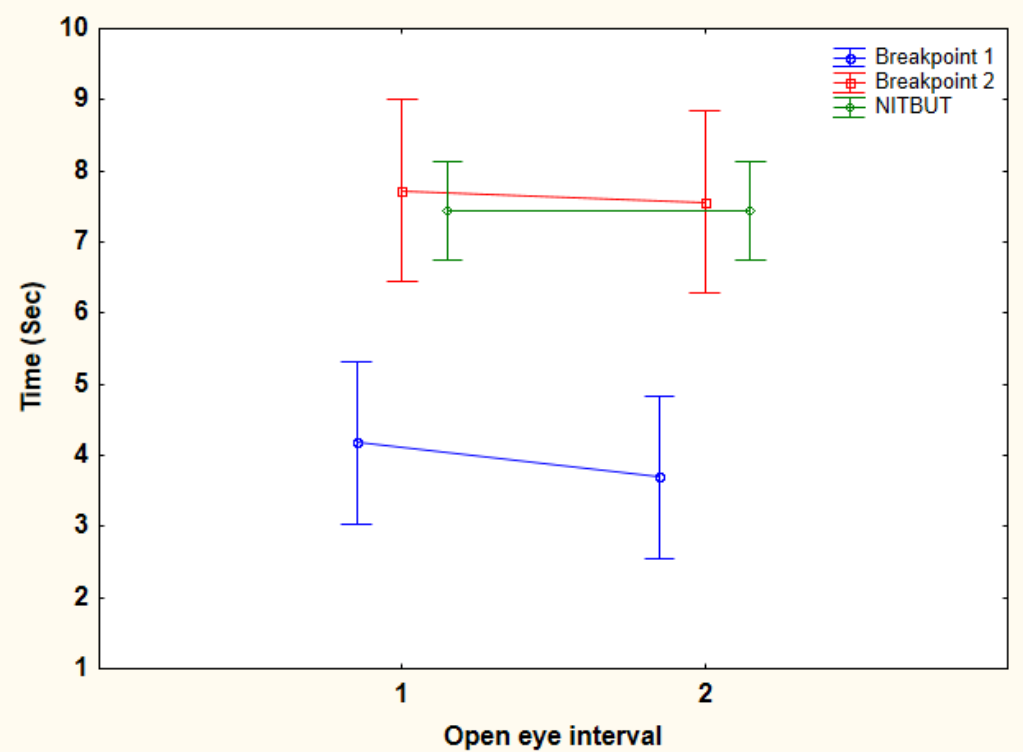

Figure 6-4: Comparison of location of the breakpoints and NITBUT values between open-eye intervals for vertical prism measures.

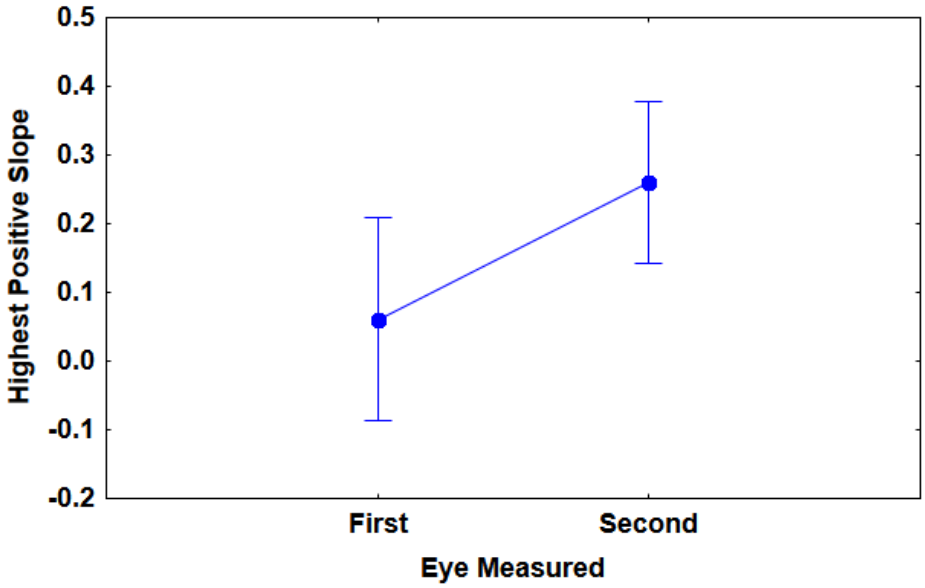

Figure 6-5: Relationship between highest positive slope and first eye measured for HOA RMS measures

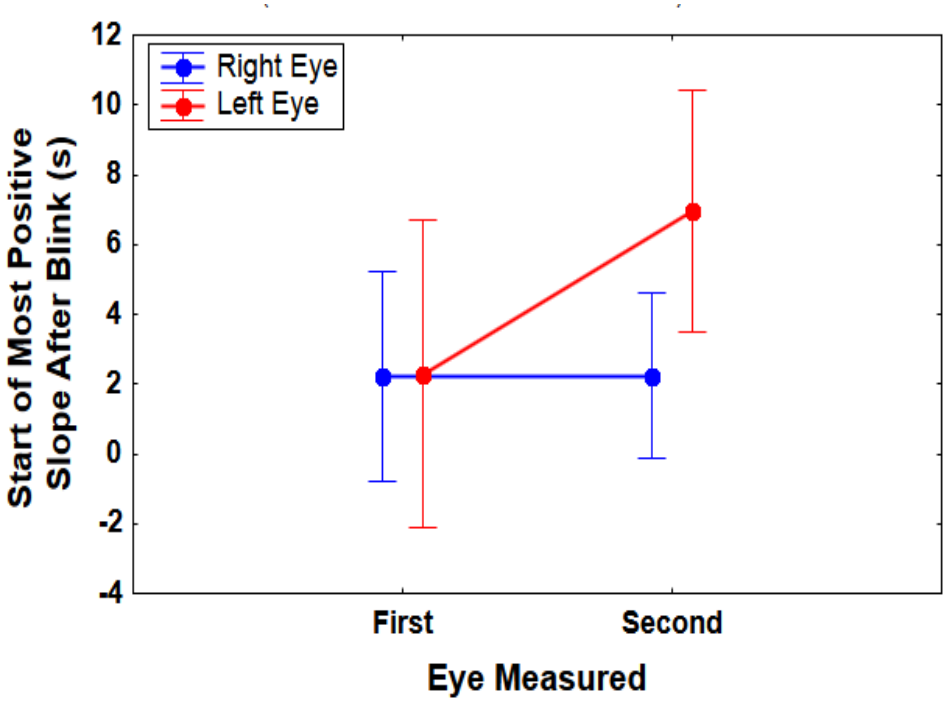

Figure 6-6: Relationship between the position of the breakpoint after the blink, the eye measured first and the eye

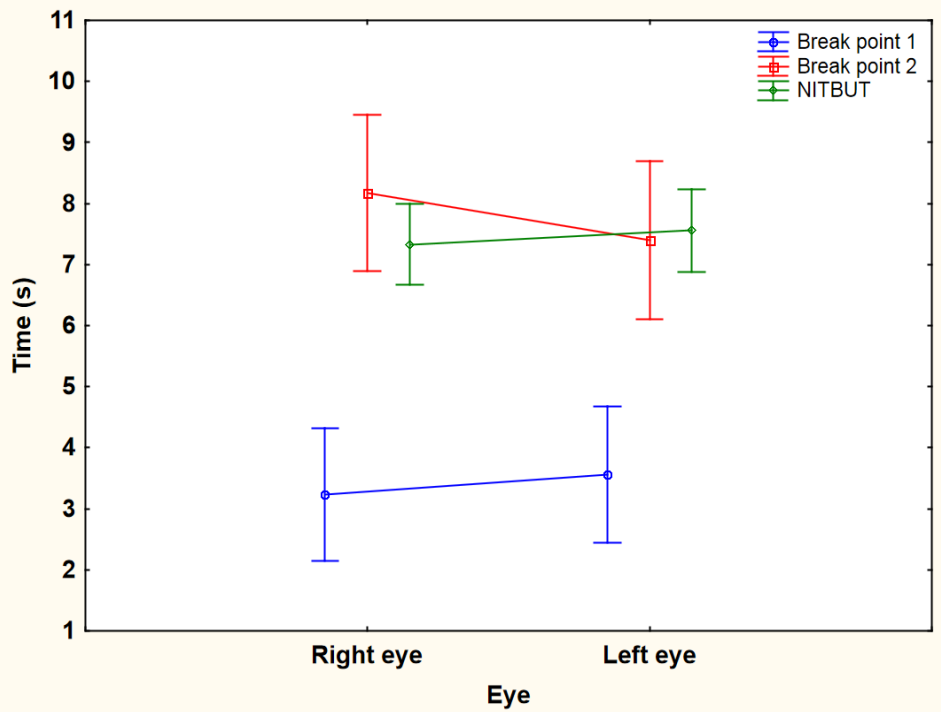

Figure 6-7: Comparison of location of the breakpoints and NITBUT between eyes for HOA RMS measures

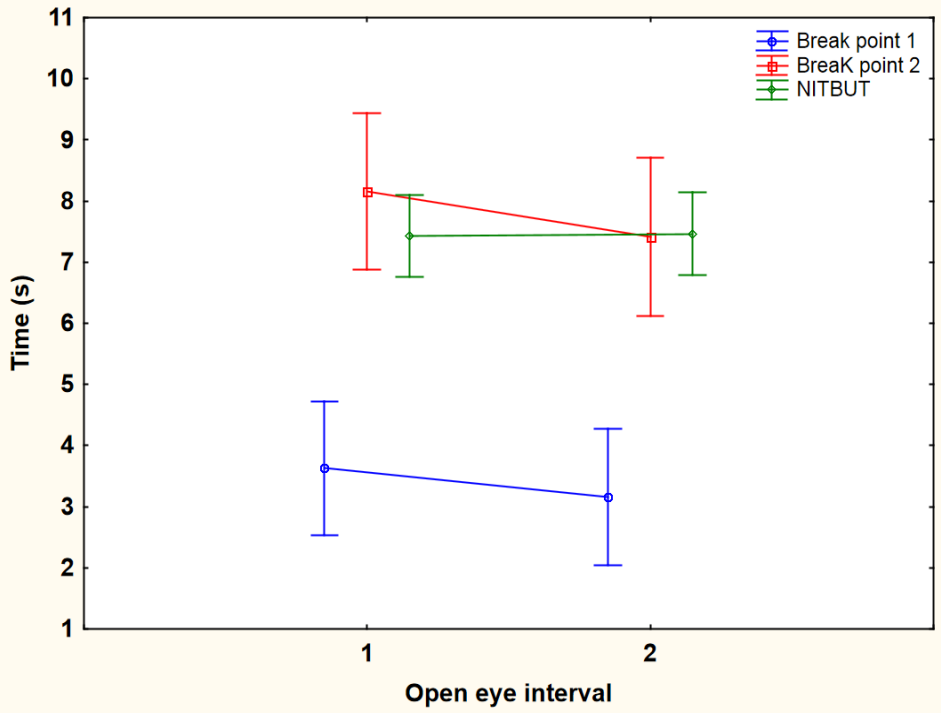

Figure 6-8: Comparison of location of the breakpoints and NITBUT between open intervals for HOA RMS measures.

6.5.2 Analysis of Individual participant data:

6.5.2.1 Vertical prism:

There was no significant difference in the location of the breakpoints between the two open-eye intervals using RM-ANOVA for the group ($p > 0.1$) (Top set of figures in Figure 6-9 and Figure 6-10). But, when individual data points were visually compared to analyse the trend in the data, a noticeable and consistent difference was observed between blink intervals, leading to a non-significant difference when analysed statistically.

The position of the breakpoint changes inversely between the open-eye intervals. This trend was observed consistently between eyes and breakpoints. The bottom set of figures in Figure 6-9 and Figure 6-10 shows the trend observed. The breakpoints of corresponding values between open-eye intervals are connected using individual lines colored according to trend observed. The green lines represent the upward trend and red represents a downward trend between the open-eye intervals.

The following trends were observed more consistently in our data; the values below the average value in the first open-eye interval tend to be higher than the average in the second open-eye interval. Similarly, the values which were higher than average in the first open-eye interval tend to be lower than the average in the second open interval, resulting in no significant difference between open-eye intervals.

6.5.2.2 HOA RMS:

Similar to the vertical prism data, the breakpoints between the two open-eye intervals were analysed. There was no significant difference in the location of the breakpoints between the

open-eye intervals using RM-ANOVA. However, when individual data were analysed, it followed trends similar to vertical prism data. Most of the values below the average of the first open-eye interval were higher in the second open-eye interval and vice versa. When compared to the vertical prism individual participant data, the observed trends of the HOA RMS data were similar and consistent (Figure 6-11 and Figure 6-12).

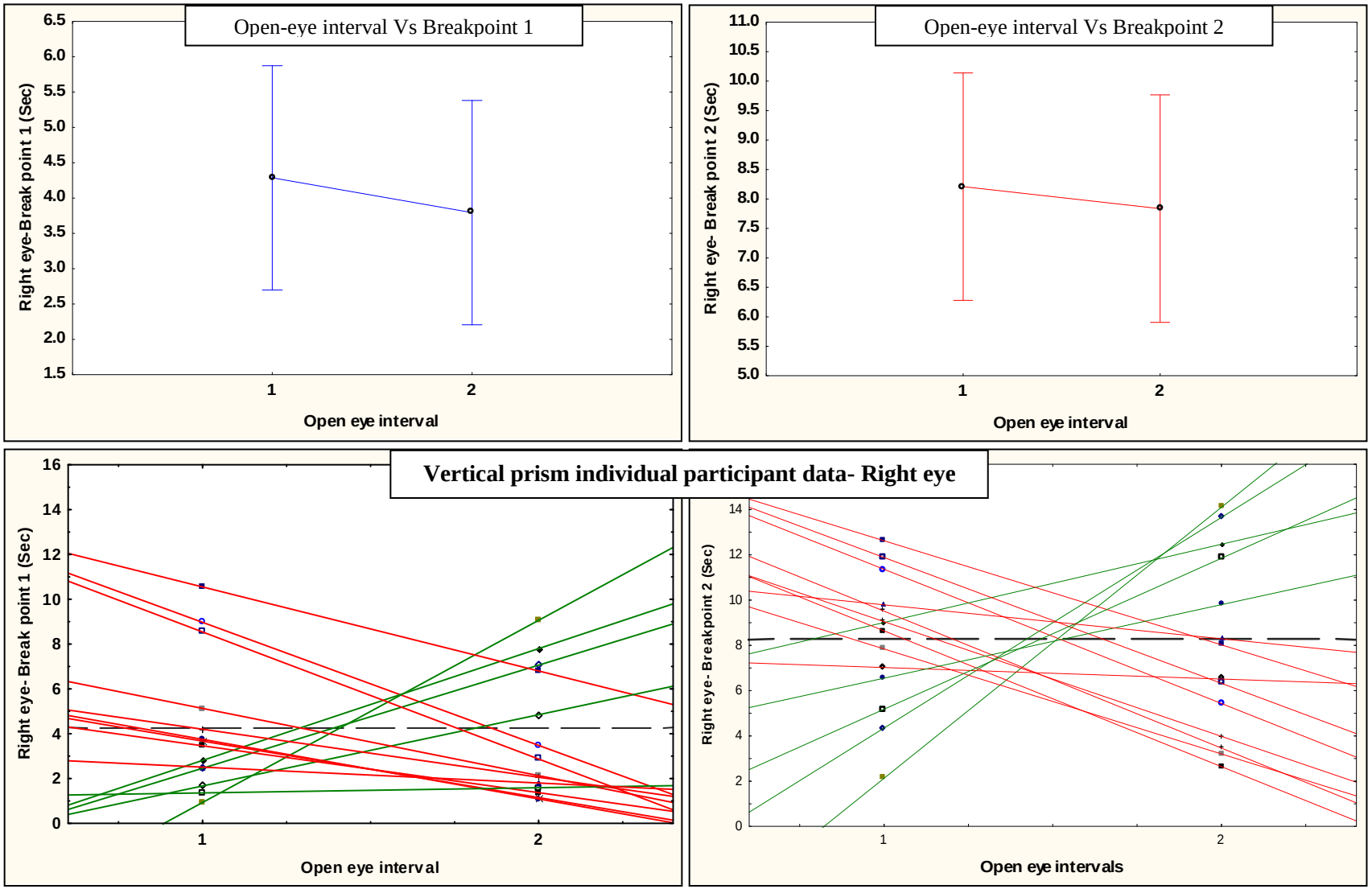

Figure 6-9: Comparison of breakpoints of right eye obtained from vertical prism data for each open-eye interval and the distribution of breakpoints between open-eye intervals. The left side graphs compares breakpoint 1 between open-eye intervals and the right side graphs compares the location of breakpoint 2 between open-eye intervals. Each line corresponds in the graphs below to a single participant data between open-eye intervals and green lines represents higher values in open-eye interval 2 compared to 1 , vice versa was denoted by red lines. The black dotted lines in the graphs below represent the mean of first open-eye interval.

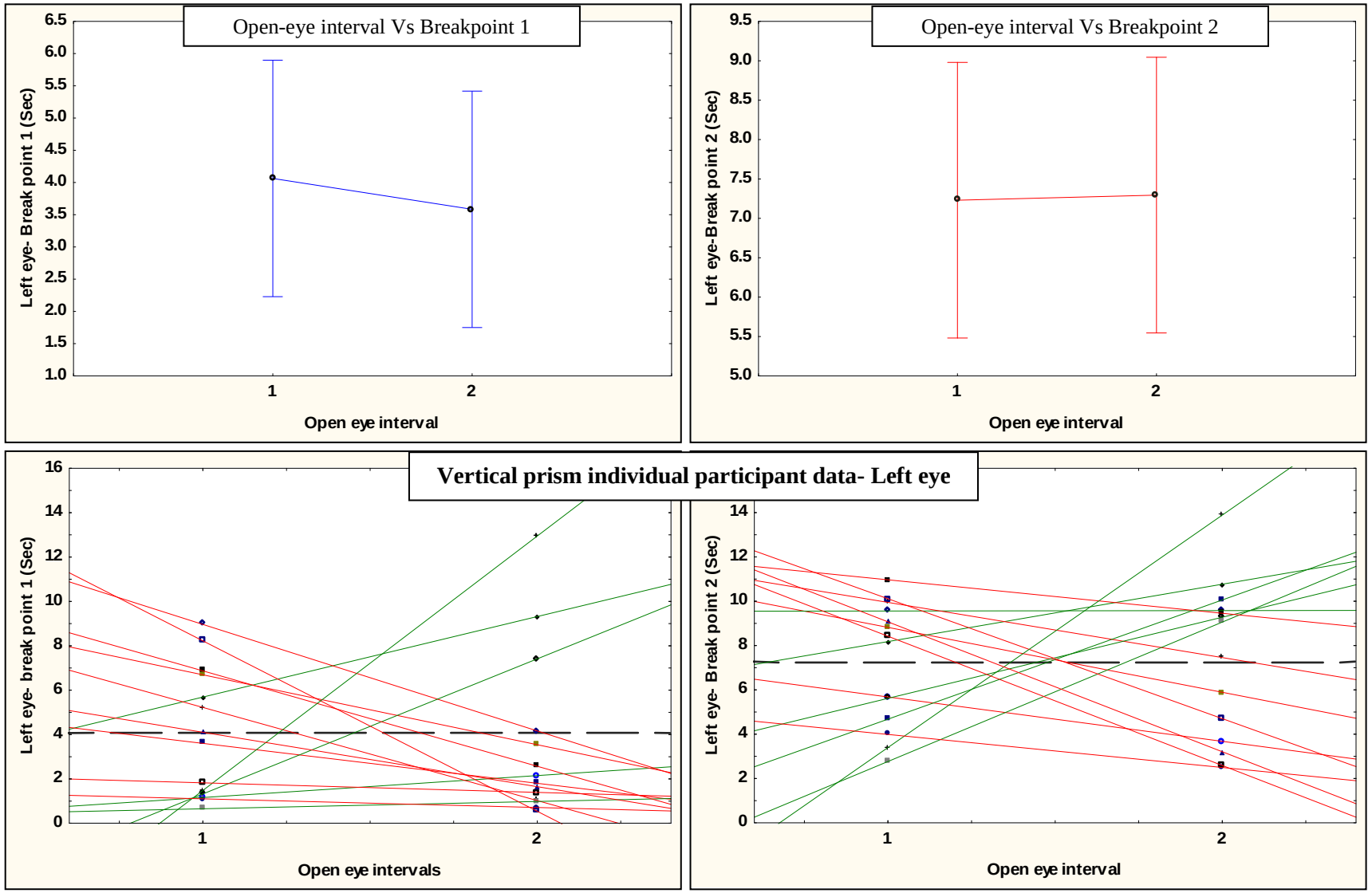

Figure 6-10: Comparison of breakpoints of left eye obtained from vertical prism data for each open-eye interval and the distribution of breakpoints between open-eye intervals. The left side graphs compares breakpoint 1 between open-eye intervals and the right side graphs compares the location of breakpoint 2 between open-eye intervals. Each line corresponds in the graphs below to a single participant data between open-eye intervals and green lines represents higher values in open-eye interval 2 compared to 1 , vice versa was denoted by red lines. The black dotted lines in the graphs below represent the mean of first open-eye interval.

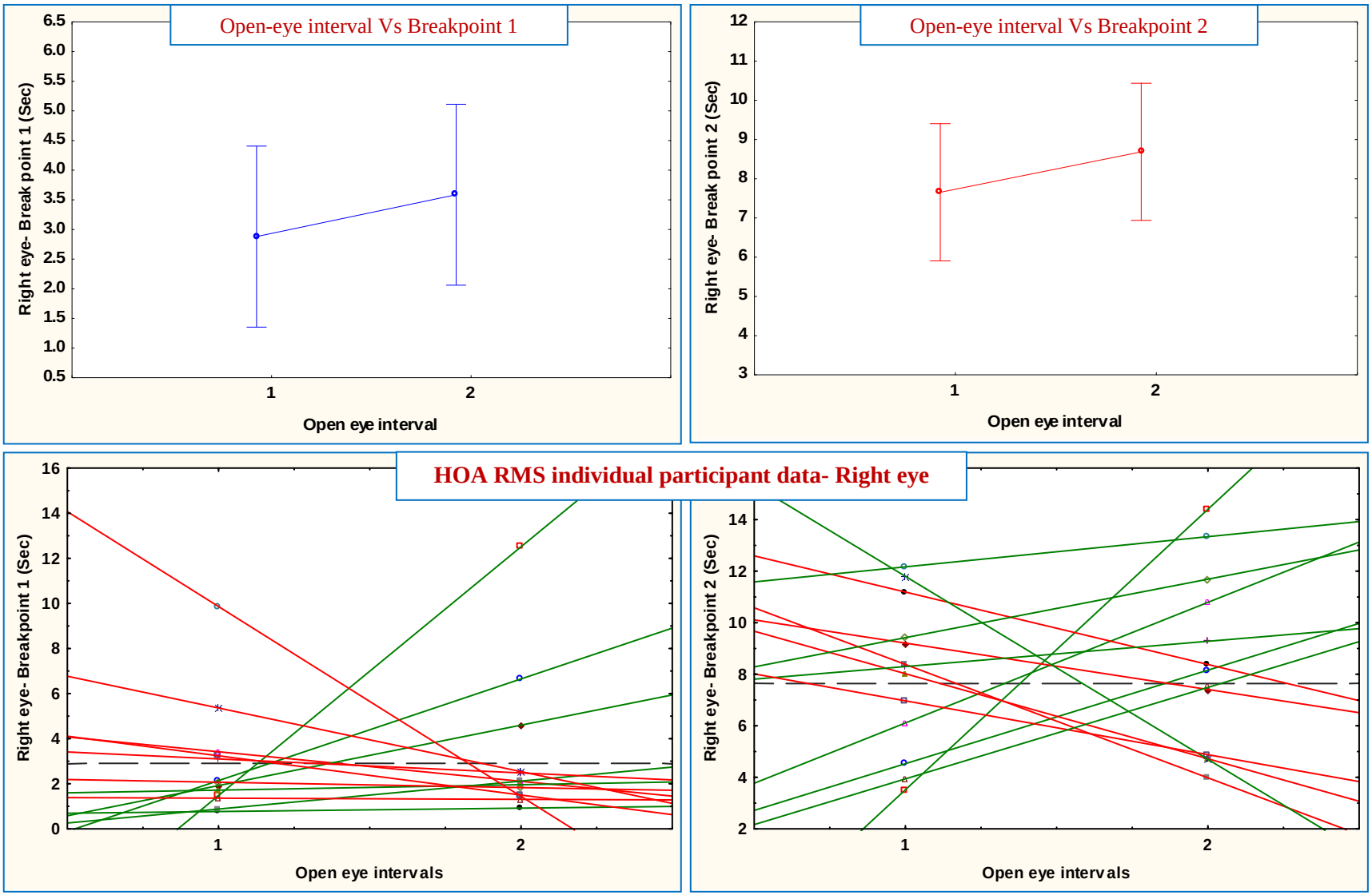

Figure 6-11: Comparison of breakpoints of right eye obtained from HOA RMS data for each open-eye interval and the distribution of breakpoints between open-eye intervals. The left side graphs compares breakpoint 1 between open-eye intervals and the right side graphs compares the location of breakpoint 2 between open-eye intervals. Each line corresponds in the graphs below to a single participant data between open-eye intervals and green lines represents higher values in open-eye interval 2 compared to 1 , vice versa was denoted by red lines. The black dotted lines in the graphs below represent the mean of first open-eye interval.

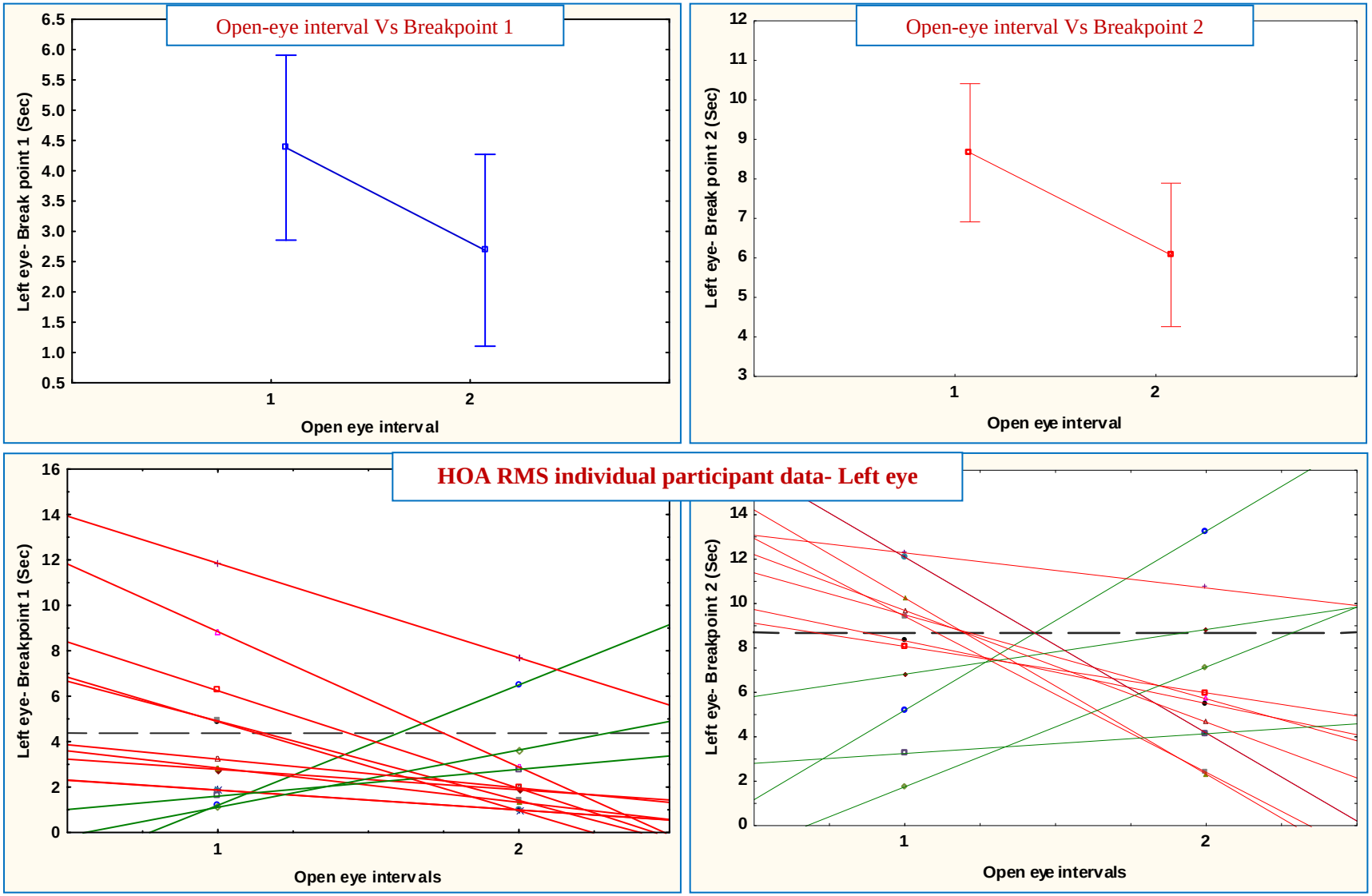

Figure 6-12: Comparison of breakpoints of left eye obtained from HOA RMS data for each open-eye interval and the distribution of breakpoints between open-eye intervals. The left side graphs compares breakpoint 1 between open-eye intervals and the right side graphs compares the location of breakpoint 2 between open-eye intervals. Each line corresponds in the graphs below to a single participant data between open-eye intervals and green lines represents higher values in open-eye interval 2 compared to 1 ,vice versa was denoted by red lines. The black dotted lines in the graphs below represent the mean of first open-eye interval.

6.5.2.3 Average HOA RMS in terms of vertical prism breakpoints:

Assuming that the vertical prism coefficient indicates the flow of the tears over the cornea and the HOA RMS or the aberrations indicates the quality of the tear film, this study investigated if the breakpoints as obtained using segmented linear regression were different for each eye of each individual participant between vertical prism and HOA RMS data (Figure 6-13). The scatter plots showed more distributed values for both breakpoints. The comparison showed a wide spread distribution on both sides of the unit slope of regression indicating higher variation between the locations of breakpoints.

Due to the above difference in the breakpoints, the average HOA RMS for first two phases of the vertical prism coefficient was obtained. The phases of vertical prism coefficient provide the stages of the tear film within blinks, whereas the average HOA RMS provides the amount of change in the anterior surface quality. Therefore, the average HOA RMS of each phase of the vertical prism explains the amount of change in the anterior surface quality during stages of the tear film within blink. The average HOA RMS corresponding to the first two phases (blink to breakpoint 1 and breakpoint 1 to 2) of the vertical prism segmented fit were calculated for each eye and each open-eye interval. The individual participant's average RMS, standard deviation, maximum and minimum of two phases were plotted for each eye and open interval (Figure 6-14 and Figure 6-15). In comparison to the first open-eye interval, the standard deviation, the maximum and minimum was observed to be larger in the second open-eye interval of both the eyes.

Non-parametric Wilcoxon paired signed rank test was used to analyse the average HOA RMS of each individual participant at each open-eye intervals and determine if the median

difference was different from zero. The results showed a significant difference ($p=0.01$) in the medians of the right eye for phase 1 (between blink and breakpoint 1) values of the first open-eye interval (Figure 6-16). Even though, the box and whisker plot shows a huge difference in range between open-eye intervals, the rest of the comparisons between medians of phase 1 and phase 2 HOA RMS values were not significantly different ($p>0.05$) from each other. (Figure 6-16)

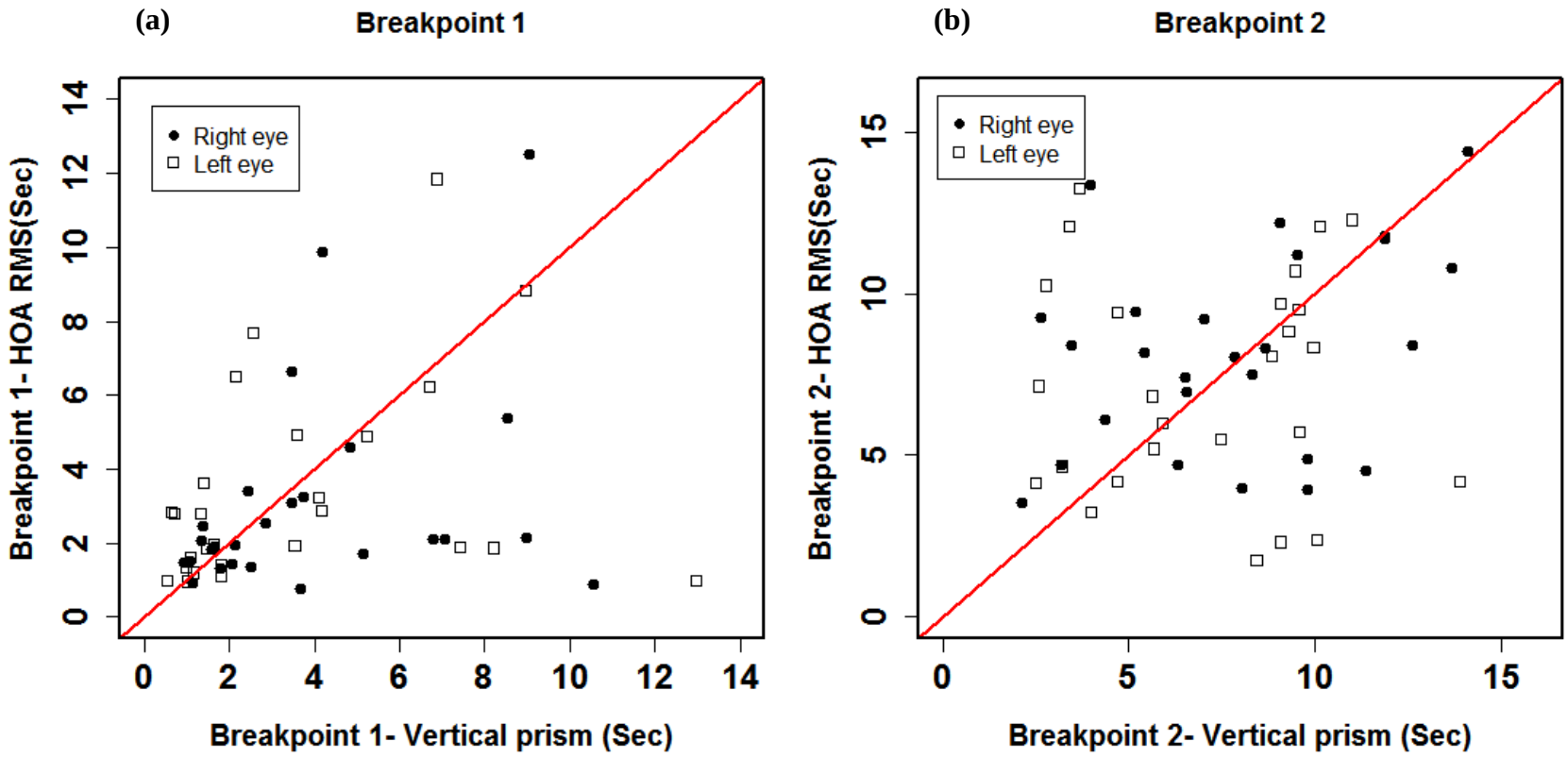

Figure 6-13: Comparison between the location of breakpoints of segmented vertical prism coefficient (x-axis) and HOA RMS (y-axis) data. Figure (a) compares the location of breakpoint 1 and (b) compares the location of breakpoint 2. The red line represents the line with unit slope.

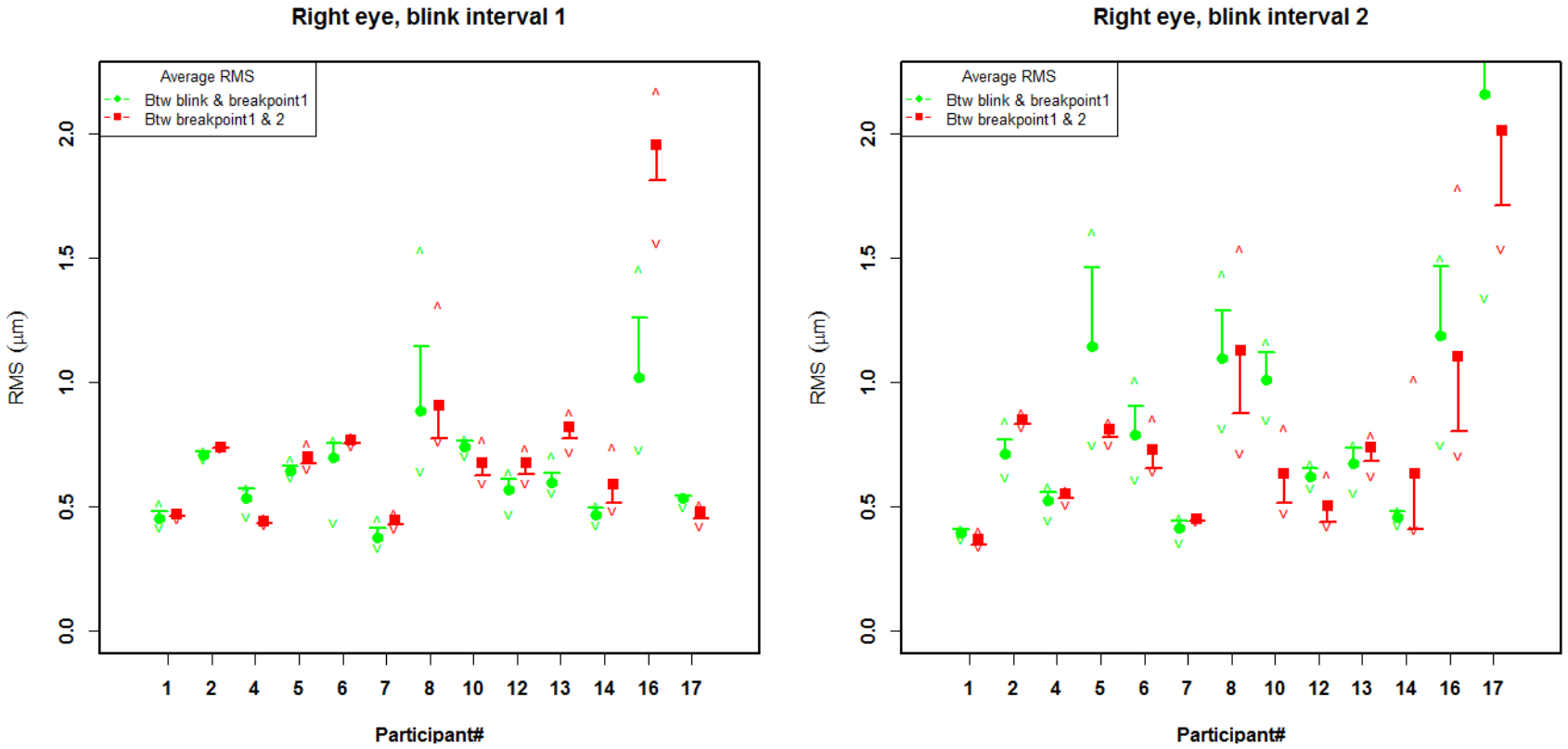

Figure 6-14: Scatter plot with error bar for the comparison of average HOA RMS between the intervals of prism breakpoints of the right eye. The green dot with upper error bar represents average HOA RMS between blink and first breakpoint, red dot with error bar represents the average RMS between breakpoint 1 &2. The error bars gives the standard deviation and the arrows represents the minimum and maximum values within the range.

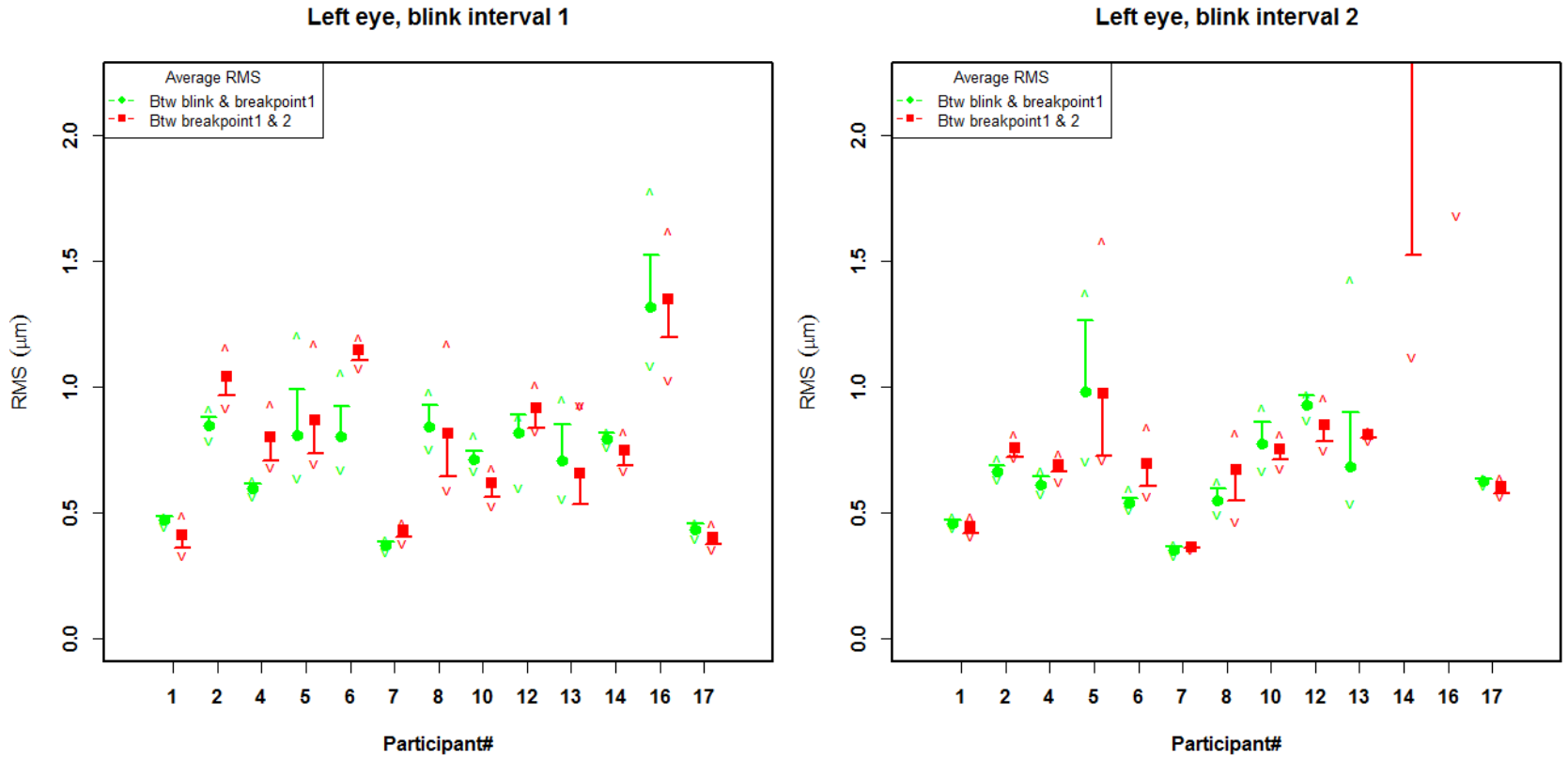

Figure 6-15: Scatter plot with error bar for the comparison of average HOA RMS between the intervals of prism breakpoints of the left eye.

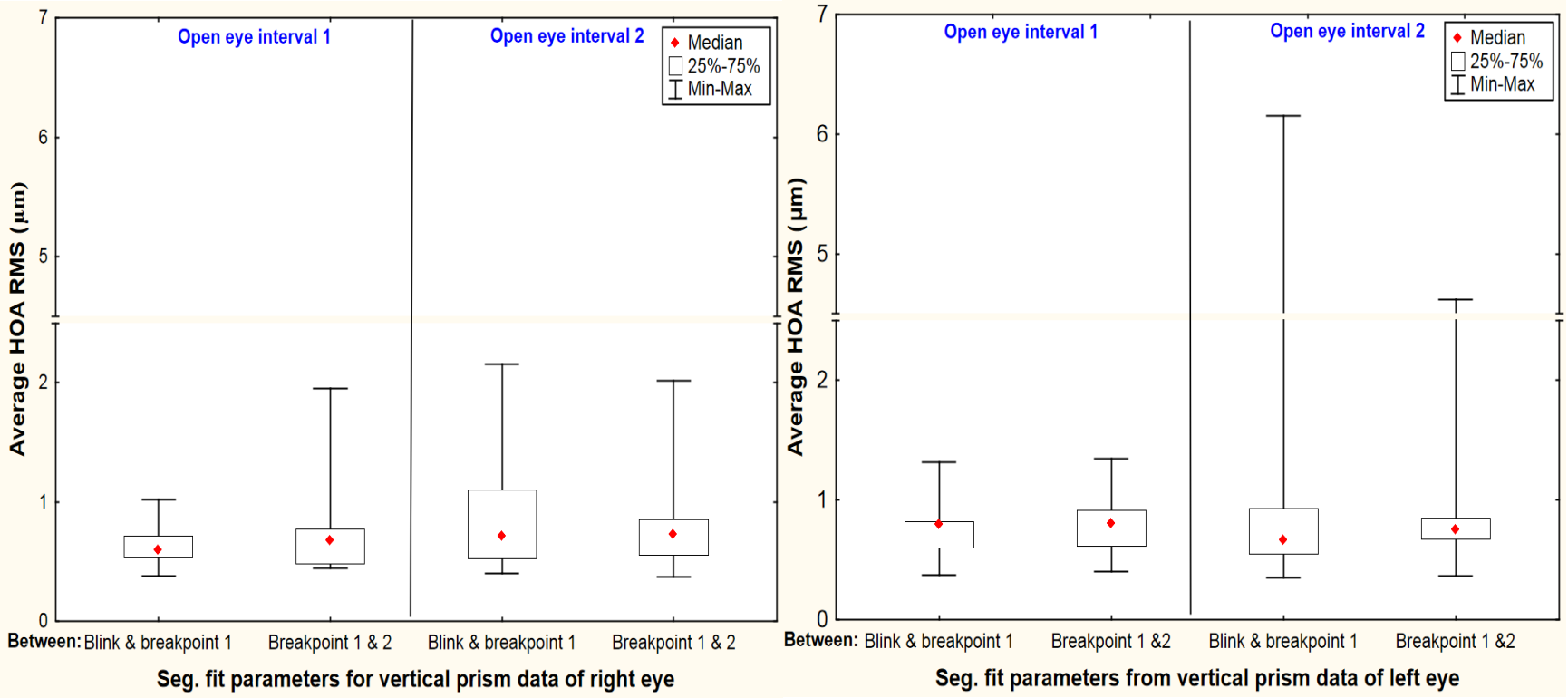

Figure 6-16: Box plot of average HOA RMS calculated between the seg.fit parameters of vertical prism data for right and left eye. The red diamond in both figures represents the median of average HOA RMS, whereas the box gives the 25 and 75% quartiles. The whiskers give the minimum and maximum average values. Note: Y-axis break between 2.5 and 4.5 µm for easier comparison between graphs.

6.5.3 Other noticeable observations from the data

A wavy pattern, as shown in Figure 6-17, was observed frequently after the second breakpoint of the dynamic vertical prism coefficients. 8 out of 26 eyes in the first open-eye interval and 12 out of 26 eyes in the second open-eye interval exhibited this wavy pattern. The wavy patterns observed were both symmetrical and non-symmetrical around the slope. The reason behind the wavy aberrations is unknown. A similar pattern was observed in the HOA RMS and horizontal prism coefficient also.

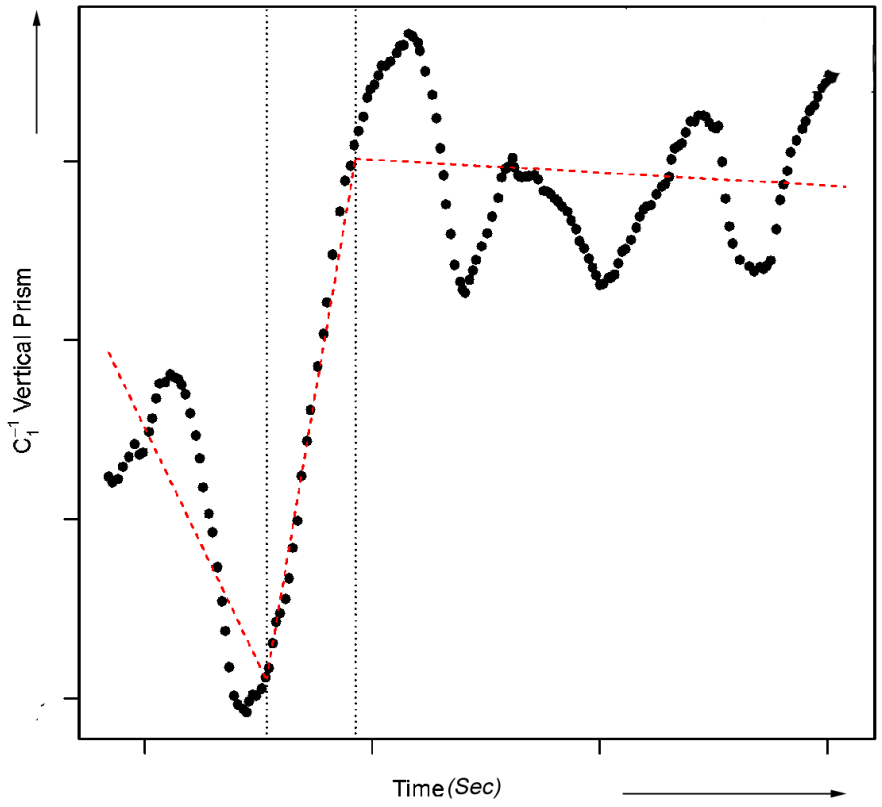

Figure 6-17: Schematic example of a wavy pattern in phase 3 of the vertical prism data.

6.6 Discussion:

In our previous study (Chapter 5), the anterior surface aberrations obtained were analysed using a linear regression technique to analyse the change over time between blinks. The slopes indicated a steep increase in the aberrations in the dry eye participants compared to normal participants, but the data was very variable compared around the fit. A study undertaken by Hampson & Mallen[78] suggested the ocular and corneal aberrations to be chaotic in nature, which contraindicates the use of linear regression to analyse the corneal aberration data. Although they proposed this based on a single participant's data, the chaos in the corneal aberrations were analysed in a study (non-thesis work) and found the chaos to be very minimal compared to the chaos obtained by Hampson and Mallen (Appendix-2).

According to Montes-Mico et al.[41,42] and Nemeth et al.[24], the tear film took approximately 3 to 10 seconds to stabilize and then start breaking up between blinks. They also found the TBUT to be comparable with the time taken to attain lowest aberrations. In contrast, our study found that the average first breakpoint was observed around 3-6 seconds post-blink and was significantly different from the NITBUT obtained. The second breakpoint, which occurs later, was found to be more similar to the NITBUT values obtained. This might be explained with the tear film stability theory proposed by Holly et al.,[8] where the tear film takes at least 3 seconds to settle down after the eye opening, forming a negative slope. If the first breakpoint indicates a settled tear film and the second phase indicates the thinning of the settled tear film commensurate with an increase in aberrations, the second breakpoint can be expected to happen at a similar instant to that at which there a noticeable break in the tear film (i.e. NITBUT measurement point) as there is a sudden rise in the irregularity of the tear film.

As suggested by Zhu,[76] the use of prism coefficient as a direct measure to analyse tear film thickness variation was analysed among our study participants. The results showed a varying amount of breakpoints between the open-eye intervals. An inverse effect was observed in this study in the location of breakpoints between open-eye intervals. This might be as a result of using a forced blinking technique to obtain aberration measurements. The breakpoints which were shorter in the first blink interval were longer in the second blink interval. It was also seen from the graphs, that the graphs with shorter breakpoints exhibit a wavy pattern in the aberration or prism coefficient after the second breakpoint. This wavy pattern may be accounted for by reflex tearing, or reflect an ocular movement or heart pulse. Since, the aberrations are more stable in the next open interval; it suggests the cause of wavy pattern to be more likely originate from the tear film than an ocular movement. If reflex tearing is the cause, a more stable or, at least, voluminous tear film during the next open interval could result and exhibit a slower change in the tear film surface. It was also observed from our experiments that the average HOA RMS is higher and more variable in the second open-eye interval compared to the first open interval. This indicates the need for more repeated measurements with shorter forced blink interval or natural blinking techniques be evaluated to address the issue of repeatability of the measurements.

6.7 Conclusion:

The three-phased segmented linear regression techniques to analyse the anterior surface aberrations can be used objectively to measure tear film stability. Even though the repeatability of the measurements from two open-eye intervals were poor, more open-eye periods and/or repeated measurements of the open-eye periods, and/or shorter open-eye

periods closer to natural blinking need to be evaluated for more detailed measure of repeatability. A criterion other than forced blinking needs to be evaluated for a more complete understanding of the natural tear film dynamics.

Chapter 7 Summary

The experimental aspects of both corneal analysers were evaluated and showed the measurements were repeatable on a given non-variable surface at optimal focus position. The repeatability of the instrument was also good when the defocus was produced by a longer working distance, suggesting that it is best to obtain anterior surface aberration measures within the optimal focus position or slightly further away from the eye than the optimal focus. The variability in aberrations produced by the initial focusing of the mires requires the omission of the initial 10-15 sec of collected data for improved measurements of surface aberrations (Chapter 3). The measurements of spectral and thermal characteristics of the light sources of two corneal analysers during the measurements of surface aberrations showed that the difference in luminance of the light source does not change the thermal characteristics of the eye (Chapter 4).

From the clinical measurements, the higher order aberrations were also found to be similar between the instruments, even though there is a possibility of the brightness of the light source inducing reflex tearing (Chapter 4). Changes in head orientation did not improve the area measured using the corneal analysers. Measurements using forced blinking were preferred compared to natural blinking procedure, when the data pertaining to the blink were not available due to the software algorithm used. The location of the blink was shown to be an important factor to analyse surface aberrations, due to significant changes in thickness of the tear film and surface aberrations that take place immediately after the blink. It was also shown that the anterior surface aberrations can be used in differentiating normal from dry eye participants, by using linear regression of the forced blink data (chapter 5).

Though the measurement in Chapter 5 showed an ability to differentiate between two groups, linear regression analysis failed to show the exact trend accompanied with the aberration data between blinks. Previous studies have shown the mechanism of tear film stability as being "three-phased" between blinks, and the measurement of vertical prism coefficients provides an estimate of the changes in the tear film thickness. In this study, the anterior surface aberrations were also assumed to be "three-phased" because the measurements of anterior surface aberrations are obtained from the surface of the tear film and the measure of anterior surface aberration gives the direct measure of tear film stability. By using segmented linear regression analysis, both our hypothesis were tested in this study. (chapter 6).

As assumed, all participant's (except 1) dynamic anterior surface aberration measurements showed a "three-phased" change in the aberrations for both open-eye intervals. The analysis of segmented linear regression of vertical prism coefficients and higher order aberrations showed that the eye measured second showed a higher rate of change in aberrations and the change occurred later after the blink, when compared to the first eye measured. The location of breakpoint 2 was not significantly different from the clinical measurements of tear breakup time, indicating a possible use of surface aberrations as an objective measure of surface quality.

Even though the breakpoints were not significantly different between each other for open-eye intervals as a group, the individual participant data showed a significant trend. The breakpoints which are earlier in the first open-eye interval occurred later in the second open-eye intervals and vice versa. This indicates a possible effect of the use of the forced blink paradigm, which causes changes in tear film stability. It was also observed that the average

higher order aberrations of each phase of vertical prism coefficient was higher and had a larger range in the second open-eye interval when compared to first open-eye interval. These results indicate the use of a criterion which is closer to natural tear film dynamics to obtain more repeatable measurements using segmented linear regression and anterior surface aberrations (chapter 6).

Based on studies undertaken in this thesis, there remain many issues which need to be analysed for better understanding of the relationship between dynamic anterior surface aberrations and tear film stability. The main issue which came up during these studies is the duration of the open-eye intervals. Even though, this study employed a blinking paradigm similar to other studies, the results showed an influence of prolonged open-eye interval on repeated measures. A wide range of blinking paradigms along with more open-eye intervals and/or repeated measurements need to be evaluated in future studies to obtain a blinking paradigm which obtains measurements without affecting the tear film stability. The results of our study using a smaller group of participants showed that the segmented linear regression analysis can be used as an objective method to analyse the tear film stability. More analysis using large sample sizes and groups has to be evaluated to test the reliability of the analysis. The groups can be categorized based on signs and anterior surface characteristics for better understanding of its reliability and to develop a criterion to differentiate clinically stable and unstable tear film. More analysis has to be carried out to examine the exact relationship between dynamic tear film thickness and vertical prism coefficient values. This analysis would be helpful in measuring dynamic variation in the tear film thickness which can provide more insight on the diagnosis of the dry eye.

Bibliography

1. Holly FJ. Tear film physiology. *Am. J. Optom. Physiol. Opt.* 1980;57(4):252–7.

2. Rolando M, Zierhut M. The ocular surface and tear film and their dysfunction in dry eye disease. *Surv. Ophthalmol.* 2001;45 Suppl 2(March):S203–10.

3. Paschides CA, Stefaniotou M, Papageorgiou J, Skourtis P, Psilas K. Ocular surface and environmental changes. *Acta Ophthalmol.* 1998;76(1):74–77.

4. Szczesna DH, Kasprzak HT. Numerical analysis of interferograms for evaluation of tear film build-up time. *Ophthalmic Physiol. Opt.* 2009;29(3):211 – 218.

5. Uchino M, Schaumberg DA. Dry eye disease: Impact on quality of life and vision. *Curr. Ophthalmol. Rep.* 2013;1(2):51–57.

6. Pinho Tavares F de. Dry eye disease. *Semin. Ophthalmol.* 2010;25(3):84 – 93.

7. Pflugfelder SCMD, Solomon AMD, Stern MEPD. The diagnosis and management of dry eye: A twenty-five-year review. *Cornea*. 2000;19(5):644–649.

8. Holly FJ. Tear physiology and dry eyes. *Surv. Ophthalmol.* 1977;22(2):69 – 87.

9. Carney L, Hill R. The nature of normal blinking patterns. *Acta Ophthalmol.* 1982;60:427–433.

10. Alonso-Caneiro D, Iskander DR, Collins MJ. Tear film surface quality with soft contact lenses using dynamic-area high-speed videokeratoscopy. *Eye Contact Lens*. 2009;35(5):227–31.

11. King-Smith PE, Reuter KS, Braun RJ, Nichols JJ, Nichols KK. Tear film breakup and structure studied by simultaneous video recording of fluorescence and tear film lipid layer images. *Invest. Ophthalmol. Vis. Sci.* 2013;54(7):4900–9.

12. Nichols JJ, King-Smith PE, Hinel EA, Thangavelu M, Nichols KK. The use of fluorescent quenching in studying the contribution of evaporation to tear thinning. *Invest. Ophthalmol. Vis. Sci.* 2012;53(9):5426–32.

13. Braun RJ. Dynamics of the tear film. *Annu. Rev. Fluid Mech.* 2011;44(1):267 – 297.

14. King-Smith PE, Ramamoorthy P, Braun RJ, Nichols JJ. Tear film images and breakup analyzed using fluorescent quenching. *Invest. Ophthalmol. Vis. Sci.* 2013:iovs.13–12628–(epub).

15. Begley C, Simpson T, Liu H, et al. Quantitative analysis of tear film fluorescence and discomfort during tear film instability and thinning. *Invest. Ophthalmol. Vis. Sci.* 2013;54(4):2645–53.

16. Chen S, Wang IJ. Effect of tear film stability on fluctuation of vision after photorefractive keratectomy. *J. Refract. Surg.* 1999;15(6):668–72.

17. Baudouin C. The pathology of dry eye. *Surv. Ophthalmol.* 2001;45:S211–S220.

18. The definition and classification of dry eye disease: Report of the definition and classification subcommittee of the international dry eye workshop. *Ocul. Surf.* 2007;5(2):75 – 92.

19. Labbe A, Wang YX, Jie Y, Baudouin C, Jonas JB, Xu L. Dry eye disease, dry eye symptoms and depression: the Beijing Eye Study. *Br. J. Ophthalmol.* 2013:bjophthalmol–2013–303838–.

20. Mengher LS, Bron AJ, Tonge SR, Gilbert DJ. A non-invasive instrument for clinical assessment of the pre-corneal tear film stability. *Curr. Eye Res.* 1985;4(1):1–7.

21. Tomlinson A, Khanal S, Ramaesh K, Diaper C, McFadyen A. Tear film osmolarity: determination of a referent for dry eye diagnosis. *Invest. Ophthalmol. Vis. Sci.* 2006;47(10):4309–15.

22. Srinivasan S, Joyce E, Jones LW. Tear osmolality and ferning patterns in postmenopausal women. *Optom. Vis. Sci.* 2007;84(7):588–592.

23. White KM, Benjamin WJ, Hill RM. Human basic tear fluid osmolality. *Acta Ophthalmol.* 2009;71(4):530–538.

24. Nemeth J, Erdelyi B, Csakany B, et al. High-speed videotopographic measurement of tear film build-up time. *Invest. Ophthalmol. Vis. Sci.* 2002;43(6):1783–1790.

25. Iskander D. R, Collins MJ, Davis B. Evaluating tear film stability in the human eye with high-speed videokeratoscopy. *IEEE Trans. Biomed. Eng.* 2005;52(11):1939 – 1949.

26. Yokoi N, Komuro A. Non-invasive methods of assessing the tear film. *Exp. Eye Res.* 2004;78(3):399–407.

27. Doane MG. An instrument for in vivo tear film interferometry. *Optom. Vis. Sci.* 1989;66(6):383–388.

28. Doane MG, Lee ME. Tear film interferometry as a diagnostic tool for evaluating normal and dry-eye tear film. *Adv. Exp. Med. Biol.* 1998;438:297–303.

29. Szczesna DH, Iskander DR. Lateral shearing interferometry for analysis of tear film surface kinetics. *Optom. Vis. Sci.* 2010;87(7):513–517.

30. Yokoi N, Takehisa Y, Kinoshita S. Correlation of tear lipid layer interference patterns with the diagnosis and severity of dry eye. *Am. J. Ophthalmol.* 1996;122(6):818–824.

31. Montes-Mico R, Caliz A, Alio JL, Montés-Micó R, Cáliz A, Alió JL. Wavefront analysis of higher order aberrations in dry eye patients. *J. Refract. Surg.* 2004;20(3):243–247.

32. Lakshminarayanan V, Fleck A. Zernike polynomials: a guide. *J. Mod. Opt.* 2011;58(7):545 – 561.

33. Porter J, Guirao A, Cox IG, Williams DR. Monochromatic aberrations of the human eye in a large population. *J. Opt. Soc. Am. A.* 2001;18(8):1793.

34. Charman W. Wavefront aberration of the eye: a review. *Optom. Vis. Sci.* 1991;68(8):574–583.

35. Hofer H, Artal P, Singer B, Aragón JL, Williams DR. Dynamics of the eye's wave aberration. *J. Opt. Soc. Am. A.* 2001;18(3):497.

36. Albarrán C, Pons AM, Lorente A, Montés R, Artigas JM. Influence of the tear film on optical quality of the eye. *Cont. Lens Anterior Eye*. 1997;20(4):129–135.

37. Montés-Micó R, Alió JL, Muñoz G, Pérez-Santonja JJ, Charman WN. Postblink changes in total and corneal ocular aberrations. *Ophthalmology*. 2004;111(4):758–767.

38. Li KY, Yoon G. Changes in aberrations and retinal image quality due to tear film dynamics. *Opt. Express*. 2006;14(25):12552–9.

39. Liu H, Thibos L, Begley CG, Bradley A. Measurement of the time course of optical quality and visual deterioration during tear break-up. *Invest. Ophthalmol. Vis. Sci.* 2010;51(6):3318–26.

40. Artal P, Guirao A, Berrio E, Williams DR. Compensation of corneal aberrations by the internal optics in the human eye. *J. Vis.* 2001;1(1):1.

41. Montés-Micó R, Alió JL, Muñoz G, Charman WN, Montes-Mico R. Temporal changes in optical quality of air–tear film interface at anterior cornea after blink. *Invest. Ophthalmol. Vis. Sci.* 2004;45(6):1752–1757.

42. Montés-Micó R, Alió JL, Charman WN. Dynamic changes in the tear film in dry eyes. *Invest. Ophthalmol. Vis. Sci.* 2005;46(5):1615–1619.

43. Buehren TDI, Collins MJPD, Iskander DRPD, Davis BBAS, Lingelbach BPD. The stability of corneal topography in the post-blink interval. *Cornea*. 2001;20(8):826–833.

44. Alonso-Caneiro D, Iskander DR, Collins MJ. Assessment of tear film surface quality using dynamic-area high-speed videokeratoscopy. *IEEE Trans. Biomed. Eng.* 2009;56(5):1473–1481.

45. IBM corporation. SPSS Statistics. 2007. Available at: www.ibm.com/software/analytics/spss.

46. R Core Team. R: A language and environment for statistical computing. 2012. Available at: http://www.r-project.org/.

47. Shoemaker L. The quantile test for homogeneity of variances. *Proc. Annu. Meet. Am. Stat. Assoc.* 2001:1–5.

48. Shoemaker L. Tests for differences in dispersion based on quantiles. *Am. Stat.* 1995;49(2):179–182.

49. Duench S, Simpson T, Jones LW, Flanagan JG, Fonn D. Assessment of variation in bulbar conjunctival redness, temperature, and blood flow. *Optom. Vis. Sci.* 2007;84(6):511–6.

50. Gugleta K, Orgül S, Flammer J. Is corneal temperature correlated with blood-flow velocity in the ophthalmic artery? *Curr. Eye Res.* 1999;19(6):496–501.

51. Maruyama K, Yokoi N, Takamata A, Kinoshita S. Effect of environmental conditions on tear dynamics in soft contact lens wearers. *Invest. Ophthalmol. Vis. Sci.* 2004;45(8):2563–8.

52. Morgan PB, Tullo AB, Efron N. Infrared thermography of the tear film in dry eye. *Eye*. 1995;9 (Pt 5)(5):615–8.

53. Hofer H, Artal P, Singer B, Aragón JL, Williams DR. Dynamics of the eye's wave aberration. *J. Opt. Soc. Am.* 2001;18(3):497–506.

54. Montés-Micó R, Cervino A, Ferrer-Blasco T, García-Lázaro S, Madrid-Costa D, Cerviño A. The tear film and the optical quality of the eye. *Ocul. Surf.* 2010;8(4):185–192.

55. Photo Research, Inc. - PR-650 SpectraScan Colorimeter. Available at: http://www.photoresearch.com/current/pr650.asp. Accessed September 21, 2013.

56. Koçak I, Orgül S, Flammer J. Variability in the measurement of corneal temperature using a noncontact infrared thermometer. *Ophthalmologica*. 1999;213(6):345–9.

57. Craig JP, Singh I, Tomlinson A, Morgan PB, Efron N. The role of tear physiology in ocular surface temperature. *Eye*. 2000;14(4):635–41.

58. Purslow C, Wolffsohn J. The relation between physical properties of the anterior eye and ocular surface temperature. *Optom. Vis. Sci.* 2007;84(3):197–201.

59. Purslow C, Wolffsohn J. Ocular surface temperature: A review. *Eye Contact Lens*. 2005;31(3):117–123.

60. Girardin F, Orgül S, Erb C, Flammer J. Relationship between corneal temperature and finger temperature. *Arch. Ophthalmol.* 1999;117(2):166–9.

61. Tan J-HH, Ng EYK, Rajendra Acharya U, Chee C. Infrared thermography on ocular surface temperature: a review. *Infrared Phys. Technol.* 2009;52(4):97–108.

62. Koh S, Maeda N, Kuroda T, et al. Effect of tear film break-up on higher-order aberrations measured with wavefront sensor. *Am. J. Ophthalmol.* 2002;134(1):115–117.

63. Mihashi T, Mihashi T, Hirohara Y, et al. Tear film break-up time evaluated by real-time Hartmann-Shack wavefront sensing. *Jpn. J. Ophthalmol.* 2006;50(2):85–89.

64. Lin Y-Y, Carrel H, Wang I-J, Lin P-J, Hu F-R. Effect of tear film break-up on higher order aberrations of the anterior cornea in normal, dry, and post-LASIK eyes. *J. Refract. Surg.* 2005;21(5):S525–S529.

65. Wang L, Dai E, Koch DD, Nathoo A. Optical aberrations of the human anterior cornea. *J. Cataract Refract. Surg.* 2003;29(8):1514–1521.

66. Roberts B, Athappilly G, Tinio B, Naikoo H, Asbell P. Higher order aberrations induced by soft contact lenses in normal eyes with myopia. *Eye Contact Lens*. 2006;32(3):138–42.

67. Rae SM, Price HC. The effect of soft contact lens wear and time from blink on wavefront aberration measurement variation. *Clin. Exp. Optom.* 2009;92(3):274–82.

68. Lindskoog Pettersson A, Jarkö C, Alvin A, Unsbo P, Brautaset R. Spherical aberration in contact lens wear. *Cont. Lens Anterior Eye*. 2008;31(4):189–93.

69. Jiang H, Wang D, Yang L, Xie P, He JC. A comparison of wavefront aberrations in eyes wearing different types of soft contact lenses. *Optom. Vis. Sci.* 2006;83(10):769–74.

70. Tuszynski J. caTools: Tools: moving window statistics. 2011. Available at: http://cran.r-project.org/package=caTools.

71. Ferreira TA, Rasband W. Image J. 2012. Available at: http://imagej.nih.gov/ij/docs/index.html.

72. IBM corporation. SPSS Statistics. 2011. Available at: www.ibm.com/software/analytics/spss.

73. King-Smith PE, Nichols JJ, Nichols KK, Fink BA, Braun RJ. Contributions of Evaporation and Other Mechanisms to Tear Film Thinning and Break-Up. *Optom. Vis. Sci.* 2008;85(8):623–630.

74. Nichols JJ, Mitchell GL, King-Smith PE. Thinning rate of the precorneal and prelens tear films. *Invest. Ophthalmol. Vis. Sci.* 2005;46(7):2353–61.

75. Sweeney DF, Millar TJ, Raju SR. Tear film stability: A review. *Exp. Eye Res.* 2013:epub.

76. Zhu M. Microfluctuations of wavefront aberrations of the eye. 2005:(QUT, Thesis).

77. Stat Soft. Inc. Statistica (data analysis software system). 2012. Available at: www.statsoft.com.

78. Hampson KM, Mallen EAH. Chaos in ocular aberration dynamics of the human eye. *Biomed. Opt. Express*. 2012;3(5):863–77.

Appendices

Appendix 1

WOLTERS KLUWER HEALTH LICENSE TERMS AND CONDITIONS

Nov 09, 2013

This is a License Agreement between Varadharajan Jayakumar ("You") and Wolters Kluwer Health ("Wolters Kluwer Health") provided by Copyright Clearance Center ("CCC"). The license consists of your order details, the terms and conditions provided by Wolters Kluwer Health, and the payment terms and conditions.

All payments must be made in full to CCC. For payment instructions, please see information listed at the bottom of this form.

License Number	3265100786637
License date	Nov 09, 2013
Licensed content publisher	Wolters Kluwer Health
Licensed content publication	Cornea
Licensed content title	The Diagnosis and Management of Dry Eye: A Twenty-five-Year Review.
Licensed content author	Pflugfelder, Stephen; Solomon, Abraham; Stern, Michael
Licensed content date	Jan 1, 2000
Volume Number	19
Issue Number	5
Type of Use	Dissertation/Thesis
Requestor type	Individual
Author of this Wolters Kluwer article	No
Title of your thesis / dissertation	Aspects of Dynamic Anterior Surface Aberrations
Expected completion date	Dec 2013
Estimated size(pages)	180
Billing Type	Invoice
Billing address	University of Waterloo, School of Optometry and Vision Science, Waterloo, ON N2L 3G1 Canada
Total	0.00 USD
Terms and Conditions	

Terms and Conditions

1. A credit line will be prominently placed and include: for books - the author(s), title of

book, editor, copyright holder, year of publication; For journals - the author(s), title of article, title of journal, volume number, issue number and inclusive pages.

2. The requestor warrants that the material shall not be used in any manner which may be considered derogatory to the title, content, or authors of the material, or to Wolters Kluwer.
3. Permission is granted for a one time use only within 12 months from the date of this invoice. Rights herein do not apply to future reproductions, editions, revisions, or other derivative works. Once the 12-month term has expired, permission to renew must be submitted in writing.
4. Permission granted is non-exclusive, and is valid throughout the world in the English language and the languages specified in your original request.
5. Wolters Kluwer cannot supply the requestor with the original artwork or a "clean copy."
6. The requestor agrees to secure written permission from the author (for book material only).
7. Permission is valid if the borrowed material is original to a Wolters Kluwer imprint (Lippincott-Raven Publishers, Williams & Wilkins, Lea & Febiger, Harwal, Igaku-Shoin, Rapid Science, Little Brown & Company, Harper & Row Medical, American Journal of Nursing Co, and Urban & Schwarzenberg - English Language).
8. If you opt not to use the material requested above, please notify Rightslink within 90 days of the original invoice date.
9. Please note that articles in the ahead-of-print stage of publication can be cited and the content may be re-used by including the date of access and the unique DOI number. Any final changes in manuscripts will be made at the time of print publication and will be reflected in the final electronic version of the issue.?Disclaimer: Articles appearing in the Published Ahead-of-Print section have been peer-reviewed and accepted for publication in the relevant journal and posted online before print publication. Articles appearing as publish ahead-of-print may contain statements, opinions, and information that have errors in facts, figures, or interpretation. Accordingly, Lippincott Williams & Wilkins, the editors and authors and their respective employees are not responsible or liable for the use of any such inaccurate or misleading data, opinion or information contained in the articles in this section.
10. 1This permission does not apply to images that are credited to publications other than Wolters Kluwer journals. For images credited to non-Wolters Kluwer journal publications, you will need to obtain permission from the journal referenced in the figure or table legend or credit line before making any use of the image(s) or table(s).
11. In case of **Disease Colon Rectum, Plastic Reconstructive Surgery, The Green Journal, Critical Care Medicine, Pediatric Critical Care Medicine, the American Heart Publications, the American Academy of Neurology** the following guideline applies: no drug brand/trade name or logo can be included in the same page as the material re-used
12. When requesting a permission to translate a full text article, Wolters Kluwer/Lippincott Williams & Wilkins requests to receive the pdf of the translated document
13. "Adaptations of single figures do not require Wolters Kluwer **further** approval if the permission has been granted previously. However, the adaptation should be credited as follows:?Adapted with permission from Lippincott Williams and Wilkins/Wolters Kluwer Health: [JOURNAL NAME] (reference citation), copyright (year of publication)" **Please note that modification of text within figures or full-text articles is strictly forbidden.**
14. The following statement needs to be added when reprinting the material in Open Access journals only: 'promotional and commercial use of the material in print, digital or mobile device format is prohibited without the permission from the publisher Lippincott Williams & Wilkins. Please contact journalpermissions@lww.com for further information".
15. Other Terms and Conditions:

v1.8

If you would like to pay for this license now, please remit this license along with your payment made payable to "COPYRIGHT CLEARANCE CENTER" otherwise you will be invoiced within 48 hours of the license date. Payment should be in the form of a check or money order referencing your account number and this invoice number RLNK501155424. Once you receive your invoice for this order, you may pay your invoice by credit card. Please follow instructions provided at that time.

Make Payment To:
Copyright Clearance Center
Dept 001
P.O. Box 843006
Boston, MA 02284-3006

For suggestions or comments regarding this order, contact RightsLink Customer Support: customercare@copyright.com or +1-877-622-5543 (toll free in the US) or +1-978-646-2777.

Gratis licenses (referencing $0 in the Total field) are free. Please retain this printable license for your reference. No payment is required.

Appendix 2

Are the fluctuations in dynamic anterior surface aberrations of the human eye chaotic?

Varadharajan Jayakumar[1],* Damber Thapa[1], Natalie Hutchings[1], Vasudevan Lakshminarayanan[1-3]

[1]*School of Optometry and Vision Science, University of Waterloo, 200 University Avenue West, Waterloo, Ontario, N2L 3G1, Canada*

[2]*Departments of Physics and Electrical and Computer Engineering, University of Waterloo, Waterloo, ON, N2L 3G1, Canada*

[3]*Departments of Physics and the Michigan Center for Theoretical Physics, University of Michigan, Ann Arbor, MI 48104, USA.*

**Corresponding author: varadhu.jayakumar@uwaterloo.ca*

Received Month X, XXXX; revised Month X, XXXX; accepted Month X, XXXX;
posted Month X, XXXX (Doc. ID XXXXX); published Month X, XXXX

The purpose of the study is to measure chaos in the dynamic anterior surface aberrations and examine how it varies between the eyes of an individual. Non-invasive tear breakup time (NITBUT) and dynamic corneal surface aberrations were measured for two open-eye intervals of 15 seconds long. Maximal Lyapunov Exponents (MLE) was calculated to test the nature of the fluctuations of the dynamic anterior surface aberration. The average MLE for total higher order aberration (HOA) was found to be small (+0.0102 ± 0.0072) μm/s. No significant difference in MLE was found between the eyes for HOA (t-test, p= 0.131). Data analysis was carried out for the Zernike coefficient of vertical prism as it gives a direct measure of the thickness of the tear film over time. The results show that, the amount of chaos was small for each Zernike coefficient and not significantly correlated between the eyes. © XXXX Optical Society of America

OCIS Codes: 330.5370, 330.7326

The tear film, approximately 10μm thick, overlays the corneal surface and provides the first and most powerful refracting surface in the eye [1]. As a result, the eye's optics and retinal image quality depends greatly on the stability of the tear film [2]. The tear film also negatively impacts visual comfort if unstable [3]. Several factors, such as evaporation and lipid layer thickness, are found to alter the tear film thickness when eyes are open between blinks [1]. Recently, a number of studies have been conducted to examine the nature of the aberrations introduced by the dynamic nature of the tear film [1-2, 4-7]. Studies show that anterior surface aberrations correlate with the optical changes caused by the dynamic nature of the tear film, and hence conclude that the aberrations are also dynamic [4].

Power spectrum analysis has been used to study the dynamic behavior of wavefront aberration in many studies [8]; however, recent studies by Hampson and Mallen [9-10], utilized chaos theory to describe fluctuations in the dynamic wavefront aberrations of the whole eye. Chaos theory studies the behavior of dynamic systems, in which simple deterministic equations can predict apparent random events [11]. Hampson and Mallen [9] suggested that the fluctuations in the aberrations of the whole eye are chaotic in nature and, therefore, the underlying equations can determine the behavior of aberrations. In a separate study [10], no correlations between eyes of an individual in the chaos of ocular aberrations for the whole eye were found.

The effect of the tear film fluctuations on the whole eye aberrations has also been examined by fitting a scleral contact lens to preserve the tear film between the eye and the lens for a single participant [9]. The authors concluded that fluctuations in the tear film may be a source of noise that 'dilutes' the chaos in the aberrations of the whole eye [9]. To examine this, we investigated chaos in the fluctuations of anterior surface aberrations only and considered the correlation of this chaos, if any, between eyes of an individual.

Methods: Twenty-eight eyes of non-symptomatic, non-contact lens wearers were included in this study. The mean age of the participants was 27.5 ± 3.3 years of age (male = 8, female = 6). NITBUT and dynamic anterior surface aberrations were measured during the study visit. NITBUT is a clinical measure of the stability of the tear film, where illuminated Placido rings are projected onto the corneal surface and the time taken from a blink to the appearance of distortion or discontinuities of the image (as the tear film 'breaks up') while the participant holds their eyes open is measured. The Atlas corneal topographer (Carl Zeiss Canada Ltd., Toronto, ON) was used to measure NITBUT and the Topcon

CA200 corneal analyzer (Topcon Canada Inc., Waterloo, ON.) was used to measure dynamic anterior surface aberrations. NITBUT was measured before the anterior surface aberrations and the order of the eye measured first was randomized across participants. In each eye, three measures of NITBUT were obtained and the average of all three measures was considered for analysis. The NITBUT ranged between 5.4 and 11.0 seconds, with a mean of 7.4 seconds in the right eye and 7.2 seconds in the left eye across all participants. The corneal analyzer uses the Placido disc principle to measure anterior surface aberrations. Dynamic measurements were obtained at a frame rate of 24Hz for two 15-second open-eye intervals between blinks. Participants were asked to hold their eyes open during the open eye measurement period. Similar to NITBUT, the order of the eye measured first was randomized across participants. The proprietary software identifies the location of the blinks and removes the blink data from further analysis. A recovery period of 10 minutes was provided between the NITBUT and anterior surface aberrations measurement to maintain the tear film in as near as normal condition. Anterior surface aberrations were calculated for a 6 mm pupil diameter.

The instrument provides the anterior surface aberrations in terms of Zernike polynomials up to the 7th order. Total higher order aberrations (HOA) were calculated as the root mean square (RMS) values of Zernike coefficients from 3rd to 7th orders [12]. For the analysis, dynamic HOA RMS and the individual Zernike coefficient for vertical prism were used. The latter is thought to give a direct measure of the thickness of the tear film over time as the tears flow vertically over the cornea after every blink [13]. Each frame captured on an open-eye interval was considered for analysis. First, the measures of each open-eye interval were separately analyzed then two data sets were combined to describe a total measurement window of 30 seconds. The blink data between the two open-eye intervals were removed for further analysis.

Chaos theory analysis: We used the analysis proposed by Rosenstein [14] to examine the chaos present in anterior surface aberrations of the eye. Lyapunov exponents were calculated for every point in the dynamic data and the largest Lyapunov exponent was chosen to make a decision. The largest Lyapunov exponent is commonly called the Maximal Lyapunov Exponent (MLE) and indicates the degree of chaos in the dynamic systems [9]. If the MLE is positive, then the data (system) is chaotic and/or the data depends on the initial condition; the larger the positive value of MLE, the greater the chaos. In contrast, a negative MLE represents a non-chaotic or predictable data [14]. In this study, MATLAB (version 2013a) was used to calculate MLEs using the lyaprosen toolbox [14]. Before performing the analysis, the HOAs were detrended to remove the linear trend. The detrending removes the best straight-line fit from the data and hence forces its mean value to zero but still it preserves the statistical properties of the data (Figure 1). The detrended data were used to obtain the MLE, which gives the amount of chaos in the dynamic anterior surface aberrations.

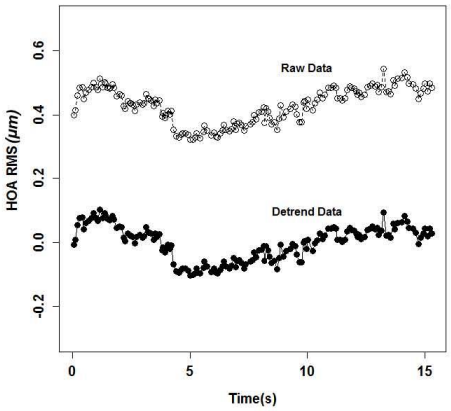

Figure 1: Example of anterior surface higher order aberrations measures obtained for a 6mm pupil diameter at 24 Hz sampling frequency for a 15sec open eye interval (top; filled black circles). The same data is also shown after detrending (bottom; open gray circles)

Chaos and anterior surface aberrations: The average HOA RMS for all the participants was +0.781 ± 0.313 μm; this indicates a high variability in anterior surface aberrations among individuals. The MLE for each open-eye interval was calculated from the HOA of each participant. The average MLE_{HOA} were +0.0325 ± 0.0429 μm/s, +0.0794 ± 0.137 μm/s, and +0.0102 ± 0.0072 μm/s for first, and second open-eye interval and the combined data set, respectively. The average MLE_{HOA} are low but positive, which indicate the presence of a low amount of chaos. Similarly, the average vertical prism and MLE corresponding to vertical prism were calculated. The average vertical prism was +0.0824 ± 0.725 μm and the average MLE_{VP} were +0.1250 ± 0.2273 μm/s, +0.0363 ± 0.0992 μm/s and +0.0193 ± 0.0150 μm/s for first and second open-eye interval, and combined data, respectively. Although the chaos was positive, the amount of chaos of vertical prism is low and similar to MLE_{HOA}. MLE values were also calculated for all coefficients upto the 4th order and are listed in Table 1. The MLE values of the 3rd and 4th orders were found to be larger compared MLE_{VP}. This would appear to support the notion that the vertical prism term describes the dynamics post-blink tear flow [13]. Similar to vertical prism the MLE values were higher in the 1st open-eye interval compared to the 2nd or combined data, except for spherical aberration. This systematic finding might be due to 'reflex tearing' [15] that occurs with

consecutive 15s intervals of forced eye-opening used in the experimental paradigm, which is prolonged compared to natural blinking.

Table 1: Average MLE values of coefficients upto 4th order.

Averages	1st open-eye interval	2nd open-eye interval	Combined data
	(μm)	(μm)	(μm)
C_1^{-1}	+0.1250	+0.0363	+0.0193
C_1^{1}	+0.0996	+0.1431	+0.0747
C_2^{-2}	+0.0601	+0.2837	+0.0164
C_2^{0}	+0.0482	+0.0811	+0.0275
C_2^{2}	+0.1801	+0.0222	+0.0189
C_3^{-3}	+0.1282	+0.2568	+0.0527
C_3^{-1}	+0.1482	+0.0922	+0.0149
C_3^{1}	+0.2704	+0.0703	+0.0136
C_3^{3}	+0.1053	+0.0655	+0.0493
C_4^{-4}	+0.1767	+0.1298	+0.0516
C_4^{-2}	+0.0586	+0.0347	+0.0183
C_4^{0}	+0.0711	+0.0296	+0.0173
C_4^{2}	+0.2255	+0.1525	+0.1892
C_4^{4}	+0.0246	+0.0523	+0.0173

The MLEs of the coefficients and higher order aberrations of the combined data were lower than the MLEs of each individual open-eye intervals. These results indicate that combining datasets reduces the MLE determined for each individual open-eye interval.

The study of Hampson and Mallen [9] examined the effect of the tear film on chaos for aberrations of the whole eye using a scleral contact lens, an MLE of +0.33 μm/s was found for the scleral contact lens case compared to +0.27 μm/s without the lens. Since the intent of the scleral contact lens was to preserve the tear film, the authors concluded that the reduction in the MLE without the lens was due to fluctuations in the tear film. Our experiment also supports this finding. When examining the anterior surface aberrations alone, small positive MLE values were obtained for both HOA and vertical prism. The tear film dynamics alters the anterior surface aberrations of the eye and, with minimal amount of chaos exhibited, is likely responsible for decreases in the chaotic nature of the ocular aberrations in total.

Correlation between eyes in chaos of the anterior surface aberrations: The chaos of the anterior surface aberrations were compared between eyes of an individual participant. A t-test was carried out to examine the difference in average values of MLE between the eyes. The MLE_{HOA} and MLE_{VP} of both the open-eye intervals and combined data set were investigated separately. There were no significant differences in MLE_{HOA} or MLE_{VP} between eyes for all 3 data sets (t-test; $p>0.05$). Since the analyses demonstrated similar results across all 3 data sets, we employed the individual open-eye interval data sets to plot illustrative figures. The comparison between the right and left eye of the MLE_{HOA} and MLE_{VP} for all participants is shown in Figure 2. The correlation of MLE_{HOA} for eight pairs of eyes was negative but was not strongly correlated ($r= -0.261$, $p=0.54$; Figure 3). Similar to the findings for MLE_{HOA}, the correlation between right and left eyes of the MLE_{VP} was also small, negative and not significant ($r=-0.2$, $p=0.71$).

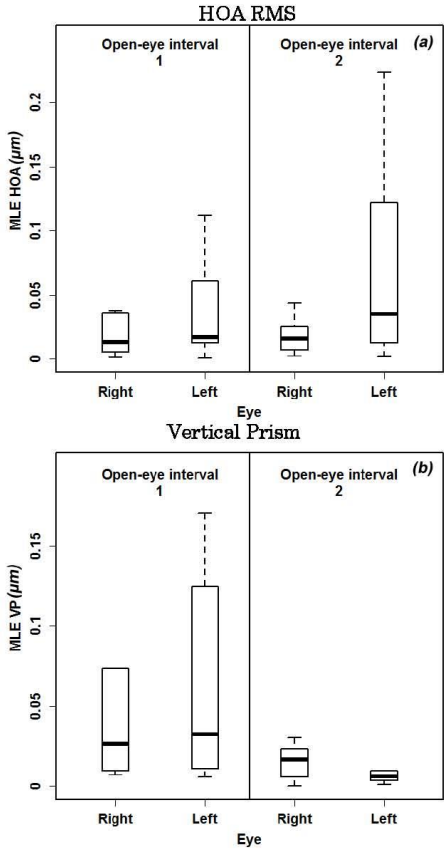

Figure 2 (a): Box plots showing the MLE values obtained for HOA RMS from each eye and open-eye interval of individual participant. 2(b): Box plots showing the MLE values obtained for vertical prism (Z_1^{-1}) coefficients from each eye and each open-eye interval of individual participant.

The difference between the chaos exhibited by the anterior surface aberrations between eyes of an individual and the lack of correlation between eyes is similar to that found in aberrations for the whole eye [10]. We have previously reported [16] that the temporal variation in anterior surface aberrations can vary between consecutive open-eye intervals within the same individual. Although, as our study indicates, the level of the chaos in anterior surface aberrations was not significantly different between eyes, differences in the tear film dynamics between eyes may result in the lack of correlation. Supporting this notion, the NITBUT values were not significantly different between eyes on average (t-test; p=0.7), yet within an individual, the between eye difference ranged between 0.4 seconds and 3.4 seconds.

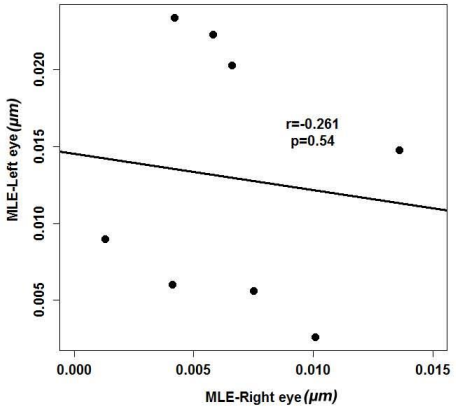

Figure 3: Correlation of maximal Lyapunov exponents obtained from HOA RMS between right and left eyes of all participants for the combined open-eye interval data.

In conclusion, we investigated the chaos in the anterior surface aberrations of the eye. The level of chaos was determined by calculating the MLE of the detrended aberration data. We found a minimal amount of chaos for the total HOA and individual Zernike coefficient of the anterior surface aberrations. The level of chaos was not significantly different between the eyes of an individual; however, likely due to the difference in the tear film dynamics, it did not correlate between the eyes. These results provide evidence of the dynamic nature of the tear film in the chaos of the anterior surface aberration of the eye. The findings may have implications for contact lens designs.

Acknowledgements: The authors would like to thank Dr. Karen Hampson from University of Bradford, UK for her help and time with the chaos analysis. We would also like to acknowledge Topcon Canada Inc. and the Centre for Contact Lens Research, University of Waterloo for providing access to the CA200 corneal analyzer.

References:

1. S. Gruppetta, L. Koechlin, F. Lacombe and P. Puget, In *SF2A-2005: Semaine de l'Astrophysique Francaise* , 237 (2005).
2. K. Y. Li and G. Yoon, *Opt. Express*, **14**, 12552 (2006)
3. D. Iskander, *IEEE Transactions on Biomedical Engineering*. **51**,1939 (2004).
4. A. Dubra, C. Paterson, and C. Dainty, *Optics Express* **12**, 6278 (2004).
5. S. Gruppetta, F. Lacombe and P. Puget, *Optics Express*. **13**, 7631– (2005).
6. R. Montés-Micó, J.L. Alió, W.N. Charman, *Invest. Ophthal. Vis.Sci.* **46**, 1615 (2005).
7. R. Montés-Micó, J.L. Alió, G. Muñoz, W.N. Charman, *Invest. Ophthal. Vis.Sci.***45**, 1752 (2004).
8. S. S. Chin, K.M. Hampson, E.A.H. Mallen , *Opt. Express*, **16**, 14731 (2008).
9. K.M. Hampson and E.A.H. Mallen, *Biomedical Optics Express*, **3**, 863 (2012).
10. K. M. Hampson, and E.A.H. Mallen, *Optics letters*, ***38***, 302 (2013).
11. H. Peitgen, H. Jürgens and D. Saupe, "*Chaos and fractals: new frontiers of science*," Springer-Verlag New York, (1992).
12. V. Lakshminarayanan and A.Fleck. *Journal of Modern Optics*, **58**, 545, (2011).
13. M. Zhu, M.J. Collins, and D. Robert Iskander, *Ophthalmic and Physiological Optics*, **24**, 562 (2004).
14. M.T. Rosenstein, J.J. Collins and C.J. De Luca, *Physica D: Nonlinear Phenomena*, **65**,117 (1993).
15. F.K. Holly, S.J. LauKaitis, E.D. Esquivel. *Current Eye Research*, **3**,897(1984).
16. V. Jayakumar, N. Hutchings, V. Lakshminaryanan and L.W. Jones. IOVS 2013, **54**: ARVO E-Abstract 2608.

Appendix 3

R source code

R.code 1 ***Few basic codings:***

```
## To read a CSV file direct from folder and assign a name for
analysis
> name <- read.csv(file=file.choose(), header=T)
## To attach the file to R console
> attach(name)
## list column headers
> ls(name)      (or)
> head (name)
## To increase outer margin area in a graph
> par(oma=c(2,2,2,2))
## To create thicker axis borders
> box(lwd=2)
## To plot a graph
> plot (x,y)
## To customize graph
>par( )
## to obtain descriptive statistics
> summary(name)
## detach the file from the R console
> detach(name)
## Remove all objects from R console
> rm(list=ls(all=TRUE))
## To install package for analysis
> library(package name)
```

R.code 2 ***Kernel density plot***

```
## Import data
## Data format: each sample arranged one below other (tall measure).
      "focus" “focusnum" "time" "zernike_rms"
      Green1      1     15.04023    1.07981
      Green2      2     15.12037    1.07326
      Green3      3     15.20037    1.07199
```

```
## install package “sm”
> library (sm)
> focus.f <- factor(focus, levels= c(1,2,3), labels=c("Green1", "Green2",
"Green3"))
## to create density plot
> sm.density.compare (zernike_rms, focus, xlab="Zernike RMS"~~(mu*m))
> title(main="Kernel density comparison plot for green focus
positions(0.25s)")
> colfill<- c(2:(2+length(levels(focus.f))))
> legend("topright", levels(focus.f), fill=colfill)
```

R.code 3 ***<u>Test for quantile distribution:</u>***

```
## Import data
## data format 3 samples (sample 2,3,and 4),median corrected samples, tall
measure of 2 median corrected samples in all probabilities.
[1] "GREEN2H” "GREEN3H" "GREEN4H" "GREEN2H_MED" "GREEN3H_MED" "GREEN4H_MED"
"GREEN2H3H" "GREEN3H4H" "GREEN2H4H"
      1.07981     1.07326     1.07199     0.002455    0.00561     0.003535
      0.002455    0.002455    0.00561
## To generate sequence for quantiles@ 2.5%
> p<- seq(0,1,0.025)
## generate quantiles for two sample combined
> measure1<- quantile(GREEN2H3H,p, na.rm=TRUE, type=1)
> measure2<- quantile(GREEN2H4H,p, na.rm=TRUE, type=1)
> measure3<- quantile(GREEN3H4H,p, na.rm=TRUE, type=1)
## generate data file for each comparison samples
> result<- data.frame (measure1, measure2, measure3)
## round the decimals to 5 digits
> round(result,5)
      measure1 measure2 measure3
0%    -0.01597 -0.01597 -0.01158
2.5%  -0.01158 -0.01139 -0.00744
5%    -0.00863 -0.00887 -0.00647
7.5%  -0.00718 -0.00744 -0.00592
10%   -0.00636 -0.00592 -0.00549
12.5% -0.00565 -0.00561 -0.00498
15%   -0.00520 -0.00520 -0.00462
17.5% -0.00473 -0.00473 -0.00410
20%   -0.00431 -0.00431 -0.00374
22.5% -0.00374 -0.00375 -0.00355
25%   -0.00341 -0.00341 -0.00339
```

```
27.5% -0.00266 -0.00307 -0.00252
30%   -0.00232 -0.00259 -0.00221
32.5% -0.00184 -0.00228 -0.00184
35%   -0.00163 -0.00181 -0.00149
37.5% -0.00137 -0.00144 -0.00137
40%   -0.00122 -0.00107 -0.00105
42.5% -0.00098 -0.00054 -0.00077
45%   -0.00054 -0.00043 -0.00042
47.5% -0.00043 -0.00029 -0.00016
50%    0.00000  0.00000  0.00000
52.5%  0.00025  0.00016  0.00011
55%    0.00040  0.00054  0.00048
57.5%  0.00086  0.00064  0.00063
60%    0.00112  0.00095  0.00094
62.5%  0.00154  0.00135  0.00108
65%    0.00192  0.00167  0.00135
67.5%  0.00213  0.00198  0.00159
70%    0.00245  0.00236  0.00193
72.5%  0.00272  0.00272  0.00217
75%    0.00312  0.00311  0.00247
77.5%  0.00353  0.00354  0.00317
80%    0.00387  0.00383  0.00368
82.5%  0.00472  0.00418  0.00403
85%    0.00514  0.00514  0.00462
87.5%  0.00533  0.00538  0.00489
90%    0.00590  0.00590  0.00538
92.5%  0.00642  0.00650  0.00584
95%    0.00734  0.00726  0.00662
97.5%  0.00864  0.00806  0.00764
100%   0.01077  0.01077  0.01001
## create a table using quantiles
> write.table(result, file=" quantile_green_0.25_30082011.csv", sep=",",
col.names=NA, qmethod="double")
## to compare outer 5% of the distribution of each sample
> quantilecombined<- quantile(GREEN2H3H, p, na.rm=TRUE, type=1)
> a<- sum (GREEN2H_MED <= -0.01158, na.rm= TRUE)
> b<- sum (GREEN2H_MED >= 0.00864, na.rm= TRUE)
> x=(a+b)
> c<- sum (GREEN2H3H <= -0.01158, na.rm= TRUE)
> d<- sum (GREEN2H3H >= 0.00864, na.rm= TRUE)
> m= (c+d)
> e<- length (GREEN2H3H)
```

```
> n= (e-m)
> k<- sum(GREEN2H_MED <1000, na.rm= TRUE)
## to compare the distributions
> dhyper(x,m,n,k)
[1] 0.1175064
## Repeat the same for comparison of other samples and between focus
positions
```

R.code 4 ***T.test and Box plot with beeswarm and axis break***

```
## Import data
## code for t-test to compare luminance of Placido disc and also
plot boxplot with data points
> t.test(Luminance~Instrument)
## create subset
> ca100<- subset(ttest, Instrument=='CA100')
> ca200<- subset(ttest, Instrument=='CA200')
#draw box plot
> boxplot(Luminance~Instrument, axes=F, ylim=c(3,11), data=ca200)
# to plot data points on box plot
> library(beeswarm)
> beeswarm(Luminance~Instrument, cex=0.8,pch=19, col="red",
data=ca200, add=T)
>axis(2,at=c(3,4,5,6,8,9,10,11),labels=c("3","4","5","6","30","31","
32","33"), cex.axis=1.5)
## Reference to create axis break using "plotrix" package
http://rss.acs.unt.edu/Rdoc/library/plotrix/html/axis.break.html
## install plotrix package
> library(plotrix)
> axis.break(2,7, style="slash")
> par(new=T)
>boxplot(Luminance~Instrument,axes=F,ylim=c(25,33),data=ca100,cex=2)
>beeswarm(Luminance~Instrument,cex=0.8,pch=19,col="green",data=ca100
,add=T)
> axis(1,at=c(1,2), labels=c("CA100", "CA200"), cex.axis=1.5)
## to add axis labels
> mtext("Instruments", side=1, line=0,cex=1.25, outer=T)
> mtext("Luminance"~~(cd/m^2), side=2, line=0, cex=1.25, outer=T)
```

R.code 5 ***ggplot***

```
## Import data
##install(ggplot2)
> library(ggplot2)
## create names for facet tittle by using labellar function
> spectrum<- list('1'="Short", '2'="Central",'3'="Long")
>spectrum_labellar<-
function(variable,value){return(spectrum[value])}
> p<- ggplot (SpectralData, aes(lambda, radiance, col=Time_point))+
facet_grid(. ~ range_no, scales="free", space="free",
labeller=spectrum_labellar)
## to plot coloured with different symbols and average with CI
>p+ geom_point()+scale_y_log10()+theme_bw()+ xlab("Wavelength
(nm)")+ylab("log
(Radiance)")+aes(shape=Time_point)+scale_shape_manual(values =
c(1,2,0,3,15,16,17,18,19,20))+
geom_smooth(aes(group=1))+aes(colour=Time_point)+theme(strip.text.x
= element_text(size = 12))
```

R.code 6 ***Scatterplot with error bars***

```
## import data
> mean.rca100<-ca100_right
> mean.lca100<- ca100_left
> mean.rca200<- ca200_right
> mean.lca200<- ca200_left
> std.rca100<- sd_ca100_right
> std.lca100<- sd_ca100_left
> std.rca200<- sd_ca200_right
> std.lca200<- sd_ca200_left
> names(mean.rca100)<-
c("1","2","3","4","5","6","7","8","9","10","11","12")
> names(mean.rca200)<-
c("1","2","3","4","5","6","7","8","9","10","11","12")
> names(std.rca100)<-
c("1","2","3","4","5","6","7","8","9","10","11","12")
```

```
> names(std.rca100)<-
c("1","2","3","4","5","6","7","8","9","10","11","12")
> names(mean.lca100)<-
c("1","2","3","4","5","6","7","8","9","10","11","12")
> names(mean.lca200)<-
c("1","2","3","4","5","6","7","8","9","10","11","12")
> names(std.lca100)<-
c("1","2","3","4","5","6","7","8","9","10","11","12")
> names(std.lca100)<-
c("1","2","3","4","5","6","7","8","9","10","11","12")
> library(plotrix)
> par(oma=c(2,2,0,0))
##plot scatterplot with error bars
> plotCI(x=(1:12), y=mean.rca100,uiw=std.rca100,lty=2, font
=2,xaxt="n",xlim=c(0,13),ylim=c(0,200),gap=0, col="green", xlab="",
ylab="")
> plotCI(x=(1:12), y=mean.rca200,uiw=std.rca200,lty=1, font
=2,xaxt="n", xlim=c(0,13),ylim=c(0,200),gap=0, add=T,col="red")
> plotCI(x=(1:12), y=mean.lca100,uiw=std.lca100,lty=3, font
=2,xaxt="n", xlim=c(0,13),ylim=c(0,200),gap=0, add=T,col="blue")
> plotCI(x=(1:12), y=mean.lca200,uiw=std.lca200,lty=4, font
=2,xaxt="n", xlim=c(0,13),ylim=c(0,200),gap=0, add=T,col="black")
> axis(side=1,at=1:12, font =2,labels=names(mean.rca100))
## legends
> legend("topright",lty=c(2,2,2,2),lwd=1.5, c("CA100 right
side","CA100 left side", "CA200 right side", "CA200 left side"),
pch=c(19,19,15,15), col=c("green","blue","red","black"))
##lines connecting points
> lines(mean.rca100,col="green", lty=2,lwd=1.5)
> lines(mean.rca200,col="red", lty=2,lwd=1.5)
> lines(mean.lca100,col="blue", lty=2,lwd=1.5)
> lines(mean.rca100,col="black", lty=2,lwd=1.5)
> lines(mean.rca100,col="green", lty=2,lwd=1.5)
> lines(mean.lca200,col="black", lty=2,lwd=1.5)
## horizontal reference lines for averages
> abline(h=92.4213, lty=3, col="green", lwd=1.5)
> abline(h=67.1414, lty=3, col="blue",lwd=1.5)
> abline(h=20.4558, lty=3, col="red",lwd=1.5)
```

```
> abline(h=15.78448, lty=3, col="black",lwd=1.5)
> mtext("Placido ring #", side=1,font =2,line=3)
> mtext("Luminance"~~(cd/m^2), side=2,font =2,line=3)
> box(lwd=1.5)
## for text annotations
> text(locator(1), "92.42",font=2, cex=0.7)
> text(locator(1), "67.14",font=2, cex=0.7)
> text(locator(1), "20.46",font=2, cex=0.7)
> text(locator(1), "15.79",font=2, cex=0.7)
```

R.code 7 ***Combining plot (boxplot with beeswarm)***

```
## to combine plot with extra outer margin space
## Import data
> par (mfrow=c(2,1), oma=c(0,1,0,0))
## boxplots with beeswarm data point.
> boxplot(luminance_100~quadrant_100,sub="CA100", xaxt="n",yaxt="n",
ylim=c(40,50), xlab="Quadrants", ylab="", font=2)
> library(beeswarm)
> beeswarm(luminance_100~quadrant_100, pch=18, cex=0.6, col="green",
add=T)
> axis(1, at=c(1,2,3,4), labels=
c("CA100\nInferior","CA100\nLeft","CA100\nRight","CA100\nSuperior"),
cex.axis= 0.8,font.axis=2, tck=-0.01)
> axis(2,
at=c(40,42,44,46,48,50),labels=c(40,42,44,46,48,50),las=2,font.axis=
2)
> mtext("Luminance"~~(cd/m^2), side=2, line=3,font=2)
> boxplot(luminance_200~quadrant_200, ylim=c(5,15),sub="CA200",
xlab="Quadrants",axes=F, font=2, ylab="" )
> beeswarm(luminance_200~quadrant_200, pch=18, cex=0.6, col="red",
add=T)
> box()
> axis(1, at=c(1,2,3,4), labels=
c("CA200\nInferior","CA200\nLeft","CA200\nRight","CA200\nSuperior"),
cex.axis= 0.8,font.axis=2, tck=-0.01)
> axis(2, at=c(5,7,9,11,13,15),labels=c(5,7,9,11,13,15),las=2,
font.axis=2)
```

R.code 8 ***Bar plot***

```
## creating combination plot of bar plots for peak wavelengths in
different experiments
## created new graph with 3 rows and one column of graphs with
custom margin widths
## import data file
> par(mfrow=c(3,1),mai=c(0.5,0.5,0.5,0.1))
## for individual ring measures
## install “gregmisc” package for creating boxplot with error bars
> library(gregmisc)
##calculate mean
> waves=tapply(Wavelength,
list(as.factor(measure_area),as.factor(ring_no)),mean)
> waves
## calculate standard error
> stderr <- function(x) sqrt(var(x,na.rm=TRUE)/(length(na.omit(x))))
> waves.stderr=tapply(Wavelength,
list(as.factor(measure_area),as.factor(ring_no)),stderr)
> waves.stderr
# calculate the range
> upper=waves+1.96*waves.stderr
> lower=waves-1.96*waves.stderr
##create boxplot
> bp<- barplot2(waves,beside=T,horiz=F,
names.arg=c("1","2","3","4","5","6","7","8","9","10","11","12"),
plot.ci=T, ci.u=upper, ci.l=lower, col=topo.colors(4),
ylim=c(638,650), legend.text=NULL,xpd=F, font=2)
> box(lwd=2)
> legend("topright",c("CA100_Left side","CA100_Right side",
"CA200_Left side", "CA200_Right side"),horiz=T, fill=
topo.colors(4))
> mtext("Placido ring #", side=1, font=2, line=2.5)
> mtext("Wavelength (nm)", side=2, font=2, line=2.5)
> mtext("Peak wavelength obtained from individual rings", side=3,
line=0.5,font=2)
## for Disc measures
## import data
```

```
##calculate mean
> waves.fullring=tapply(Wavelength_fullring,
list(as.factor(inst_fullring),as.factor(fullring_no)),mean)
> waves.fullring
## calculate standard error
> stderr <- function(x) sqrt(var(x,na.rm=TRUE)/(length(na.omit(x))))
> waves_full.stderr=tapply(Wavelength_fullring,
list(as.factor(inst_fullring),as.factor(fullring_no)),stderr)
> waves_full.stderr
# calculate the range
> upper=waves.fullring+1.96*waves_full.stderr
> lower=waves.fullring-1.96*waves_full.stderr
##create boxplot
> bp<- barplot2(waves.fullring,beside=T,horiz=F,
names.arg=c("1","2","3","4","5","6","7","8","9","10","11","12"),
plot.ci=T, ci.u=upper, ci.l=lower, col=c("green","red"),
ylim=c(638,650), legend.text=NULL,xpd=F, font=2)
> box(lwd=2)
> legend("topright",c("CA100", "CA200"),horiz=T, fill=
c("green","red"))
> mtext("Placido ring #", side=1, font=2, line=2.5)
> mtext("Wavelength (nm)", side=2, font=2, line=2.5)
> mtext("Peak wavelength obtained from each dics measure", side=3,
line=0.5,font=2)
##for quadrant measures
## Import data
##calculate mean
> waves.quad=tapply(Wavelength_quad,
list(as.factor(inst_quad),as.factor(quad)),mean)
> waves.quad
## calculate standard error
> stderr <- function(x) sqrt(var(x,na.rm=TRUE)/(length(na.omit(x))))
> waves_quad.stderr=tapply(Wavelength_quad,
list(as.factor(inst_quad),as.factor(quad)),stderr)
> waves_quad.stderr
# calculate the range
> upper=waves.quad+1.96*waves_quad.stderr
> lower=waves.quad-1.96*waves_quad.stderr
```

```
##create boxplot
> bp<- barplot2(waves.quad,beside=T,horiz=F,
names.arg=c("Inferior","Superior","Right","left"), plot.ci=T,
ci.u=upper, ci.l=lower, col=c("green","red"), ylim=c(638,650),
legend.text=NULL,xpd=F, font=2)
> box(lwd=2)
> legend("topright",c("CA100", "CA200"),horiz=T, fill=
c("green","red"))
> mtext("Quadrants", side=1, font=2, line=2.5)
> mtext("Wavelength (nm)", side=2, font=2, line=2.5)
> mtext("Peak wavelength obtained from each quadrant", side=3,
line=0.5,font=2)
```

R.code 9 ***Scatterplot***

```
##multiple scatter plot for unanimous object measures
## Import data
> par(mfrow=c(3,1),oma=c(0,0.5,0,0))
## plot for air
> plot(time, ca100_air,  pch=16,cex=1.25 ,xlab="", ylab="",
ylim=c(24.5, 26.5), cex.axis=1.25)
> box(lwd=2)
> points(time, ca200_air, pch=1, cex=1.25)
> mtext("Time (sec)", font=2, side=1, line=3)
> mtext("Temperature"~~(degree*C), font=2, side=2, line=3)
> lines(time,ca100_air, lty=1, lwd=1.5)
> lines(time,ca200_air, lty=4, lwd=1.5)
> text(140,25.7, "Mean=25.31")
> text(140,24.9, "Mean=25.15")
> legend("topright", pch=c(16,1), c("CA100", "CA200"), lty=c(1,4))
> title(main="Air")
##plot for tissue
> plot(time, ca100_tissue,  pch=17,cex=1.25 ,xlab="", ylab="",
ylim=c(25.5, 27.5), cex.axis=1.25)
> box(lwd=2)
> points(time, ca200_tissue, pch=2, cex=1.25)
> mtext("Time (sec)", font=2, side=1, line=3)
> mtext("Temperature"~~(degree*C), font=2, side=2, line=3)
```

```
> lines(time,ca100_tissue, lty=2, lwd=1.5)
> lines(time,ca200_tissue, lty=3, lwd=1.5)
> text(140,26.8, "Mean=26.57")
> text(140,26, "Mean=26.36")
> legend("topright", pch=c(17,2), c("CA100", "CA200"), lty=c(2,3))
> title(main="Tissue paper")
##plot for model eye
> plot(time, ca100_modeleye,  pch=18,cex=1.25 ,xlab="", ylab="",
ylim=c(25.5, 27.5), cex.axis=1.25)
> box(lwd=2)
> points(time, ca200_modeleye, pch=5, cex=1.25)
> mtext("Time (sec)", font=2, side=1, line=3)
> mtext("Temperature"~~(degree*C), font=2, side=2, line=3)
> lines(time,ca100_modeleye, lty=5, lwd=1.5)
> lines(time,ca200_modeleye, lty=6, lwd=1.5)
> text(140,26.8, "Mean=26.39")
> text(140,25.7, "Mean=26.06")
> legend("topright", pch=c(18,5), c("CA100", "CA200"), lty=c(5,6))
> title(main="Model eye")
```

R.code 10 ***<u>Multilevel plots</u>***

```
## import data
## choose file for eyelid(or) conjunctiva (or) cornea
## subset data using following commands
> infra<- subset(mlplots, inst=="CA100")
> red<- subset(mlplots, inst=="CA200")
## find linear regression for each participant
> reg11<- lm(temp1~time,data=infra)
> reg12<- lm(temp1~time,data=red)
> reg21<- lm(temp2~time,data=infra)
> reg22<- lm(temp2~time,data=red)
> reg31<- lm(temp3~time,data=infra)
> reg32<- lm(temp3~time,data=red)
> reg41<- lm(temp4~time,data=infra)
> reg42<- lm(temp4~time,data=red)
> reg51<- lm(temp5~time,data=infra)
> reg52<- lm(temp5~time,data=red)
```

```
> reg61<- lm(temp6~time,data=infra)
> reg62<- lm(temp6~time,data=red)
> reg71<- lm(temp7~time,data=infra)
> reg72<- lm(temp7~time,data=red)
> reg81<- lm(temp8~time,data=infra)
> reg82<- lm(temp8~time,data=red)
> reg91<- lm(temp9~time,data=infra)
> reg92<- lm(temp9~time,data=red)
> reg01<- lm(temp10~time,data=infra)
> reg02<- lm(temp10~time,data=red)
## plot an empty graph with type=”n”
> plot(temp1~time, data=mlplots, type="n", xlab="Time (s)",
ylab="Temperature"~~(degree~c),ylim=c(30,36),cex.axis=1.25)
## create slope lines using following codes
> abline(reg11,lty=1,lwd=2,col="green")
> abline(reg12,lty=1,lwd=2,col="red")
> abline(reg21,lty=1,lwd=2,col="green")
> abline(reg22,lty=1,lwd=2,col="red")
> abline(reg31,lty=1,lwd=2,col="green")
> abline(reg32,lty=1,lwd=2,col="red")
> abline(reg41,lty=1,lwd=2,col="green")
> abline(reg42,lty=1,lwd=2,col="red")
> abline(reg51,lty=1,lwd=2,col="green")
> abline(reg52,lty=1,lwd=2,col="red")
> abline(reg61,lty=1,lwd=2,col="green")
> abline(reg62,lty=1,lwd=2,col="red")
> abline(reg71,lty=1,lwd=2,col="green")
> abline(reg72,lty=1,lwd=2,col="red")
> abline(reg81,lty=1,lwd=2,col="green")
> abline(reg82,lty=1,lwd=2,col="red")
> abline(reg91,lty=1,lwd=2,col="green")
> abline(reg92,lty=1,lwd=2,col="red")
> abline(reg01,lty=1,lwd=2,col="green")
> abline(reg02,lty=1,lwd=2,col="red")
> legend("bottomright",title=
"Instruments",c("CA100","CA200"),lty=c(1,1),col=c("green","red"))
```